The Pennsylvania State University

The Graduate School

Department of Energy and Geo-Environmental Engineering

AN INTEGRATED HYDRODYNAMIC / PVT VERTICAL WELLBORE MODEL FOR TWO-PHASE NATURAL GAS / LIQUID SYSTEMS

A Thesis in

Petroleum and Natural Gas Engineering

by

Abdallah A. Sadegh

Submitted in Partial Fulfillment
of the Requirements
for the Degree of

Doctor of Philosophy

August 2006

The thesis of Abdallah A. Sadegh was reviewed and approved* by the following:

Michael A. Adewumi
Professor of Petroleum and Natural Gas Engineering and Quentin E. and Louise L. Wood University Endowed Fellow in Petroleum and Natural Gas Engineering
Thesis Advisor
Chair of Committee

Turgay Ertekin
Professor and Program Chair of Petroleum and Natural Gas Engineering, Graduate Program Chair of Petroleum and Natural Gas Engineering and George E. Trimble Chair in Earth and Mineral Sciences

Robert W. Watson
Associate Professor of Petroleum and Natural Gas Engineering and Geo-Environmental Engineering

M. Thaddeus Ityokumbul
Associate Professor of Mineral Processing and Geo-Environmental Engineering

Dr. Mark S. Klima
Associate Professor of Mineral Processing and Geo-Environmental Engineering

*Signatures are on file in the Graduate School

ABSTRACT

Multiphase flow in the wellbore poses a challenge for production engineers since characterization of prevailing flow regime determines the appropriate pressure drop calculation method. The problem is further complicated when the flowing fluid undergoes phase changes. The key objective was to develop a wellbore flow model based on sound physical principles, incorporating state of the art hydrodynamic and thermodynamic tools.

The model developed comprises a flow pattern detection routine, hydrodynamic model, and an equation-of-state-based phase behavior package. The model was extensively tested with 30 field cases, proving to accurately predict pressure drop for single and two-phase (gas/condensate) flow giving an average absolute error of 6.3%.

The inherent challenges were handling phase changes as pressure, temperature and/or composition vary. Accurate prediction of fluid properties was also crucial. The model provides a convenient tool for the production engineer for well design and can be readily incorporated in NODAL analysis.

TABLE OF CONTENTS

LIST OF FIGURES

LIST OF TABLES

NOMECLATURE

$(a\alpha)_i$ =Peng-Robinson pure component interaction parameter

b_i=Peng-Robinson pure component co-volume

A_C=Core cross-sectional area

A_P=Pipe cross-sectional area

d_{crit} =Bubble diameter above which bubble may remain intact in turbulent flow by deforming

d_{max} =Maximum stable diameter for gas bubble in turbulent flow

D_{HL} =Liquid film hydraulic diameter

D_P =Pipe diameter

D_{Pmin} =Minimum pipe diameter for bubbly flow existence

f =Taitel et al friction factor used in dispersed bubbly flow

f_i =Interface friction factor

f_{Gi} =Fugacity of the gas phase

f_L =Liquid film friction factor in Hasan and Kabir model

f_{LF} =Liquid film friction factor in Hasan and Kabir model

f_{Lg} =Interface drag friction factor in annular mist flow

f_{Li} =Fugacity of the liquid phase

f_{LS} =Liquid slug friction factor

f_{SLF} =Superficial liquid film friction factor in annular mist flow

f_{TP} =two phase friction factor used in bubbly flow model

F_{DG}=Drag for on the gas phase per unit volume

F_E =Entrained liquid fraction in gas core (annular mist flow)

F_{FG}=Friction force per unit volume between pipe and gas phase

F_{FL}=Friction force per unit volume between pipe and liquid phase

F_{FSU} =Friction force per unit volume for entire slug unit

F_G=Combined force cause by gas phase

F_{GG}=Force of gravity per unit volume acting on the gas phase

F_{GL}=Force of gravity per unit volume acting on the liquid phase

F_i=Interface drag force in annular mist model

F_L=Combined force cause by liquid phase

F_{LF}=Friction force at pipe wall

F_{Lg}= Friction force at liquid/core interface in annular mist flow

F_{wL}= Friction force due to liquid in annular mist flow

F_{wLS}= Friction force due to slug flow

g =Acceleration of gravity

G_{SU} =Gravity force per unit volume for entire slug unit

H_{GLS} =Gas holdup in liquid slug

H_L =Liquid holdup

H_L' =Liquid holdup factor in Hagedorn and Brown correlation

H_{LF} =Liquid film holdup

L =Length (for instance length of Taylor bubble is L_{TB})

MW = Molecular weight

N_D =Dimensionless pipe diameter number

N_{GV} =Dimensionless gas velocity number

N_L =Dimensionless liquid viscosity number

N_{LV} =Dimensionless liquid velocity number

N_{Re} =Reynolds number

N_S =Dimensionless slip velocity number

P =Pressure

P_{ci} =Pure component critical pressure

P_{SC} =Pressure at standard conditions (14.73 Psia and 65 °F)

R =Gas constant

S_i =Interface perimeter

S_{LF} =Liquid film perimeter

t = time

T =Temperature

T_{ci} =Pure component critical temperature

v_{crit} =Critical gas velocity required to keep entrained liquid droplets (annular mist flow)

v_M =Mixture velocity

v_S =Slip velocity

v_{SC} =Superficial gas core velocity

v_{SG} =Superficial gas velocity

v_{SL} =Superficial liquid velocity

$\tilde{v}$ =Molar volume

x_i =Pure component mole fraction in gas phase

X_M =Modified Lockhart and Martinelli parameter

Xv_{SG} =Dimensionless superficial gas velocity number in Aziz et al. model

y_i =Pure component mole fraction in liquid phase

Y_M =Modified Lockhart and Martinelli parameter

Yv_{SL} =Dimensionless superficial liquid velocity number in Aziz et al. model

z_i =Pure component mole fraction in the feed

Z =Film thickness correlating factor in annular mist flow model

GREEK:

α =Gas fraction in hydrodynamic formulation

β =Ratio of length of Taylor bubble to entire length of slug unit

δ =Film thickness (annular mist flow)

ε =Absolute roughness of pipe

λ_L =Liquid entrainment coefficient (annular mist flow)

μ_G =Gas viscosity

μ_M =Mixture viscosity

μ_L =Liquid viscosity

μ_{SC} =Core fluid viscosity

ω_i=*Accentric factor*

ρ_C =Core fluid density (annular mist flow)

ρ_G =Gas density

ρ_L =Liquid density

ρ_M =Mixture density

ρ_W =Water density

σ =Surface tension

θ =Pipe inclination angle

τ_i =Interfacial surface stress

Φ_{Gi} =Pure component fugacity coefficient in the gas phase

Φ_{Li} =Pure component fugacity coefficient in the liquid phase

Ψ =Liquid holdup correction factor in Hagedorn and Brown correlation

ACKNOWLEDGEMENTS

Praise and thanks are due to God Almighty for his endless blessings. I would like to thank my thesis advisor Dr. Michael A. Adewumi for his patience and continued support during the completion of this work. This endeavor would not have been possible without his guidance. I would also like to extend my gratitude to Dr. Turgay Ertekin, Dr. Robert W. Watson, Dr. M. Thaddeus Ityokumbul, Dr. Mark S. Klima, and Dr. Osama O. Awadelkarim for their interest in serving on the thesis committee and for their valuable and insightful recommendations.

I would like to thank from all my heart Ms Huda A. Jerri for her friendship and support and for painstakingly reviewing this thesis.

This work is dedicated to my parents Mariam Ahmed El-Shaikh and Ahmed El-Sadeg and to my children Mohamed and Asma.

Chapter 1

INTRODUCTION AND STATEMENT OF PROBLEM

1.1 Introduction

As the demand for energy rises, petroleum and natural gas production companies are exploring and exploiting more complex reservoir systems. It is a business necessity to optimize the production and to conserve the natural drive mechanisms within the reservoirs. One of the major challenges facing production engineers is optimization of the production system. The production system comprises the reservoir, the near wellbore region, the wellbore, and the surface production facility.

Optimization of this system requires accurate prediction of pressure drop in the wellbore. This is a challenging task because single-phase flow seldom occurs in the wellbore. More commonly, multiphase flow prevails in the wellbore and also in gas and oil transmission and distribution pipelines. The engineering calculations required to design and operate oil and gas production, processing, and transmission systems are complicated by a number of physical phenomena. These phenomena include flow regime transitions, turbulence, and thermodynamic phase changes with pressure and temperature. Hence, use of empirical correlations based on limited laboratory or field data often lead to erroneous predictions.

Most of the tools currently in use by production engineers are based on empirical correlations. The approach taken in developing these models was to generate an extensive database by varying parameters thought to impact pressure drop. The parameters include gas flow rate, liquid flow rate, pipe diameter, fluid viscosities, and liquid surface tension. The pressure drop data are then correlated to dimensionless groups based on the relevant variables. One of the major limitations of this approach is that it cannot be safely extrapolated to prediction in situations where the actual well parameters are outside the range of data initially used to develop the correlation. In

additionally, it was observed that different pressure gradients arose for varied distribution of the flowing phases in the pipe. The regime transitions were also a function of the physical parameters of the flow system under consideration. Therefore it is necessary to predict the prevailing flow regime and then use a pressure drop prediction method suitable for that particular flow regime.

Another disadvantage of using current pressure drop prediction methods is that the fluid properties are usually based on empirical correlations. This becomes especially critical if the wellbore model is coupled with a compositional reservoir simulator. Internal inconsistencies can arise since the compositional simulator is based on an equation of state. The correlations used with the wellbore model may predict different fluid properties for the same pressure, temperature, and fluid composition than the properties given by the reservoir simulator.

Flow of gas condensate, in addition to the complexities inherent in all two-phase flow modeling is further complicated by the fact that retrograde condensation can occur. The in-situ liquid fraction may change due to change in pressure, temperature or fluid composition. This particular problem requires the incorporation of compositional modeling in the prediction of fluid splits and gas and liquid properties.

Considering the disadvantages of using current pressure drop prediction methods for gas condensate wellbore modeling, it is necessary to integrate hydrodynamic modeling, with hydrocarbon phase behavior modeling, and flow regime transition determination in order to obtain reasonable predictions. The premise of the research was to address the formidable challenges of accurately predicting pressure drop, liquid holdup and fluid compositions for gas condensate wells.

1.2 Statement of Problem

The objective of this research is to develop an integrated wellbore model for gas/condensate wells. The model should be capable of predicting pressure drop, liquid

holdup, and composition at the wellhead of the gas and/or liquid stream. The model incorporates state-of-the art methods in hydrodynamic modeling, hydrocarbon phase behavior modeling, and flow regime transition prediction.

Chapter 2

LITERATURE REVIEW

2.1 Early Research

Research in two-phase flow was probably first documented by Davis and Weidner [1914]. They investigated vertical flow of a mixture of air and water in a glass tube and concluded that the pressure drop depended on the water to air ratio. They suspected the increase in pressure drop was due to air "slowing-down" (slippage) in response to interfacial friction with water. Pressure drop was formulated as a function of the interface velocity by Versluys [1930]. In his theoretical investigation, analyses were conducted for limiting flow regimes, namely liquid mist entrapped in a gas stream and dispersed gas bubbles carried by a liquid stream. Uren et al [1930] performed experiments on oil-air mixtures and used their results to relate the pressure drop to a friction factor for the mixture.

The contribution of inertia to two-phase pressure drop was investigated by Moore and Wilde [1931]. They devised a procedure to determine the combined pressure drop by giving a correlation for liquid holdup and mixture friction factor. Bergelin et al. [1946] observed annular flow when they conducted experiments in which a mixture of air and water flowed downward in a vertical pipe. This was the first time geometric distribution of the flowing phases was observed in laboratory experiments.

2.2 Empirical Models

The first correlation to find wide acceptance in the petroleum industry was introduced by Poettman and Carpenter [1952]. They developed an empirical correlation based on flow of oil-water-gas mixtures in producing wells. The fluids were treated as a mixture, and a combined friction factor was determined empirically. In this study the effect of acceleration of the fluid was neglected.

Baxendell and Thomas [1961] collected high flow rate field data from La Paz oil field in Venezuela. They followed a similar approach to Poettman and Carpenter and fitted the observed pressure drops using the combined mass and momentum balance equations. A range of friction factor values were substituted into the pressure drop formula until agreement with experimental data was obtained. A graph was then constructed on semi-log paper relating the numerator of the Reynolds number to the friction factor. It is noted that Baxendell and Thomas' data extended to much higher flow rates and that at these conditions the friction factor is approximately a linear function of the numerator of the Reynolds number. This is expected due to dominance of turbulence at such high flow rates.

Fancher and Brown [1963] expanded the Poettman and Carpenter correlation by using the gas-liquid-ratio as a second correlating parameter. They first classified field data based on gas-liquid-ratio and then correlated each subset of pressure drop data to the numerator of the Reynolds number. Using this approach, plots for friction factor versus numerator of Reynolds number where obtained. They claimed their correlation agreed with field data to within 10%.

2.3 Semi-Empirical Models

Hagedorn and Brown [1964] conducted an extensive study of air-oil and air-water mixtures in an experimental well. They developed a correlation requiring both friction factor and liquid holdup inputs. The pressure drop was attributed to acceleration effects, potential energy effects, and friction effects. The mixture approach was not found to fit the data properly and as such Hagedorn proposed a two-phase Reynolds number based on the use of liquid holdup as a mixing parameter for the densities and viscosities of the fluids. The liquid holdup was correlated to the four dimensional groups proposed by Duns and Ros [1963] (the liquid velocity number, the gas velocity number, the pipe diameter number, and the liquid viscosity number).

The liquid holdup "factor" was found to correlate to the combination of the gas velocity number, liquid velocity number and dimensionless pressure. This combination is given mathematically by

$$H_L^{'} = f\left(\frac{N_{LV}}{N_{GV}^{0.575}} \left[\frac{P}{P_{SC}} \right]^{0.1} \right) \qquad \textbf{2.1}$$

A secondary correction was applied to account for scatter caused by viscosity and pipe diameter effects. The corrected liquid holdup is given by

$$H_L = H_L^{'} \psi \left(\frac{N_{GV} N_L^{0.38}}{N_D^{2.14}} \right) \qquad \textbf{2.2}$$

2.4 Semi-Mechanistic Models

Duns and Ros [1963] noted the inadequacy of Poettman and Carpenter's correlation for application when low pressure, low flow rate, high gas-oil-ratio (low liquid holdup) or high viscosity oils are encountered. They postulated that the shortcomings of previous method was due to lumping the acceleration pressure drop (due to gas slip past liquid) into a generalized pressure drop. To alleviate this issue, they conducted extensive testing with various fluids, pipe diameters, inlet pressure, and flow rates (they claim to have compiled 20,000 data points).

Duns and Ros noted that if dimensionless pressure drop is plotted against superficial gas velocity, a decreasing pressure drop is observed as superficial gas velocity increases. The rate of decrease, however, is dependent on the liquid superficial velocity. They also noted a sharp increase in pressure drop at very high gas velocity (>1.5 m/s). They attributed this to the transition to mist flow regime and subsequent increase in frictional pressure loss. It should be noted that these observations were all made for a single fluid and single pipe diameter.

Duns and Ros proposed that in order to obtain better pressure drop correlations, a different correlation may be necessary for each geometric distribution of in-situ gas and liquid (flow regime). To do this, they proposed four dimensionless numbers to represent the effect of liquid velocity, gas velocity, liquid viscosity, and pipe diameter. The four numbers are given by:

$$N_{LV} = v_{SL}\left(\frac{\rho_L}{g\sigma}\right)^{0.25} \qquad \textbf{2.3}$$

$$N_{GV} = v_{SG}\left(\frac{\rho_G}{g\sigma}\right)^{0.25} \quad \textbf{2.4}$$

$$N_D = D\sqrt{\frac{\rho_L g}{\sigma}} \quad \textbf{2.5}$$

$$N_L = \mu_L\left(\frac{g}{\sigma^3\rho_L}\right)^{0.25} \quad \textbf{2.6}$$

A "map" was generated by plotting the liquid velocity number versus the gas velocity numbers. Major flow regime transitions were then plotted on this map.

In order to determine the holdup, Duns and Ros defined slip velocity as:

$$v_S = \frac{v_{SG}}{1-H_L} - \frac{v_{SL}}{H_L} \quad \textbf{2.7}$$

The slip velocity was expressed in dimensionless form by:

$$N_S = v_S\left(\frac{\rho_L}{g\sigma}\right)^{0.25} \quad \textbf{2.8}$$

Correlations for the slip velocity were then proposed for the case where the gas is the dispersed phase (named region I), the segregated region (II), and liquid mist region (III). Duns and Ros proposed slip velocity and frictional pressure drop correlations for each of the three zones.

Orkiszewski [1967] proposed a pressure drop correlation based on the extension of the slug flow model of Griffith and Wallis [1961] taking into consideration a flow regime spectrum spanning from bubbly flow to mist flow, and including slug flow. The criterion of Griffith and Wallis for transition from bubbly to slug flow was used along with the transition from separated flow to mist flow proposed by Duns and Ros. The friction factor was calculated using a flow regime-specific correlation.

Aziz et al. [1972] proposed a model to predict pressure drops for wells production from under-saturated oil reservoirs. The mixture density and velocity wer determined using liquid holdup based on the existing flow pattern. Aziz et al. used the regime map of Govier et al. [1957].

The flow regime transition limits were based on the modified superficial gas and liquid velocities defined, respectively, as:

$$Xv_{SG} = \left(\frac{\rho_G}{\rho_{Air,SC}}\right)^{1/3}\left(\frac{\rho_L\sigma_{Air-Water,SC}}{\rho_W\sigma_L}\right)^{1/4} v_{SG} \qquad \textbf{2.9}$$

$$Yv_{SL} = \left(\frac{\rho_L\sigma_{Air-Water,SC}}{\rho_W\sigma_L}\right)^{1/4} v_{SL} \qquad \textbf{2.10}$$

The pressure drop was composed of the contribution of the hydrostatic pressure head, the friction pressure loss, and the acceleration loss. Symbolically this is written as

$$\left(\frac{\Delta P}{\Delta Z}\right)_T = \left(\frac{\Delta P}{\Delta Z}\right)_H + \left(\frac{\Delta P}{\Delta Z}\right)_F + \left(\frac{\Delta P}{\Delta Z}\right)_A \qquad \textbf{2.11}$$

In order to determine the liquid holdup for bubbly flow regime, the bubble drift velocity was determined from the expression proposed by Zuber et al. [1967] , that is

$$v_S = 1.2(v_{SG} + v_{SL}) + 1.41\left[\frac{g\sigma(\rho_L - \rho_G)}{\rho_L^2}\right]^{0.25} \qquad \textbf{2.12}$$

This velocity was then used to determine the liquid holdup from

$$H_L = 1 - \frac{v_{SG}}{v_S} \qquad \textbf{2.13}$$

The Aziz et al. method did not cover the annular mist flow regime.

The methods discussed so far can predict pressure drop only in vertical pipes and as a result, available correlation did not perform as required for design of pipe in hilly terrain or for deviated wells. Beggs [1972] conducted an extensive research program to investigate pressure drops for inclinations spanning 0 to 90 º. Beggs and Brill [1973] reported results of the data analysis. They concluded that pressure drop due to friction was significantly affected by liquid holdup. Also, for their particular data set they found that the liquid holdup can be correlated to the input gas/liquid ratio and the Froude number. Beggs and Brill fitted the data and produced a correlation for liquid holdup and pressure drop for the investigated range of inclinations. They provided separate liquid holdup correlations for segregated (stratified, wavy, and annular), intermittent (slug and plug), and distributed flow (mist and bubbly) regimes. Beggs and Brill were probably the first to quantify the significance of pressure recovery in downhill flow and to emphasize the importance of its inclusion in design considerations.

Mukherjee [1980] performed an extensive experimental investigation of two-phase flow for inclinations spanning 0 to 90 º to provide a flow pattern map, liquid holdup correlation, and two-phase friction factor correlation. A mixture of kerosene and water or light lube oil and water was used to investigate the effect of viscosity on two-phase flow. Analysis of the data and testing of the proposed pressure drop correlations with field data from Prudhoe Bay flow lines and North Sea wells was presented by Mukherjee and Brill [1985]. Liquid holdup was generally correlated to a gas velocity number and to a liquid viscosity number using regression analysis. Three separate holdup correlations were proposed for horizontal and uphill flow, for downhill stratified flow, and for all other downhill flow patterns. Frictional pressure loss was correlated to a Moody [1944] friction factor based on mixture velocity, inlet liquid-fraction averaged viscosity, and density. The expression for the frictional pressure drop was scaled with a liquid holdup factor obtained by averaging using input specific weight fractions.

2.5 Mechanistic Models

Hasan and Kabir [1988] presented a study on the mechanics of multiphase flow phenomena. Their approach was to develop hydrodynamic expressions for pressure drop based on the prevailing mechanism of two-phase configuration at a given well depth. Integral to this study was the definition of a transition criterion between two successive flow patterns.

For transition from bubbly to slug flow they concluded from previous studies ([Radovich and Moissis, 1962],[Griffith and Snyder, 1964], [Hasan et al., 1988]) that a

gas fraction of 0.25 was sufficient for gas bubbles to coalesce and from gas slugs in the liquid phase. They proposed the following superficial gas velocity (gas flow rate divided by entire pipe area) as an appropriate transition criterion. The expression is

$$v_{SG} = 0.49v_{SL} + 0.546\left[\frac{g\sigma(\rho_L - \rho_G)}{\rho_L^2}\right]^{0.25} \qquad \textbf{2.14}$$

They stated that this equation was limited to low to moderate flow rates. At high flow rates turbulence tends to break up the large bubbles allowing the so called dispersed bubbly flow to exist for gas fractions higher than 0.25. Thus, the authors adopted the Taitel et al. [1980] criterion for predicting the mixture velocity above which bubbly flow will exist despite a gas fraction greater that 0.25. This expression is

$$v_M = \left[4.68D_P^{0.48}\left[\frac{g(\rho_L - \rho_G)}{\sigma}\right]^{0.5}\left(\frac{\sigma}{\rho_L}\right)^{0.6}\left(\frac{\rho_M}{\mu_L}\right)^{0.08}\right]^{1/1.12} \qquad \textbf{2.15}$$

At higher gas flow rates, friction between the elongated bubbles and the liquid slugs breaks the gas bubbles resulting in a chaotic flow regime referred to as churn flow. Hasan and Kabir proposed the use of the following boundaries to predict transition to churn flow:

$$\frac{\rho_G v_{SG}^2}{\left(\rho_L v_{SL}^2\right)^{1.7}} \le 0.00673 \quad \text{,if } \rho_L v_{SL}^2 < 50 \qquad \textbf{2.16}$$

$$\frac{\rho_G v_{SG}^2}{17.10\log\left(\rho_L v_{SL}^2\right)-23.2} \le 1.0 \quad \text{, if } 50 < \rho_L v_{SL}^2 < 3{,}300 \qquad \textbf{2.17}$$

if

$$\rho_L v_{SL}^2 > 3{,}300 \qquad \textbf{2.18}$$

then flow is either bubbly or annular depending on the gas fraction. At high gas flow rates, transition from churn flow to annular flow occurs. The authors used the expression proposed by Taitel et al. [1980] to predict transition to annular flow. This transition occurred at a superficial gas velocity given by

$$v_{SG} = 3.1\left[\frac{g\sigma\left(\rho_L-\rho_G\right)}{\rho_L^2}\right]^{0.25} \qquad \textbf{2.19}$$

Hasan and Kabir proposed a correlation for friction factor dependent on the prevailing flow regime. For the annular case, the liquid film friction factor was estimated using

$$f_{LF} = 0.079[1+75H_L]\times\left(\frac{\rho_G v_{SG} D_P}{\mu_G}\right)^{-0.25} \qquad \textbf{2.20}$$

The friction factor for all other flow regimes was estimated from the Moody chart using the mixture Reynolds number

$$N_{\mathrm{Re}M} = \frac{\rho_M v_M D_P}{\mu_M} \qquad \textbf{2.21}$$

Ansari et al. [1994] proposed a mechanistic model for determining pressure drop and liquid holdup based on prevailing flow regime. The Taitel et al. [1980] flow regime transition map was used. The friction force due to slug flow was modeled using the expression

$$F_{wLS} = \frac{f_{LS}\rho_{LS}v_m^2}{2D_P}(1-\beta) \qquad \textbf{2.22}$$

where β was defined as the ratio of the slug unit comprising the liquid slug with entrained gas bubbles and the Taylor bubble. In equation [2.22], *LS* referred to liquid slug. Pressure drop for bubbly flow regime was handled in a similar manner to that used by Hasan and Kabir [1988]. For annular flow, the gas core was expected to have entrained liquid droplets. Therefore the proposed friction force expression for the interaction of the liquid film used in Ansari model was given by

$$F_{wL} = \frac{(1-F_E)^2}{64\delta^3(1-\delta)^3}\frac{f_L\rho_L v_{sL}^2}{2D_P} \qquad \textbf{2.23}$$

The film friction factor was determined from a Moody type correlation using the following Reynolds number

$$N_{\mathrm{Re}L} = \frac{(1-F_E)\rho_L v_{sL} D_P}{\mu_L} \qquad \textbf{2.24}$$

In [2.23] and [2.24], δ was the film thickness, and F_E was the entrained liquid fraction in the gas core. This fraction was given by

$$F_E = 1-\exp\left[-0.125\left(v_{crit}-1.5\right)\right] \qquad \textbf{2.25}$$

The critical velocity was found empirically to be

$$v_{crit} = 10,000 \frac{v_{sg}\mu_g}{\sigma_L}\left(\frac{\rho_g}{\rho_L}\right)^{0.5} \quad \textbf{2.26}$$

The surface tension of the liquid was denoted by σ_L an the interface friction force was given by

$$F_{Lg} = \frac{Z}{(1-2\sigma)^5}\frac{f_{Lg}\rho_C v_{sC}^2}{2D_P} \quad \textbf{2.27}$$

where f_{Lg} is the interface drag friction factor which they correlated to the film thickness using the correlating factor Z given by

$$Z = 1 + 300\sigma \qquad \text{for } F_E < 0.9 \quad \textbf{228}$$

and

$$Z = 1 + 24\left(\frac{\rho_g}{\rho_L}\right)^{\frac{1}{3}}\sigma \qquad \text{for } F_E > 0.9 \quad \textbf{2.29}$$

The core drag friction factor was determined using the following Reynolds number

$$N_{\mathrm{Re}L} = \frac{\rho_C v_{sC} D_P}{\mu_{sC}} \quad \textbf{2.30}$$

and the core density was given by

$$\rho_C = \left(\frac{F_E v_{sL}}{v_{sg} + F_E v_{sL}}\right)\rho_L + \left(1 - \frac{F_E v_{sL}}{v_{sg} + F_E v_{sL}}\right)\rho_g \quad \textbf{2.31}$$

and the core viscosity by

$$\mu_C = \left(\frac{F_E v_{sL}}{v_{sg} + F_E v_{sL}} \right) \mu_L + \left(1 - \frac{F_E v_{sL}}{v_{sg} + F_E v_{sL}} \right) \mu_g \qquad \textbf{2.32}$$

It should be noted that churn flow was not considered.

Ansari et al performed a statistical analysis on the relative performance of their model using a data bank of 1712 cases. They compared the model to Hagedorn and Brown, Aziz et al., Duns and Ros, Hasan and Kabir, Beggs and Brill, Orkiszewski, and Mukherjee and Brill. It was found that overall the Hagedorn and Brown model performed the best. The same model also outperformed for the 1086 vertical well cases. Hasan and Kabir model provided the best predictions for the 29 test cases where bubble flow persisted for over 75% of the time. Hagedorn and Brown performed the best for the 1052 cases where flow regime was 100% slug. It should be noted, however, that Hagedorn and Brown data comprised the majority of test cases. When these data were removed, Ansari's model outperformed all other models indicating that the mechanistic approach may be more appropriate for a wide range of cases, and not only for specific data set as is the case for empirical correlations.

Kaya et al. [2001] reported the results of a project to develop a mechanistic model for deviated wells. They used the flow regime transition criteria of Barnea [1987]. The flow prediction model for bubbly flow was performed using the drift-flux concept. The liquid holdup was determined iteratively from

$$1.53 \left[\frac{g\left(\rho_L - \rho_g\right)\sigma_L}{\rho^2} \right]^{0.25} \sqrt{H_L \sin\theta} = \frac{v_{sg}}{\left(1 - H_L\right)} - 1.2\left[\left(1 - H_L\right) v_{sg} + H_L v_{sL} \right] \qquad \textbf{2.33}$$

After the liquid holdup was computed, the mixture density and viscosity were also computed. The Reynolds number was determined and used to estimate the friction factor from the Moody chart.

The procedure for dispersed bubble flow is similar to the approach used by Hasan and Kabir [1988]. For the slug flow case, the Kaya et al. model was mainly an extension for the Ansari et al. model to account for varying inclination angles.

For the churn flow model, a procedure similar to that for slug model was used with the exception of a new expression for the gas in the liquid slug is used. This expression was given by:

$$H_{GLS} = \frac{v_{SG}}{1.126 v_M + 1.41 \left[\frac{g\left(\rho_L - \rho_g\right)\sigma_L}{\rho_L^2} \right]^{0.25} \sqrt{\sin\theta}} \qquad \textbf{2.34}$$

The annular-mist flow model is identical to that of Ansari [1994]. Kaya et al. claim their model was compared to the Hagedorn and Brown, Aziz et al., Hasan and Kabir, and Ansari models using an extensive data set comprising 2,052 data points and was found to give the best approximation for pressure drop.

2.6 Two-Fluid Model

Bendikson et al. [1991] discussed the development of a commercial code: OLGA. Their approach was to use a two fluid model incorporating three mass balance equations for segregated liquid, dispersed liquid, and gas respectively. The formulation also included combined momentum for the gas and dispersed liquid, a momentum equation

for the segregated liquid and combined energy equations. The effect of transients was taken into account by including accumulation terms in the governing equations. This formulation was apparently influenced by advances in modeling of sudden loss of pressurization of nuclear reactor core chamber (RELAP5/MOD1 Code Manual, [NUREGCR 3567, 1984]).

Thermodynamic and thermo-physical properties needed for model closure were supplied as table data which were interpolation as necessary during runtime. For segregated flow, friction forces were calculated in a manner very similar to that discussed by Hasan and Kabir [1988]. For dispersed flow, empirical correlations were used in the majority of the cases.

Chapter 3

FLOW REGIME TRANSITIONS

3.1 Overview

In the current project, the Taitel, Dukler and Barnea [1980] approach is used to predict the transition boundary from bubbly to slug flow and from bubbly to dispersed bubbly flow if bubbly flow exists. The transition from slug flow to annular mist flow is treated with a combination of the approach suggested by Taitel et al. and that proposed by Barnea [1987].

Even though many flow regime maps exist in the literature e.g. [Duns and Ros, 1963; Aziz et al., 1972; Beggs and Brill, 1973 and Mukherjee and Brill, 1985] the aforementioned approach was selected because it is based on physical understanding of the problem and on generalizing the transitions as not to be limited to one set of flowing fluids and pipe diameters. Also, empirical data is only used when a first principles approach can not tractably be used. It should be noted that the area of flow regime transitions is an active research area [Mukherjee and Brill 1999] and thus the understanding of the physical mechanisms involved is still undergoing. The flow regime transition criteria are discussed in the next sections.

3.2 Existence of Bubbly Flow Regime

When gas is introduced into a flowing stream of liquid in a pipe, gas first appears as small dispersed bubbles. Bubbles introduced at the pipe inlet may travel at a higher velocity than the bubbles already in the pipe and thus trailing bubbles can overtake leading bubbles and coalesce to form Taylor bubbles. Taylor bubbles are large bullet shaped bubble with a diameter slightly smaller than the pipe diameter. The front of the bubble is shaped like an ellipsoid while the trailing edge is relatively flat.

If the gas rise velocity is higher than the average velocity of the gas, then dispersed gas bubbles travel at the trailing end of the Taylor bubble and coalesce with it. Since the rise of the Taylor bubble has been shown by Nicklin et al. [1962] to only be a function of the pipe diameter then there exists a minimum pipe diameter under which bubbly flow can not exist. Taitel et al. [1980] found that this critical diameter is a function of the relative density of the gas and liquid and also of the surface, and gravity forces that exist in the pipe. They proposed the following relation to describe the diameter:

$$D_{P\min} = 19.01\sqrt{\frac{(\rho_L - \rho_G)\sigma}{g\rho_L^2}} \qquad \textbf{3.1}$$

3.3 Transition from Bubbly Flow to Slug Flow

For pipes of a diameter larger than the minimum diameter presented in equation [3.1], it is possible for bubbles to exist and rise relative to the liquid stream. The

likelihood of bubble collisions increases with increased in-situ gas fraction. The critical gas fraction has been found experimentally [Davis and Taylor, 1949] to be about 0.25. To quantify the transition criterion to slug flow the gas slip velocity is expressed as a difference between the actual gas velocity and the actual liquid velocity using

$$v_S = v_G - v_L \qquad \textbf{3.2}$$

The superficial liquid velocity is then expressed explicitly as a function of the slip velocity and the superficial gas velocity. That is:

$$v_{SL} = \left(\frac{H_L}{1 - H_L} \right) v_{SG} - H_L v_S \qquad \textbf{3.3}$$

Harmathy [1960] has shown that for Taylor type bubbles, the slip velocity is a function of the gas and liquid densities and the surface tension of the liquid. He proposed

$$v_S = 1.53 \left[\frac{g\sigma(\rho_L - \rho_G)}{\rho_L^2} \right]^{0.25} \qquad \textbf{3.4}$$

At a gas fraction of 0.25, the transition boundary can thus be expressed as:

$$v_{SL} = 3.0 v_{SL} - 1.15 \left[\frac{g\sigma(\rho_L - \rho_G)}{\rho_L^2} \right]^{0.25} \qquad \textbf{3.5}$$

3.4 Transition to Dispersed Bubbly Flow

Turbulence due to high liquid flow rate can cause breakup of large bubbles and dispersion of colliding bubbles. Turbulent mixing can cause bubbly flow to exist at gas fractions higher than 0.25. The maximum stable diameter for a gas bubble in turbulent conditions has been given by Taitel et al. as:

$$d_{\max} = 1.15\left(\frac{\sigma}{\rho_L}\right)^{3/5}\left[\frac{2f}{D_P}v_M^3\right]^{-2/5} \qquad \textbf{3.6}$$

For highly turbulent flow, it can be assumed that slip between the gas and liquid is negligible. Using this assumption, the mixture velocity can be estimated with

$$v_M = v_{SG} + v_{SL} \qquad \textbf{3.7}$$

where the friction factor in equation [3.6] can be estimated using

$$f = 0.046\left(\frac{v_m D_P}{\mu_L}\right)^{-0.2} \qquad \textbf{3.8}$$

By substituting [3.7] and [3.8] in [3.6] it is found that

$$d_{\max} = 2.99\left(\frac{\sigma}{\rho_L}\right)^{3/5}\left[\frac{1}{\mu_L^{0.2} D_P^{1.2}}\right]^{-0.4}\left(v_{SG} + v_{SL}\right)^{2.4} \qquad \textbf{3.9}$$

Brodkey [1967] reported that if the bubbles in such turbulent flow deform rather than break, slug flow may prevail. He showed that breakup can only occur for bubbles smaller than a critical size determined by the surface tension of the liquid and the density difference between liquid and gas phases. He proposed that the critical size is given by

$$d_{crit} = \sqrt{\frac{0.4\sigma}{g\left(\rho_L - \rho_G\right)}} \qquad \textbf{3.10}$$

The transition boundary can thus be found by equation [3.9] and [3.10]. The transition occurs when:

$$v_{SL} = -v_{SL} + 4\left[\frac{D_P^{0.429}\left(\frac{\sigma}{\rho_L}\right)^{0.089}}{\mu_L^{0.072}}\left[\frac{g\left(\rho_L - \rho_G\right)}{\rho_L}\right]^{0.446}\right] \qquad \textbf{3.11}$$

3.5 Transition from Dispersed Bubbly Flow to Slug Flow

At high gas flow rates, the available volume of bubbles can exceed the physical space available in a given pipe segment which forces the bubbles to coalesce to conserve volume. Scott and Kouba [1990] found that this occurs at a gas fraction of 0.76. Noting that the slip velocity can be assumed negligible at these conditions, it is determined from equation [3.3] that:

$$v_{SL} = 3.17 v_{SG} \qquad \textbf{3.12}$$

3.6 Transition to Annular Mist Flow

Transition to annular flow occurs at high gas flow rates. It is necessary for the gas to flow at a high enough velocity to prevent down-flow of liquid film. Taitel et al. found that for a particular gas and liquid phase, a superficial gas velocity given by:

$$v_{SG} = 3.1\left[\frac{g\sigma\left(\rho_L - \rho_G\right)}{\rho_L^2}\right]^{0.25} \qquad \textbf{3.13}$$

is sufficient to prevent liquid back flow. Barnea [1987] reported that formation of liquid slugs must also be considered. She also reported that the liquid holdup needs to be smaller than that necessary to form the liquid slugs and this minimum holdup is attained at

$$\left(H_{LF} + \lambda_L \frac{A_C}{A_P}\right) > 0.12 \qquad \textbf{314}$$

The term $\lambda_L \frac{A_C}{A_P}$ takes into account the liquid entrained in the gas core. This liquid film holdup H_{LF} is given by:

$$\begin{aligned} H_{LF} &= 4\underline{\delta}\left(1-\underline{\delta}\right) \\ \underline{\delta} &= \frac{\delta}{D_P} \end{aligned} \qquad \textbf{3.15}$$

The dimensionless film thickness was determined by solving the combined dimensionless momentum equation

$$Y_M - \frac{Z}{\left(1-H_{LF}\right)^{2.5} H_{LF}} + \frac{1}{H_{LF}^3} X_M^2 = 0 \qquad \textbf{3.16}$$

where the modified Lockhart and Martinelli [1949] parameters are defined as:

$$\begin{aligned} X_M &= \sqrt{\frac{\left(1-F_E\right)^2 \left(dP/dZ\right)_{SL}}{\left(dP/dZ\right)_{SC}}} \\ Y_M &= \frac{g\left(\rho_L - \rho_G\right)}{\left(dP/dZ\right)_{SC}} \end{aligned} \qquad \textbf{3.17}$$

Wallis [1969] provided an empirical correlation for the liquid entrainment based on experimental data. He reported that

$$F_E = 1 - \exp\left[-0.125\left(v_{crit} - 1.5\right)\right] \qquad \textbf{3.18}$$

The critical velocity is given by:

$$v_{crit} = 10,000 \frac{v_{SG}\mu_G}{\sigma_L}\left(\frac{\rho_G}{\rho_L}\right)^{1/2} \qquad \textbf{3.19}$$

The term Z is a correction factor depending on liquid entrainment. It was reported [Ansari et. al., 1994] that this term is best approximated by

$$\begin{aligned} &Z = 1 + 300\underline{\delta} \quad \text{for } F_E > 0.9 \\ &\text{and} \\ &Z = 1 + 24\left(\frac{\rho_L}{\rho_G}\right)^{1/3} \underline{\delta} \quad \text{for } F_E < 0.9 \end{aligned} \qquad \textbf{3.20}$$

The superficial core pressure drop present in the Lockhart-Martinelli formulation is given by

$$\left(\frac{dP}{dZ}\right)_{SC} = \frac{f_{SC}\rho_C v_{SC}^2}{2D_P} \qquad \textbf{3.21}$$

The superficial friction factor is determined using the Colebrook correlation from the superficial Reynolds number

$$N_{\mathrm{Re}SC} = \frac{v_{SC}\rho_C D_P}{\mu_{SC}} \qquad \textbf{3.22}$$

The core density is given by

$$\rho_C = (1-\lambda_{LC})\rho_G + \lambda_{LC}\rho_L \qquad \textbf{323}$$

and the liquid entrainment coefficient λ_{LC} is evaluated from the drift flux concept using

$$\lambda_{LC} = \frac{F_E v_{SL}}{F_E v_{SL} + v_{SG}} \qquad \textbf{3.24}$$

The superficial pressure drop of the liquid film is given by

$$\left(\frac{dP}{dZ}\right)_{SLF} = \frac{f_{SLF}\rho_L v_{LF}^2}{2D_P} \qquad \textbf{3.25}$$

The superficial friction factor is determined using the Colebrook correlation and the following superficial liquid film Reynolds number

$$N_{\mathrm{Re}SLF} = \frac{v_{LF}\rho_L D_P}{\mu_L} \qquad \textbf{3.26}$$

where the liquid film velocity is given by

$$v_{LF} = \frac{v_{SL}(1-F_E)}{4\underline{\delta}(1-\underline{\delta})} \qquad \textbf{3.27}$$

Having determined that slug flow may not exist from the liquid holdup criterion, Barnea's second criterion must also be met. The second criterion is that the liquid film must be thick enough to withstand shear instabilities (waves). The minimum liquid thickness is obtained by solving the following implicit equation:

$$Y_M - \frac{2-1.5H_{LF}}{H_{LF}^3(1-1.5H_{LF})H_{LF}} X_M^2 = 0 \qquad \textbf{3.28}$$

Annular flow will prevail when the gas velocity is sufficient to prevent liquid backflow, liquid holdup is insufficient to support liquid slugs, and the surface of the liquid annulus is thick enough to withstand wave instabilities.

Chapter 4

HYDRODYNAMIC MODEL

4.1 Model Overview

The hydrodynamic model is composed of four sub-models corresponding to each of the four expected flow regimes. A model has been implemented for slug flow, bubbly flow, dispersed bubbly flow, and annular mist flow. The oil flow rate, gas-oil-ratio, pressure, temperature, gas and oil compositions, as well as flow string length and diameter are provided as the inputs. Each of the four models is discussed in detail in this chapter.

4.2 Slug Flow Model

4.2.1 Formulation

In order to fully capture the physics of gas-liquid slug flow, transient multi-fluid modeling is recommended Error! Not a valid link.. Due to the complexities of the closure relationships required for a fully defined system of equations it is desired to use a simpler approximation. Application of mechanistic models has provided remarkably good agreement with experimental data [Error! Not a valid link.; Hasan and Kabir, 1988; and Ansari et al., 1994]. The mechanistic approach is therefore adopted in the current research.

In the present model, the fully developed slug flow pattern is represented by large gas bubbles of the same average length traveling at the same translational velocity. These bubbles are separated by liquid slugs of equal lengths with small spherical gas bubbles entrained within each liquid slug. The liquid continuity is preserved by a falling film of liquid surrounding the large bullet shaped gas bubbles (Taylor bubbles). The model is shown schematically in Figure 4.1. It was reported that such geometric representation of slug flow agrees satisfactorily with experimental observations [Nicklin et al. 1962, Error! Not a valid link.; Error! Not a valid link.].

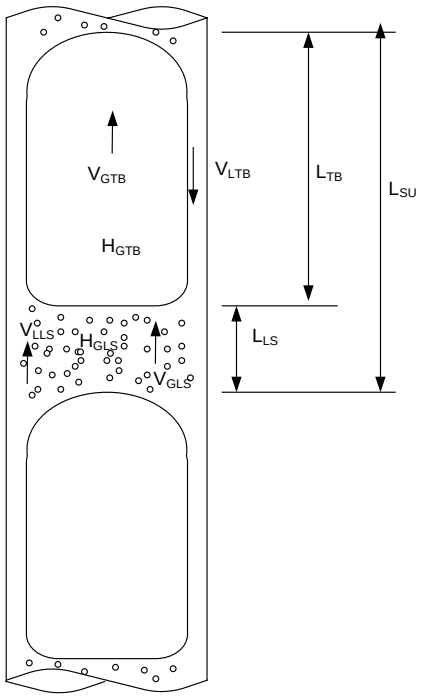

Figure **4-1**: Idealized representation of slug flow

Considering Figure 4.1, we can establish a continuity equation for each of the four phases namely: The gas in the Taylor bubble, the gas entrained as bubbles in liquid slug,

the liquid in the liquid slug and the liquid in the falling film. Since we assume steady state we can write

$$\begin{cases} \alpha_{LTB}\rho_l \dfrac{dv_{LTB}}{dx} + \rho_l v_{LTB} \dfrac{d\alpha_{LTB}}{dx} = 0 \\ \alpha_{GTB} v_{GTB} \left.\dfrac{\partial \rho_g}{\partial P}\right|_T \dfrac{dP}{dx} + \alpha_{GTB}\rho_g \dfrac{dv_{GTB}}{dx} + \rho_g v_{GTB} \dfrac{d\alpha_{GTB}}{dx} = 0 \\ \alpha_{LLS}\rho_l \dfrac{dv_{LLS}}{dx} + \rho_l v_{LLS} \dfrac{d\alpha_{LLS}}{dx} = 0 \\ \alpha_{GLS} v_{GLS} \left.\dfrac{\partial \rho_g}{\partial P}\right|_T \dfrac{dP}{dx} + \alpha_{GLS}\rho_g \dfrac{dv_{GLL}}{dx} + \rho_g v_{GLS} \dfrac{d\alpha_{GLS}}{dx} = 0 \end{cases} \quad \textbf{4.1}$$

These four equations can be combined to give a mixture continuity equation. The liquid was assumed to be incompressible in this case. The continuity equation is given then by

$$\rho_l v_{LTB} \frac{d\alpha_{LTB}}{dZ} + \alpha_{GTB}\rho_g \frac{dv_{GTB}}{dZ} + \alpha_{LTB}\rho_l \frac{dv_{LTB}}{dZ} + \alpha_{GLS}\rho_g \frac{dv_{GLL}}{dZ} = -\left[\alpha_{GTB} v_{GTB} \left.\frac{\partial \rho_g}{\partial P}\right|_T \frac{dP}{dZ} + \alpha_{GLS} v_{GLS} \left.\frac{\partial \rho_g}{\partial P}\right|_T \frac{dP}{dZ} \right] \quad \textbf{4.2}$$

Similarly, the four momentum equations are given as

$$\frac{dP}{dZ} + \left(\alpha_{GTB} v_{GTB}^2 \left.\frac{\partial \rho_g}{\partial P}\right|_T + \alpha_{GLS} v_{GLS}^2 \left.\frac{\partial \rho_g}{\partial P}\right|_T \right) \frac{dP}{dZ} + 2 \left[\begin{array}{l} \alpha_{GTB}\rho_g \dfrac{dv_{GTB}}{dZ} + \alpha_{LTB}\rho_l \dfrac{dv_{LTB}}{dZ} + \\ \alpha_{GLS}\rho_g \dfrac{dv_{GLS}}{dZ} + \alpha_{LLS}\rho_l \dfrac{dv_{LLS}}{dx} \end{array} \right] \quad \textbf{4.3}$$
$$= -F_{fSU} - G_{SU}$$

where:

F_{fSU} is the friction force per unit volume for the entire slug unit.

G_{SU} is the gravity force per unit volume for the entire slug unit.

By substituting for the bracketed term in equation [4.3] using the right hand side of equation [4.2] and rearranging we get

$$\frac{dP}{dZ} = -\frac{F_{fSU} + G_{SU}}{\left(1 + \alpha_{GTB} v_{GTB}^2 \left.\frac{\partial \rho_g}{\partial P}\right|_T + \alpha_{GLS} v_{GLS}^2 \left.\frac{\partial \rho_g}{\partial P}\right|_T\right)} \qquad \textbf{4.4}$$

Equation [4.4] gives the approximate pressure drop per unit length when the right hand side is evaluated. Note that equation [4.4] is only valid for reasonably small pressure drops and therefore the entire well length must be divided into appropriate pressure intervals. Orkiszewski [1967] suggested that these pressure intervals should be about 10% of the reference pressure (usually the wellhead pressure) and not exceed 100 Psi.

The necessary closure relationships for equation [4.4] are the liquid holdup, the gravity force and the friction force. The necessary relations for determining these parameters are discussed in the next section.

4.2.2 Closure to the Slug Flow Model

Let's consider Figure 4.1. In order to provide adequate closure for equation [4.4], it is necessary to determine the exact geometrical configuration of the slug unit. The development here follows a simplified version of that presented by Error! Not a valid link.. The total gas fraction in the slug unit may be written as

$$\alpha_{GSU} = \frac{V_G}{V_{SU}} \qquad \textbf{4.5}$$

Considering Figure 4.1, equation [4.5] can be rewritten as

$$\begin{cases} V_G = L_{SU} A_P = L_{TB} A_{GTB} + L_{LS} A_{GLS} \\ \alpha_{GSU} = \beta \alpha_{GTB} + (1-\beta)\alpha_{GLS} \\ \beta = \dfrac{L_{TB}}{L_{SU}} \end{cases} \quad \textbf{4.6}$$

The average time required for an entire slug unit to pass through any arbitrary plane is given by

$$\Delta t_{TB} = \frac{L_{TB}}{v_{SU}}$$

$$\Delta t_{LS} = \frac{L_{LS}}{v_{SU}} \quad \textbf{4.7}$$

Since we are evaluating steady state flow, it suffices for mass conservation to consider volume conservation of the gas entering the pipe. The volume of the gas phase entering the pipe is given by

$$V_G = v_{SG} A_P \left(\frac{L_{SU}}{v_{SU}} \right) \quad \textbf{4.8}$$

and the volume conservation may be written as

$$\begin{aligned} v_{SG} A_P \left(\Delta t_{TB} + \Delta t_{LS} \right) &= V_{GTB} + V_{GLS} \\ &= \alpha_{GTB} A_P L_{GTB} \frac{v_{GTB}}{v_{TB}} + \alpha_{GLS} A_P L_{LS} \frac{v_{GLS}}{v_{TB}} \end{aligned} \quad \textbf{4.9}$$

By equating [4.8] and [4.9] it is found that

$$v_{SG}A_P\left(\frac{L_{SU}}{v_{TB}}\right)=\alpha_{GTB}A_PL_{GTB}\frac{v_{GTB}}{v_{TB}}+\alpha_{GLS}A_PL_{LS}\frac{v_{GLS}}{v_{TB}} \qquad \textbf{4.10}$$

Equation [4.10] reduces to a relationship between the superficial gas velocity and the velocities of the gas in the liquid slug and the rise velocity of the Taylor bubble. This relationship is given by

$$v_{SG}=\alpha_{GTB}\beta v_{GTB}+\alpha_{GLS}\left(1-\beta\right)v_{GLS} \qquad \textbf{4.11}$$

Considering liquid volume conservation, and using a similar approach, it is found that

$$v_{SL}=\alpha_{LTB}\beta v_{LTB}-\alpha_{LLS}\left(1-\beta\right)v_{LLS} \qquad \textbf{4.12}$$

Finally, to solve equations [4.11] and [4.12] which contain eight unknowns, namely $\alpha_{LTB},\alpha_{LLS},v_{GTB},v_{LTB},v_{GLS},v_{LLS},v_{TB},\beta$, six additional equations are required to obtain a fully define system. These are presented next.

4.2.2.1 Mass Exchange around the Taylor Bubble

The liquid from a leading slug unit is transferred to the flowing film surrounding the rising Taylor bubble to keep the liquid slugs at the same length. Therefore, mass exchange occurs between the falling liquid film and the slug unit traveling at the translational velocity of the leading edge of Taylor bubble. So to conserve the liquid

volume, the liquid lost by the liquid slug has to be balanced by the liquid gained by the film surrounding the Taylor bubble. That is

$$\text{[Volume lost by LS]} + \text{[Volume gained by LTB]} = 0 \qquad \textbf{4.13}$$

Expressing equation [4.13] in terms of unit velocities it is found that

$$-v_{LLS}\alpha_{LLS}A_P = v_{LTB}\alpha_{LTB}A_P \qquad \textbf{4.14}$$

Also the mass transfer of liquid occurring at the pipe entrance is given by

$$\left(v_{TB} - v_{LLS}\right)\alpha_{LLS} = \left(v_{TB} + v_{LTB}\right)\alpha_{LTB} \qquad \textbf{4.15}$$

A similar balance for the gas yields:

$$\left(v_{TB} - v_{GLS}\right)\alpha_{GLS} = \left(v_{TB} + v_{GTB}\right)\alpha_{GTB} \qquad \textbf{4.16}$$

4.2.2.2 Taylor Bubble Rise Velocity

In general, the Taylor bubble rise is due to the combination of the effect of the mixture velocity and the bubble rise relative to the mean velocity of the mixture. This is given by

$$v_{TB} = C_0\left(v_{SG} + v_{SL}\right) + C_1\left[\frac{gD_p\left(\rho_L - \rho_G\right)}{\rho_L}\right]^{1/2} \qquad \textbf{4.17}$$

The second term in equation [4.17] refers to bubble rise in stagnant liquid. Experimental investigation by Fernandes, [1983], showed that $C_0 = 1.29$ and $C_1 = 0.35$. These values are incorporated in the present model to give:

$$v_{TB} = 1.29 v_M + 0.35 \left[\frac{g D_p \left(\rho_L - \rho_G \right)}{\rho_L} \right]^{1/2} \qquad \textbf{4.18}$$

4.2.2.3 Velocity of Gas in Liquid Slug

Error! Not a valid link. modified Harmathy [1960], expression for single bubble rise in liquid to account for turbulence effects on bubble flow. They proposed that the average bubble velocity in the liquid slug is given by

$$v_{GLS} = 1.29 v_M + 1.53 \left[\frac{g \sigma \left(\rho_L - \rho_G \right)}{\rho_L^2} \right]^{1/4} \qquad \textbf{4.19}$$

4.2.2.4 Velocity of Falling Liquid Film Surrounding Taylor Bubble

Error! Not a valid link. proposed a relationship for flowing film thickness surrounding the Taylor bubble. This relationship was adapted by Sylvester [1987] using geometric considerations in terms of the liquid fraction in the Taylor bubble wherein he proposed:

$$v_{LTB} = 9.916 \left[g D_p \left(1 - \sqrt{\alpha_{LTB}} \right) \right]^{1/2} \qquad \textbf{4.20}$$

4.2.2.5 Gas Fraction in Liquid Slug

Sylvester [1987] used experimental data from the literature [Error! Not a valid link.; Fernandes 1983] to correlate this fraction to the mixture velocity and gas superficial velocity. He proposed:

$$\alpha_{GLS} = \frac{v_{SG}}{0.425 + 2.65 v_M} \qquad \textbf{4.21}$$

Vo and Shoham [1989] combined equations [4.11, 4.12, 4.15, and 4.16] and [4.18-21] to obtain an implicit expression for the liquid fraction in the Taylor bubble segment. They found that:

$$\left(9.916\sqrt{gD_p}\right)\left(1-\sqrt{1-\alpha_{LTB}}\right)^{1/2}\alpha_{LTB} - v_{TB}\left(1-\alpha_{LTB}\right) + \overline{A} = 0 \qquad \textbf{4.22}$$

where

$$\overline{A} = \alpha_{GLS}\left(v_{TB} - v_{GLS}\right) + v_M \qquad \textbf{4.23}$$

In the present work, equation [4.22] is solved using a fail-safe combination of Newton-Raphson and Bisection methods. The Newton-Raphson expression is given by:

$$\alpha_{LTB}^{n+1} = \alpha_{LTB}^{n} - \frac{F\left(\alpha_{LTB}\right)}{F'\left(\alpha_{LTB}\right)} \qquad \textbf{4.24}$$

The objective function F is given by:

$$F(\alpha_{LTB}) = 9.916\left[gD_P\left(1-\sqrt{1-\alpha_{LTB}}\right)\right]^{1/2}\alpha_{LTB} - v_{TB}(1-\alpha_{LTB}) + \overline{A} \qquad \textbf{4.25}$$

And its derivative F' is given by:

$$F'(\alpha_{LTB}) = v_{LTB} + 9.916\left[gD_P\left(1-\sqrt{1-\alpha_{LTB}}\right)\right]^{1/2} + \frac{\alpha_{LTB}}{4\sqrt{1-\alpha_{LTB}\left(1-\sqrt{1-\alpha_{LTB}}\right)}} \qquad \textbf{4.26}$$

4.2.2.6 Gravity Force

Having determined the geometric configuration of the slug unit and noting that the downward traveling film does not contribute to the hydrostatic pressure loss, the gravity force can be expressed as:

$$G_{SU} = \left[(1-\beta)\rho_{LS} + \beta\rho_G\right] \qquad \textbf{4.24}$$

where

$$\rho_{LS} = \alpha_{LLS}\rho_L + (1-\alpha_{LLS})\rho_G \qquad \textbf{4.25}$$

4.2.2.7 Friction Force

The friction force due to the Taylor bubble segment is considered negligible compared to the liquid slug segment. Thus the friction force is given by:

$$F_{SU} = \frac{f_{LS}\rho_{LS}v_M^2}{2D_p}(1-\beta) \qquad \textbf{4.26}$$

where the slug friction factor is determined from the Colebrook [1939] equation using

$$N_{\mathrm{Re}LS} = \frac{\rho_{LS}v_M D_P}{\mu_{LS}} \qquad \textbf{4.27}$$

The viscosity of the liquid slug mixture is given as

$$\mu_{LS} = \alpha_{LLS}\mu_L + (1-\alpha_{LLS})\mu_G \qquad \textbf{4.28}$$

and the Colebrook implicit expression for friction factor is given by

$$\frac{1}{\sqrt{f}} = \left[1.74 - 2\log\left(\frac{2\varepsilon}{D_P} + \frac{18.7}{N_{\mathrm{Re}}\sqrt{f}}\right)\right] \qquad \textbf{4.29}$$

4.2.3 Slug Flow Model Testing

The slug model was tested using 19 data point from experiments conducted by Error! Not a valid link. using a 30.5ft long test section of 1-1/2 inches steel tubing. This data set was selected because flow regime observations were made during the experimental runs. Consequently, the performance of the flow regime transition model developed in

chapter 3 was also evaluated. The pipe was assumed to have an absolute roughness of 0.00005 ft. The testing results are summarized in Table 4.1 and shown graphically in Figure 4.2.

Table **4-1**: Pressure drop and flow regime predictions for an air and kerosene mixture. Slug Flow regime was observed in the lab. (APE = Absolute Percent Error, MDL = Model, SL = Slug, DB = Dispersed Bubbly, BB = Bubbly, AAPE = Average APE)

Test No.	Dp [pred.]	DP	Regime [Pred.]	Regime [Obs.]	APE [MDL]
8786	3.20	4.86	SL	SL	34.20
8784	2.99	3.82	SL	SL	21.86
9249	1.29	0.68	SL	SL	89.41
8787	3.59	4.99	SL	SL	27.98
8773	10.21	9.71	SL	SL	5.15
8804	1.66	2.56	SL	SL	35.35
8783	2.95	3.62	SL	SL	18.48
9253	1.70	1.92	SL	SL	11.72
9256	1.54	1.69	SL	SL	9.11
9254	1.66	1.86	SL	SL	10.54
9255	1.59	1.74	SL	SL	8.39
8803	1.45	1.92	SL	SL	24.53
8806	2.01	2.73	SL	SL	26.41
8782	3.29	3.71	SL	SL	11.24
8772	3.29	12.00	DB	SL	72.56
8778	3.86	4.41	SL	SL	12.45
8777	3.86	5.21	DB	SL	25.89
8816	8.26	7.59	SL	SL	8.76
9257	8.26	8.32	BB	SL	0.78
				AAPE	**23.94**
				AAPE (SL)	**22.23**

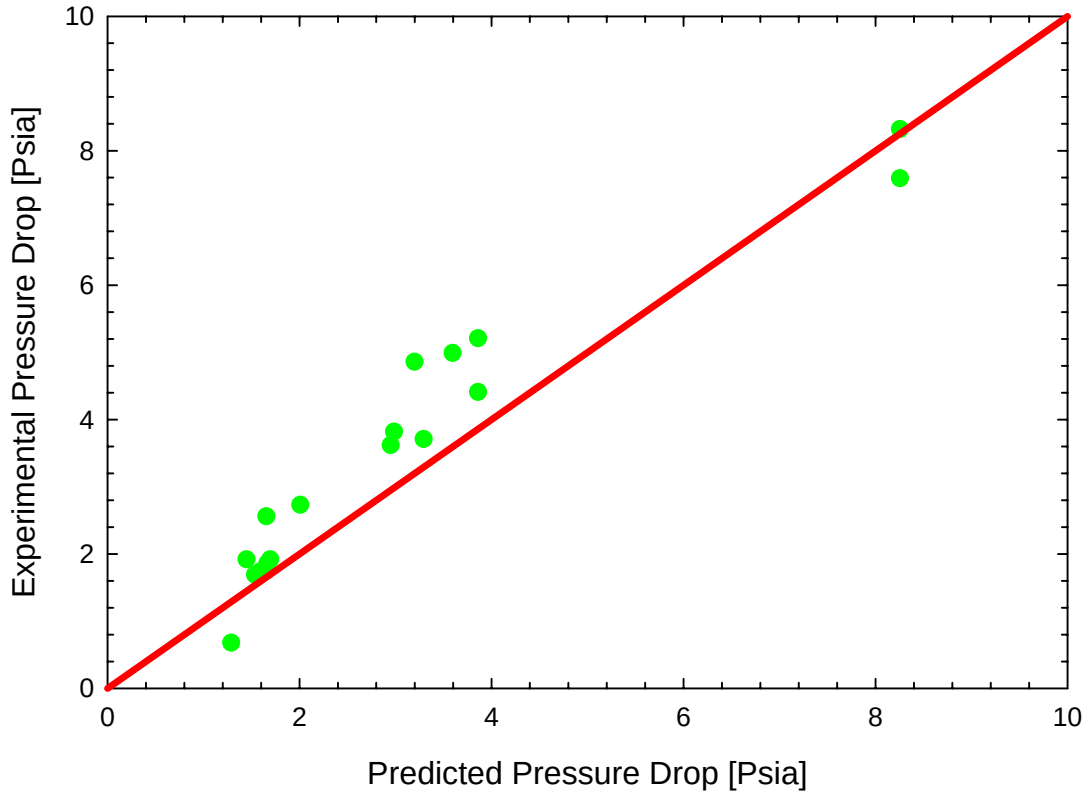

Figure **4-2**: Comparison of model performance for slug flow with experimental data of Mukherjee [1980]

4.3 Bubbly/Dispersed Bubbly Flow Model

4.3.1 Formulation

For the bubbly and dispersed bubbly flow, the gas phase exists as dispersed bubbles in a continuous liquid phase. These two flow regimes are depicted schematically in Figure 4.3.

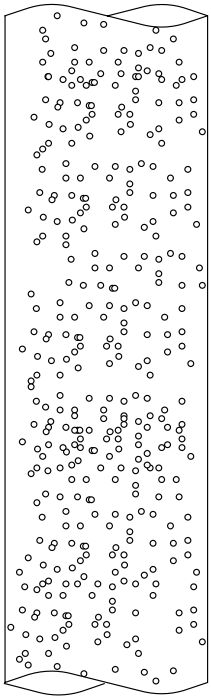

Figure **4-3**: Schematic representation of bubbly flow in a vertical wellbore

The bubbly flow model is based on mass and momentum balance equations for the liquid and the dispersed gas phase. The mass balance equations are given by

$$\begin{cases} (1-H_L)v_G \left.\dfrac{\partial \rho_G}{\partial P}\right|_T \dfrac{dP}{dZ} + (1-H_L)\rho_G \dfrac{dv_G}{dZ} - \rho_G v_G \dfrac{dH_L}{dZ} = 0 \\ H_L \rho_L \dfrac{dv_L}{dZ} + \rho_L v_L \dfrac{dH_L}{dZ} = 0 \end{cases} \quad \textbf{4.30}$$

These equations can be rearranged as follows

$$\begin{cases} (1-H_L)\rho_G \dfrac{dv_G}{dZ} = -\left[(1-H_L)v_G \left.\dfrac{\partial \rho_G}{\partial P}\right|_T \dfrac{dP}{dZ} + \rho_G v_G \dfrac{dH_L}{dZ} \right] \\ H_L \rho_L \dfrac{dv_L}{dZ} = -\rho_L v_L \dfrac{dH_L}{dZ} \end{cases} \quad \textbf{4.31}$$

The momentum balance equations, meanwhile are given by

$$\begin{cases} \left(\left[1-H_L\right] v_G^2 \left.\dfrac{\partial \rho_G}{\partial P}\right|_T \right) \dfrac{dP}{dZ} + \left[1-H_L\right] \dfrac{dP}{dZ} + 2\left[1-H_L\right] \rho_G v_G \dfrac{dv_G}{dZ} \\ -\rho_G v_G^2 \dfrac{dH_L}{dZ} = -F_{GG} - F_{DG} - F_{FG} \\ H_L \dfrac{dP}{dZ} + 2H_L \rho_L v_L \dfrac{dv_L}{dZ} + \rho_L v_L^2 \dfrac{dH_L}{dZ} = -F_{GL} + F_{DG} - F_{FL} \end{cases} \quad \textbf{4.32}$$

Equation [4.34] and [4.35] are combined to obtain

$$\left[1 + \left(\left[1-H_L\right] v_G^2 \left.\dfrac{\partial \rho_G}{\partial P}\right|_T \right) \right] \dfrac{dP}{dZ} + \left(\rho_G v_G^2 \dfrac{dH_L}{dZ} - \rho_L v_L^2 \dfrac{dH_L}{dZ} \right) = -F_G - F_F \quad \textbf{4.33}$$

Equation [4.36] is given in terms of liquid holdup by

$$\left[1+\left(\frac{v_{SG}^2}{(1-H_L)}\frac{\partial\rho_G}{\partial P}\bigg|_T\right)\right]\frac{dP}{dZ}+\left[\rho_G\left(\frac{v_{SG}}{(1-H_L)}\right)^2-\rho_L\left(\frac{v_{SL}}{H_L}\right)^2\right]\frac{dH_L}{dZ}$$
$$+\rho_{TP}g+\frac{f_{TP}\rho_{TP}v_{TP}^2}{2D_p}=0 \qquad \textbf{4.34}$$

where

$$\rho_{TP}=(1-H_L)\rho_G+H_L\rho_L$$
$$v_{TP}=v_{SG}+v_{SL} \qquad \textbf{4.35}$$

The two-phase friction factor is determined from the Colebrook correlation using the following two-phase Reynolds number:

$$N_{\mathrm{Re}TP}=\frac{\rho_{TP}v_{TP}D_P}{\mu_{TP}} \qquad \textbf{4.36}$$

The mixture viscosity is determined by using liquid holdup as the weighing parameter. That is

$$\mu_{TP}=(1-H_L)\mu_G+H_L\mu_L \qquad \textbf{4.37}$$

For small pressure intervals, it can be assumed that the in-situ liquid holdup remains relatively constant. With this assumption, equation [4.37] can be written as

$$\frac{dP}{dZ}=-\frac{\rho_{TP}g+\frac{f_{TP}\rho_{TP}v_{TP}^2}{2D_p}}{1+\left(\frac{v_{SG}^2}{(1-H_L)}\frac{\partial\rho_G}{\partial P}\bigg|_T\right)} \qquad \textbf{4.38}$$

For the case of bubbly flow it is necessary to determine the liquid holdup in order to evaluate equation [4.41]. Liquid holdup is obtained by expressing the drift velocity of the gas relative to the mixture. The drift velocity is given by Zuber and Hench [1962] as

$$v_s = 1.53\left[\frac{g\sigma_L(\rho_L-\rho_G)}{\rho_L^2}\right]H_L^n \qquad \textbf{4.39}$$

Ansari et. al. [1994] found that the liquid holdup exponent *n* in equation [4.42] is best approximated by 0.5. Error! Not a valid link. proposed that the gas velocity can be expressed as

$$v_G = 1.2v_{TP} + 1.53\left[\frac{g\sigma_L(\rho_L-\rho_G)}{\rho_L^2}\right]H_L^n \qquad \textbf{4.40}$$

That is

$$1.2(v_{SG}+v_{SL}) + 1.53\left[\frac{g\sigma_L(\rho_L-\rho_G)}{\rho_L^2}\right]H_L^{1/2} - \frac{v_{SG}}{1-H_L} = 0 \qquad \textbf{4.41}$$

Equation [4.44] is solved in this model using a fail-safe Newton-Raphson, bisection method combination. The objective function is given by:

$$F(H_L) = 1.2(v_{SG}+v_{SL}) + 1.53\left[\frac{g\sigma_L(\rho_L-\rho_G)}{\rho_L^2}\right]H_L^{1/2} - \frac{v_{SG}}{1-H_L} \qquad \textbf{4.42}$$

and the derivative is given by

$$F'(H_L) = 0.765\left[\frac{g\sigma_L(\rho_L - \rho_G)}{\rho_L^2}\right]H_L^{-1/2} + \frac{v_{SG}}{(1-H_L)^2} \qquad \textbf{4.43}$$

When dispersed bubbly flow exists it is assumed that the slip velocity is negligible. Therefore the liquid fraction predicted from the phase behavior package is used to determine the mixture density, and viscosity. The bubbly flow pressure drop model was tested using Mukherjee [1980] data. The results are presented in Table

4.3.2 Bubbly Flow Model Testing

Table **4-2**: Pressure drop and flow regime prediction for bubbly flow regime

Test No.	Dp [pred.]	DP	Regime [Pred.]	Regime [Obs.]	APE [MDL]
8785	7.61	7.94	SL	BB	4.14
8812	9.56	11.16	BB	BB	14.36
8813	8.78	9.77	BB	BB	10.12
8817	9.39	10.59	BB	BB	11.34
8818	9.14	9.18	BB	BB	0.48
8819	8.34	9.00	SL	BB	7.38
8820	8.79	9.26	BB	BB	5.10
8821	9.23	10.32	BB	BB	10.55
8822	8.91	9.26	BB	BB	3.79
8824	8.90	10.06	BB	BB	11.49
8825	9.15	10.24	BB	BB	10.65
				AAPE	**8.13**
				AAPE (BB)	**8.65**

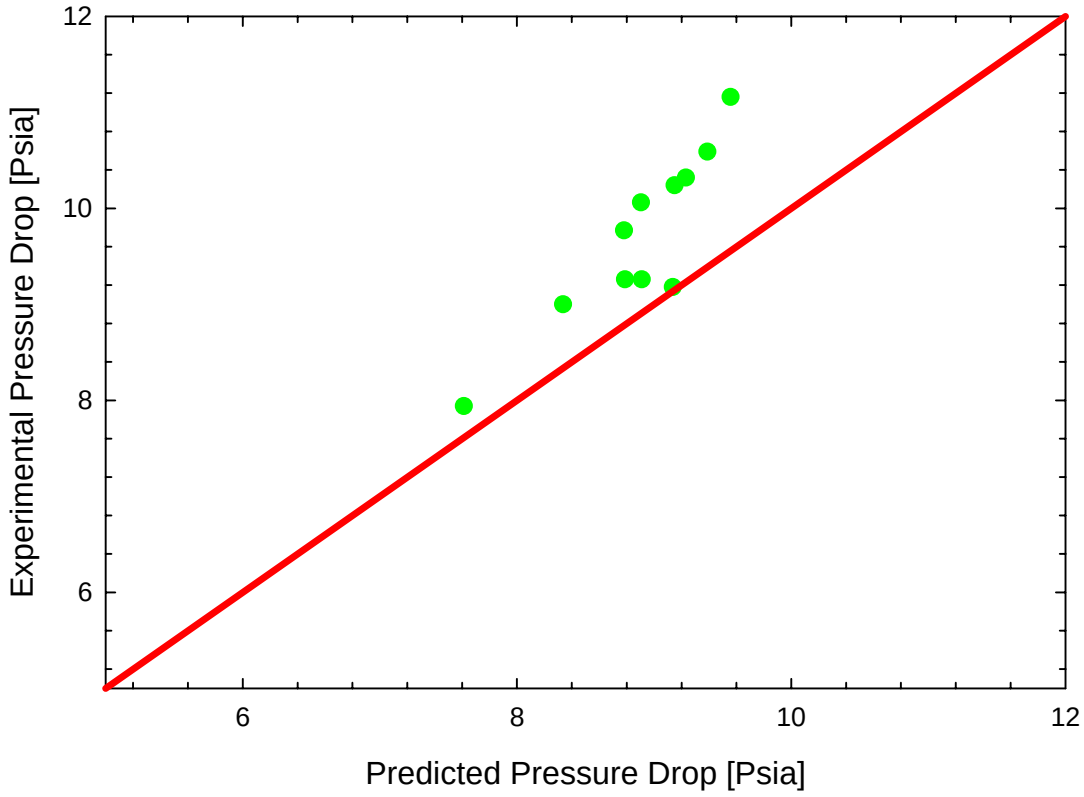

Figure **4-4**: Comparison of experimental pressure drop [Mukherjee, 1980] and model predictions for bubbly flow regime

It is expected that the errors found in pressure drop prediction when slug flow prevails may be due to entrance effects.

4.4 Annular Mist Flow Model

4.4.1 Formulation

The annular mist flow regime takes place at high gas flow rates. Under such conditions, the liquid forms an annulus and the gas slips as a core with entrained liquid. This model can be formulated using a momentum equation for the core and a momentum equation for the liquid film surrounding it. The system is considered as two phases, a homogeneous core and a liquid annulus as shown in Figure 4.5.

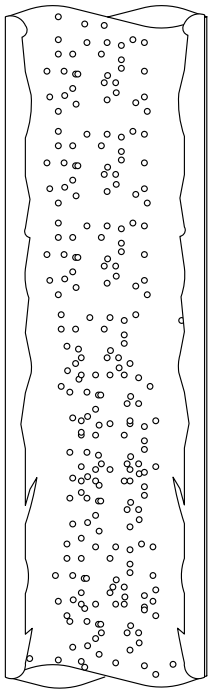

Figure **4-5**: Schematic representation of annular mist flow in a vertical wellbore

The core and liquid film pressure drops are given respectively by

$$\begin{cases} \left(\frac{dP}{dZ}\right)_C = \frac{-F_{GC} - F_i}{\left(1 + v_C^2 \left.\frac{\partial \rho_C}{\partial P}\right|_T\right)} \\ \left(\frac{dP}{dZ}\right)_{LF} = -F_{GL} + F_i - F_{FL} \end{cases} \quad \textbf{4.44}$$

The core mixture density is obtained by weighting the liquid and gas velocity using the parameter λ_{LC}

$$\rho_C = \left(1 - \lambda_{LC}\right)\rho_G + \lambda_{LC}\rho_L \quad \textbf{4.45}$$

$$\lambda_{LC} = \frac{F_E v_{SL}}{F_E v_{SL} + v_{SG}} \quad \textbf{4.46}$$

Wallis [1969] provided an empirical correlation for the liquid entrainment based on experimental data. He reported

$$F_E = 1 - \exp\left[-0.125\left(v_{crit} - 1.5\right)\right] \quad \textbf{4.47}$$

The critical gas velocity sufficient for entraining liquid is related to the gas velocity, density, and surface tension, as well as the liquid density and surface tension. The relationship is given by

$$v_{crit} = 10,000 \frac{v_{SG}\mu_G}{\sigma_L}\left(\frac{\rho_G}{\rho_L}\right)^{1/2} \quad \textbf{4.48}$$

The core velocity is given from geometric considerations by

$$v_C = \frac{v_{SC}}{\left(1-2\underline{\delta}\right)^2} \qquad \textbf{4.49}$$

and the dimensionless film thickness is given by

$$\underline{\delta} = \frac{\delta}{D_P} \qquad \textbf{4.50}$$

Closure relationships for the momentum equations are discussed next.

4.4.2 Closure relationships for the momentum equations

The drag force can be expressed using the development proposed by Wallis [1969] as follows

$$F_i = \tau_i \frac{S_i}{A_C} \qquad \textbf{4.51}$$

where the interfacial surface stress is given by

$$\tau_i = \frac{f_i \rho_C v_C^2}{8} \qquad \textbf{4.52}$$

The interface friction factor is given by Wallis such that

$$f_i = f_{SC} Z \qquad \textbf{4.53}$$

where the parameter Z is a correction factor dependent on liquid entrainment. It was reported [Ansari et. al., 1994] that this parameter is better correlated by considering the high entrainment case and low and moderate entrainment cases separately. They proposed

$$\begin{aligned} &Z = 1 + 300\underline{\delta} \quad \text{for } F_E > 0.9 \\ &\text{and} \\ &Z = 1 + 24\left(\frac{\rho_L}{\rho_G}\right)^{1/3} \underline{\delta} \quad \text{for } F_E < 0.9 \end{aligned} \qquad \textbf{4.54}$$

Combining equations [4.56] and [4.61] we obtain

$$\tau_i = \frac{D_P}{4} \frac{Z}{\left(1 - 2\underline{\delta}\right)^4} \left(\frac{dP}{dZ}\right)_{SC} \qquad \textbf{4.55}$$

The perimeter of the core is given by

$$S_i = \pi D_P \left(1 - 2\underline{\delta}\right) \qquad \textbf{4.56}$$

and the cross sectional area of the core is given by

$$A_C = \frac{\pi}{4} D_P^2 \left(1 - 2\underline{\delta}\right)^2 \qquad \textbf{4.57}$$

Thus

$$\frac{S_i}{A_C} = \frac{4}{D_P\left(1-2\underline{\delta}\right)} \qquad \textbf{4.58}$$

Substituting [4.58] and [4.61] into [4.54] we obtain

$$F_i = \frac{Z}{\left(1-2\underline{\delta}\right)^5}\left(\frac{dP}{dZ}\right)_{SC} \qquad \textbf{4.59}$$

where the superficial pressure drop of the core is given by

$$\left(\frac{dP}{dZ}\right)_{SC} = \frac{f_{SC}\rho_C v_{SC}^2}{2D_P} \qquad \textbf{4.60}$$

The superficial friction factor is determined using Colebrook correlation and the superficial core Reynolds number

$$N_{\mathrm{Re}SC} = \frac{v_{SC}\rho_C D_P}{\mu_{SC}} \qquad \textbf{4.61}$$

The pressure drop associated with the core can be written as

$$\left(\frac{dP}{dZ}\right)_C = \frac{-\left[g\rho_C + \frac{Z}{\left(1-2\underline{\delta}\right)^5}\left(\frac{dP}{dZ}\right)_{SC}\right]}{\left(1+v_C^2\left.\frac{\partial\rho_C}{\partial P}\right|_T\right)} \qquad \textbf{4.62}$$

Next the liquid film pressure drop is evaluated. First we evaluate the wall friction force. This force is given by:

$$F_{LF} = \tau_{LF} \frac{S_{LF}}{A_{LF}} \quad \textbf{4.63}$$

where

$$\tau_{LF} = \frac{f_{LF} \rho_L v_{LF}^2}{8} \quad \textbf{4.64}$$

$$N_{\mathrm{Re}\,LF} = \frac{v_{LF} \rho_L D_{HL}}{\mu_L} \quad \textbf{4.65}$$

The hydraulic diameter of the liquid film is given by:

$$D_{HL} = 4\underline{\delta}\left(1-\underline{\delta}\right) D_P \quad \textbf{4.66}$$

and the liquid velocity is given by

$$v_{LF} = \frac{v_{SL}\left(1-F_E\right)}{4\underline{\delta}\left(1-\underline{\delta}\right)} \quad \textbf{4.67}$$

Combining equations [4.67] and [4.70] we obtain

$$\tau_{LF} = \frac{f_{LF}}{8}\left(1-F_E\right)^2 \rho_L \left[\frac{v_{SL}}{4\underline{\delta}\left(1-\underline{\delta}\right)}\right]^2 \quad \textbf{4.68}$$

The perimeter of the liquid film is given by

$$S_{LF} = \pi D_P \quad \textbf{4.69}$$

and the cross sectional area of the liquid film is given by

$$A_{LF} = \pi D_P^2 \underline{\delta}\left(1-\underline{\delta}\right) \qquad \textbf{4.70}$$

Thus

$$\frac{S_{LF}}{A_{LF}} = \frac{1}{D_P \underline{\delta}\left(1-\underline{\delta}\right)} \qquad \textbf{4.71}$$

Substituting [4.71] and [4.74] into [4.66] we obtain

$$F_{LF} = \frac{\left(1-F_E\right)^2}{64\underline{\delta}^3\left(1-\underline{\delta}\right)^3}\frac{f_{LF}}{f_{SL}}\left(f_{SL}\frac{\rho_L v_{SL}^2}{2D_P}\right) \qquad \textbf{4.72}$$

This can be written as

$$F_{LF} = \frac{\left(1-F_E\right)^2}{64\underline{\delta}^3\left(1-\underline{\delta}\right)^3}\frac{f_{LF}}{f_{SLF}}\left(\frac{dP}{dZ}\right)_{SLF} \qquad \textbf{4.73}$$

where the superficial pressure drop of the liquid film is given by

$$\left(\frac{dP}{dZ}\right)_{SLF} = \frac{f_{SLF}\rho_L v_{LF}^2}{2D_P} \qquad \textbf{4.74}$$

The superficial friction factor is determined using the Colebrook correlation and the superficial core Reynolds number

$$N_{\mathrm{Re}SLF} = \frac{v_{LF}\rho_L D_P}{\mu_L} \qquad \textbf{4.75}$$

The pressure drop of the liquid film can therefore be given by:

$$\left(\frac{dP}{dZ}\right)_{LF} = -\left[\begin{array}{l} \dfrac{\left(1-F_E\right)^2}{64\underline{\delta}^3\left(1-\underline{\delta}\right)^3}\dfrac{f_{LF}}{f_{SLF}}\left(\dfrac{dP}{dZ}\right)_{SLF} \\ +g\rho_L + \dfrac{Z}{2\underline{\delta}\left(1-\underline{\delta}\right)\left(1-2\underline{\delta}\right)^3}\left(\dfrac{dP}{dZ}\right)_{SC} \end{array}\right] \qquad \textbf{4.76}$$

By equating the pressure drop experienced by the liquid fluid to the pressure drop expressed by the gas core, it is found that

$$\left[\frac{\left(1-F_E\right)^2}{64\underline{\delta}^3\left(1-\underline{\delta}\right)^3}\frac{f_{LF}}{f_{SLF}}\left(\frac{dP}{dZ}\right)_{SLF} + g\rho_L + \frac{Z}{2\underline{\delta}\left(1-\underline{\delta}\right)\left(1-2\underline{\delta}\right)^3}\left(\frac{dP}{dZ}\right)_{SC}\right]$$

$$= \frac{\left[g\rho_C + \dfrac{Z}{\left(1-2\underline{\delta}\right)^5}\left(\dfrac{dP}{dZ}\right)_{SC}\right]}{\left(1+v_C^2\left.\dfrac{\partial\rho_C}{\partial P}\right|_T\right)} \qquad \textbf{4.77}$$

Equation [4.80] is an implicit equation with film thickness being the unknown. This equation was solved using a fail-safe Newton-Raphson / Bisection method combination. Results of testing the annular mist flow predictive model are presented in Table 4.3 and shown in Figure 4.6

4.4.3 Annular mist flow model testing

Table **4-3**: Pressure drop and flow regime prediction for annular mist flow of air and kerosene

Test No.	Dp [pred.]	DP [Obs.]	Regime [Pred.]	Regime [Obs.]	APE [MDL]
8792	2.05	1.80	ANM	ANM	14.11
9235	1.31	1.44	ANM	ANM	9.31
9236	1.65	1.74	ANM	ANM	5.34
9704	1.27	1.13	SL	ANM	12.57
9705	1.25	1.04	SL	ANM	20.00
				AAPE	**12.27**
				AAPE (BB)	**9.59**

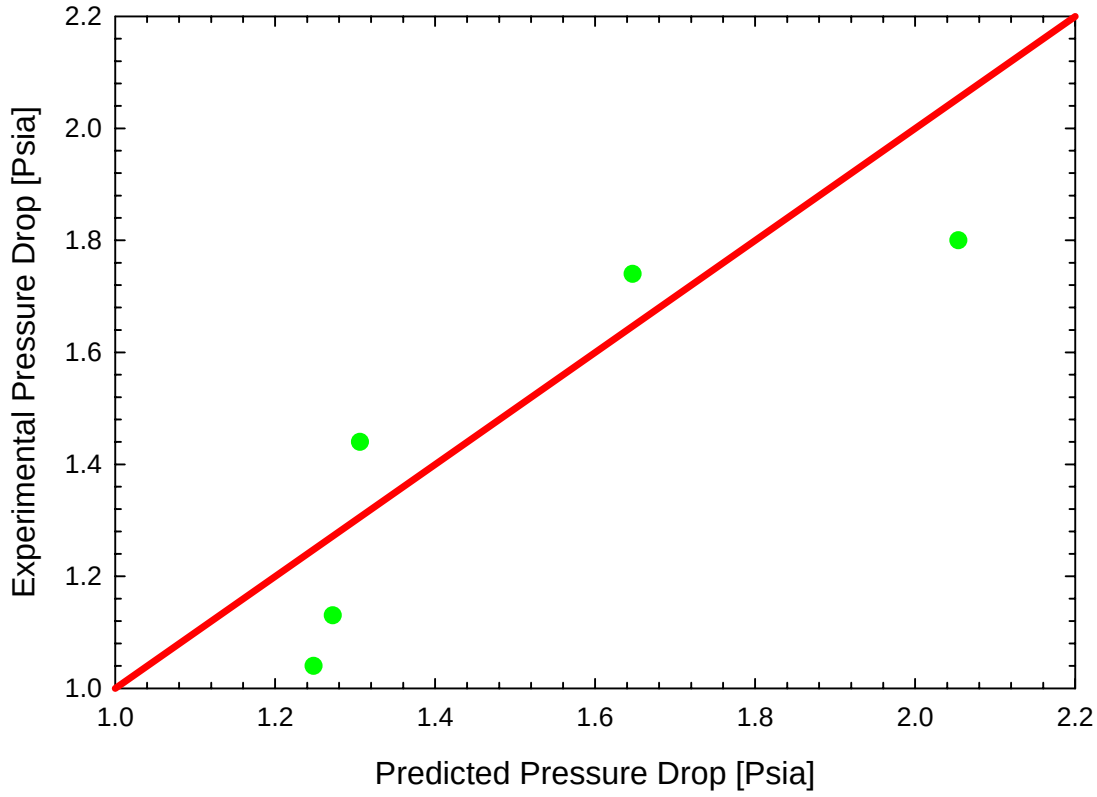

Figure **4-6**: Comparison of experimental pressure drop reported by Mukherjee [1980] with model predictions for annular mist flow

4.5 Extension to Deviated Wells

In this section, a brief discussion is provided on how to extend the model presented in this dissertation to predicting flow behavior of deviated wells. It should be noted that the intention here is to provide a starting point for more comprehensive future work.

Based on our investigation we recommend using the flow transition methodology presented by Kaya et al [2001]. The flow regime transitions are similar to those discussed in Chapter 3 with the difference of taking the inclination effect into account. Table 4-4 presents the equations necessary to construct a flow transition map. The pressure drops equations proposed by Kaya et al [2001] are modified to account for gas expansion due to pressure, temperature, and composition changes. These expressions are presented in Table 4-5. It should be noted that Kaya et al model was not verified in this study and therefore it is recommended that independent investigation of performance and limitations of this model be conducted.

Table **4-4**: Flow transitions in inclined upward two phase flow.

Transition	**Limiting Boundary**
Bubbly flow to Slug flow	$v_{SG} = 0.333 v_{SL} + 0.3825 \left[\frac{g\sigma(\rho_L - \rho_G)}{\rho_L^2} \right]^{1/4} \sin^{1/2}(\theta)$
Transition to Dispersed Bubbly flow	$d_{CB} = \frac{3}{8} \frac{\rho_L}{\rho_L - \rho_G} \frac{f_M v_M^2}{g \cos\theta}, \quad \lambda = \frac{v_{SL}}{v_{SG} + v_{SL}} \le 0.48$ $v_{SG} = 1.083 v_{SL}, \quad \lambda > 0.48$
Slug to Churn	$v_{SG} = 12.19(1.2 v_{SL} + v_0)$ $v_0 = (0.35 \sin\theta + 0.54 \cos\theta) \left[\frac{g(\rho_L - \rho_G) D}{\rho_L} \right]^{1/2}$
Annular to Slug or Churn	$\left(H_{LF} + \frac{\lambda_{LC} A_C}{A} \right) > 0.12,$ *and* $Y_M \ge \frac{2 - 1.5 H_{LF}}{H_{LF}^3 (1 - 1.5 H_{LF})}$

Table **4-5**: Pressure drop expressions for inclined upward two phase flow

Flow Regime	Pressure Drop
Bubbly flow	$1.53\left[\frac{g\sigma(\rho_L-\rho_G)}{\rho_L^2}\right]^{1/4}\sqrt{H_L\sin\theta}=\frac{v_{SG}}{1-H_L}-1.2(v_{SG}+v_{SL})$ $\frac{dP}{dZ}=-\frac{\frac{f_M\rho_M v_M^2}{2D_P}}{1+\left(\frac{v_{SG}^2}{1-H_L}\frac{\partial\rho_G}{\partial P}\right)}-\rho_M g\sin\theta$ $\rho_M=H_L\rho_L+(1-H_L)\rho_G$ $\mu_M=H_L\mu_L+(1-H_L)\mu_G$
Dispersed Bubbly flow	$H_L=\frac{v_{SL}}{v_{SL}+v_{SG}}$ $\frac{dP}{dZ}=-\frac{\frac{f_M\rho_M v_M^2}{2D_P}}{1+\left(\frac{v_{SG}^2}{1-H_L}\frac{\partial\rho_G}{\partial P}\right)}-\rho_M g\sin\theta$
Slug flow	$H_{GLS}=\frac{v_{SG}}{1.208v_M+1.41\left[\frac{g\sigma(\rho_L-\rho_G)}{\rho_L^2}\right]^{1/4}\sqrt{\sin\theta}}$ $\frac{dP}{dZ}=-\frac{\beta\frac{f_M\rho_{LS}v_M^2}{2D_P}}{1+\left(\frac{v_{SG}^2}{1-H_L}\frac{\partial\rho_G}{\partial P}\right)}-\beta\rho_{LS}g\sin\theta$ $\rho_{LS}=\rho_L(1-H_{GLS})+H_{GLS}\rho_G$
Churn flow	$H_{GLS}=\frac{v_{SG}}{1.126v_M+1.41\left[\frac{g\sigma(\rho_L-\rho_G)}{\rho_L^2}\right]^{1/4}\sqrt{\sin\theta}}$ $\frac{dP}{dZ}=-\frac{\beta\frac{f_M\rho_{LS}v_M^2}{2D_P}}{1+\left(\frac{v_{SG}^2}{1-H_L}\frac{\partial\rho_G}{\partial P}\right)}-\beta\rho_{LS}g\sin\theta$ $\rho_{LS}=\rho_L(1-H_{GLS})+H_{GLS}\rho_G$
Annular Mist	Same as model presented in section 4.4 except for the gravity term being multiplied by $\sin\theta$

Chapter 5

PHASE BEHAVIOR MODEL

5.1 Model Overview

The phase behavior calculations necessary for the wellbore model are divided into two parts. Flash calculations are requisite to determine the fraction of gas and liquid condensate as well as the composition of each stream. Fluid properties are imperative for closure of the hydrodynamic model. These properties are densities of the liquid and gas phases, gas and liquid viscosities, liquid interfacial tension, and density variations with pressure. In the following sections, these three categories will be discussed in detail.

5.2 Flash Calculations

The flash calculator used in this model is based on the Peng-Robinson [1976] equation of state (PR EOS). This is a cubic equation of state developed for natural gas property predictions. This equation can be expressed by:

$$P = \frac{RT}{\tilde{v} - b_i} - \frac{(a\alpha)_i}{\tilde{v}^2 + 2b_i\tilde{v} - b_i^2} \qquad \textbf{5.1}$$

where the molar volume $\tilde{v}$ is defined as

$$\tilde{v} = \frac{ZRT}{P} \qquad \textbf{5.2}$$

The pure component properties $(a\alpha)_i$ and b_i are given by

$$
\begin{aligned}
(a\alpha)_i &= 0.45724\frac{R^2T_{ci}^2}{P_{ci}}\left[1+\Psi(\omega_i)\left(1-\sqrt{T_{ri}}\right)\right]^2 \\
T_{ri} &= \frac{T}{T_{ci}} \\
\Psi(\omega_i) &= 0.37464+1.54226\omega_i-0.26992\omega_i^2 \\
b_i &= 0.00780\frac{RT_{ci}}{P_{ci}}
\end{aligned}
\qquad \textbf{5.3}
$$

Note that the flowing temperature and the critical temperatures are in Rankine and the flowing and critical pressures are in psia. The gas constant for practical field units is 10.7315 psia-ft3/lbmol-°R.

The mixing rules applied to the equation of state are

$$
\begin{aligned}
b_m &= \sum_{i=1}^{nc} z_i b_i \\
(a\alpha)_m &= \sum_{i=1}^{nc}\sum_{j=1}^{nc} x_i x_j \sqrt{(a\alpha)_i (a\alpha)_j}\left(1-k_{ij}\right)
\end{aligned}
\qquad \textbf{5.4}
$$

For thermodynamic equilibrium to occur, the fugacity of each of the chemical components must be equal in both phases. That is:

$$f_{Li} = f_{Gi} \qquad \textbf{5.5}$$

Fugacity coefficients can be defined for the gas and liquid phases and used to define an equilibrium composition ratio. The equilibrium ratio may then be used to converge upon the equilibrium split of the two phases. This equilibrium ratio is defined as:

$$K_i = \frac{\Phi_{Li}}{\Phi_{Gi}} = \frac{\frac{f_{Li}}{x_i P}}{\frac{f_{Gi}}{y_i P}} = \frac{y_i}{x_i}\frac{f_{Li}}{f_{Gi}} \qquad \textbf{5.6}$$

Note that at equilibrium

$$K_i = \frac{y_i}{x_i} \qquad \textbf{5.7}$$

The Successive Substitution Method (SSM) is used in the flash calculator when its convergence is reasonable. If the convergence is not computationally acceptable, then accelerated SSM is used.

The SSM method is an iterative method whereby starting form an initial "reasonable" guess for the gas mole fractions y_i and the liquid mole fractions x_i, the actual equilibrium composition is converged upon. The flash calculation procedure is as follows

1. Estimate equilibrium ratios using Wilson's [1966] correlation:

$$K_i = \frac{1}{P_{ri}} = \exp\left[5.37\left(1+\omega_i\right)\left(1-\frac{1}{T_{ri}}\right)\right] \qquad \textbf{5.8}$$

2. Compute the gas fraction using the Newton-Raphson procedure, expressly:

$$\alpha_g^{n+1} = \alpha_g^n - \frac{\Gamma}{\Gamma'} \qquad \textbf{5.9}$$

where the Rachford-Rice objective function Γ and its derivative are defined by

$$\Gamma = \sum_{i=1}^{nc} \frac{z_i (K_i - 1)}{1 + \alpha_g (K_i - 1)}$$
$$\Gamma' = -\sum_{i=1}^{nc} \frac{z_i (K_i - 1)^2}{\left[1 + \alpha_g (K_i - 1)\right]^2} \qquad \textbf{5.10}$$

3. Determine the mole fractions of components in the gas and liquid using:

$$x_i = \frac{z_i}{1 + \alpha_g (K_i - 1)}$$
$$y_i = \frac{z_i (K_i - 1)}{1 + \alpha_g (K_i - 1)} \qquad \textbf{5.11}$$

4. Determine the compressibility factors by solving the cubic equation:

$$Z^3 + a_3 Z^2 + a_4 Z + a_5 = 0$$
$$a_1 = \frac{(a\alpha)_i P}{(RT)^2}$$
$$a_2 = \frac{b_i P}{RT} \qquad \textbf{5.12}$$
$$a_3 = -(1 - a_2)$$
$$a_4 = a_1 - 3a_2^2 - 2a_2$$
$$a_5 = -\left(a_1 a_2 - a_2^2 - a_2^3\right)$$

5. Determine the fugacity coefficient of the gas and liquid phases using:

$$\ln\Phi_{Gi} = (BB)_i (Z_G - 1) - \ln(Z_G - a_2)$$
$$-\frac{a_1}{2\sqrt{2}B}\left[(AA)_i - (BB)_i\right]\ln\left[\frac{Z_G + (\sqrt{2}+1)a_2}{Z_G - (\sqrt{2}-1)a_2}\right]$$
$$(AA)_i = \frac{2}{(\alpha a)_m}\left[\sum_{j=1}^{nc} z_j \sqrt{(\alpha a)_i (\alpha a)_j}\,(1 - k_{ij})\right] \qquad \textbf{5.13}$$
$$(BB)_i = \frac{b_i}{b_m}$$

6. Use the SSM formula to update the equilibrium ratios. Specifically:

$$K_i^{n+1} = K_i^n \left(\frac{f_{Li}}{f_{Li}}\right)^n \qquad \textbf{5.14}$$

7. Check for convergence using:

$$\sum_{i=1}^{nc}\left(\frac{f_{Li}}{f_{Gi}} - 1\right) < \varepsilon \qquad \textbf{5.15}$$

8. Repeat steps 2-7 until convergence is attained.

5.3 Fluid Properties Calculators

5.3.1 Density Calculator

Having determined the compressibility factors for the gas and liquid phases in addition to the chemical composition of both phases, the densities are determined using:

$$\rho_G = \frac{P}{RT}\left(\frac{\sum_{i=1}^{nc} y_i MW_i}{Z_G}\right)$$
$$\rho_L = \frac{P}{RT}\left(\frac{\sum_{i=1}^{nc} x_i MW_i}{Z_L}\right) \qquad \textbf{5.16}$$

5.3.2 Volume Translation

5.3.2.1 Introduction

Cubic equations of states are known to poorly predict liquid hydrocarbon density [Gmehling and Wang, 1999]. To improve the predictions of hydrocarbon liquid density, a volume translation is incorporated in this phase behavior package.

5.3.2.2 Theoretical Development

An equation of state is a functional relationship between the pressure, temperature, volume, and composition of a system. This relationship can be stated in general as

$$P = F(T, V, z_1, ..., z_i, ..., z_n) \qquad \textbf{5.17}$$

The fugacity coefficients used to establish equilibrium conditions (see section 4) are given by:

$$\ln \phi_i = \int_0^P \left(\frac{v_i}{RT} - \frac{1}{P} \right) dP \qquad i = 1, n \qquad \textbf{5.18}$$

where v_i is the partial molar volume with respect to composition and is symbolically given by:

$$v_i = \left(\frac{\partial V}{\partial z_i} \right)_{T,P,z_j} \qquad j \neq i; \quad i = 1, n \qquad \textbf{5.19}$$

It has been reported by several authors that the Soave-Redlich-Kowng equation of state (SRKEOS) inaccurately predicts the volume of heavy hydrocarbons ([Peneloux et al., 1982], [Gmehling and Wang, 1999]). It is therefore imperative to correct this volume discrepancy. The same can be stated regarding the PREOS.

Peneloux et al. proposed the concept of volume translation. They argued that the volume obtained using the SRKEOS is a "pseudo-volume" which is given symbolically by:

$$v_{actual} = v_{SRKEOS} - c \qquad \textbf{5.20}$$

They further claimed that a translation along the volume axis will improve volume prediction without changing the equilibrium conditions, and they provided the following proof:

They defined the "pseudo volume" as:

$$\widetilde{V} = V + \sum_{i=1}^{n} c_i z_i \qquad \textbf{5.21}$$

A translated functional relationship was then used to describe pressure in the following form:

$$P = \widetilde{F}(T, \widetilde{V}, z_1, ..., z_i, ..., z_n) \qquad \textbf{5.22}$$

A "pseudo partial volume" was defined as:

$$\widetilde{v}_i = \left(\frac{\partial \widetilde{V}}{\partial z_i}\right)_{T,P,z_j} = v_i + c_i \qquad j \neq i;\ i = 1, n \qquad \textbf{5.23}$$

Using the former definition, the "pseudo fugacity coefficients" were defined as:

$$\ln \widetilde{\phi}_i = \int_0^P \left(\frac{\widetilde{v}_i}{RT} - \frac{1}{P}\right) dP \qquad i = 1, n \qquad \textbf{5.24}$$

A short manipulation of equation [5.24] shows that:

$$\ln \tilde{\phi}_i = \int_0^P \left(\frac{\tilde{v}_i}{RT} - \frac{1}{P} \right) dP = \int_0^P \left(\frac{v_i}{RT} - \frac{1}{P} \right) dP + \int_0^P \frac{c_i}{RT} dP = \ln \phi_i + \frac{c_i P}{RT} \qquad \textbf{5.25}$$

"Pseudo" phase equilibrium is reached when the concentration and activity of a given compound in the liquid phase is balanced by its composition and activity in the gas phase. This can be stated symbolically by:

$$x_i \tilde{\phi}_i^L = y_i \tilde{\phi}_i^V \qquad \textbf{5.26}$$

Equation [5.26] can be rewritten using equation [5.25] as follows:

$$x_i \phi_i^L \exp\left(\frac{c_i P}{RT} \right) = y_i \phi_i^V \exp\left(\frac{c_i P}{RT} \right) \qquad \textbf{5.27}$$

Equation [5.27] is the same as:

$$x_i \phi_i^L = y_i \phi_i^V \qquad \textbf{5.28}$$

which is the equilibrium criterion for the Peng-Robinson equation of state.

Peneloux et al. proposed the following volume correction formula for the SRKEOS:

$$c = 0.40768\frac{RT_c}{P_c}\left(0.29441 - z_{RA}\right) \qquad \textbf{5.29}$$

where z_{RA} is the Rackett compressibility factor [Spencer and Danner, 1973]. Peneloux et al. used values published by Spencer and Adler [1978].

For this study we used the volume translation techniques proposed by Gmehling and Wang [1999].

The Gmehling and Wang method accounts for temperature variation and is based on a large data bank incorporating inorganic compounds normally present in natural gas/condensate fluids.

5.3.2.3 Volume Correction Procedure

Gmehling and Wang provide the following relations for determining the translated volume using the SRKEOS for mixtures normally found in natural gas. Here their method is extended to PREOS. The following steps are taken to correct volume:

The experimental molar volumes at the critical pressure and temperature are compared to the volumes obtained using PREOS and the volume difference is estimated. The mixture critical volume and volume deviation terms are determined with:

$$c_m = \sum_{i=1}^{n} z_i c_i \qquad \textbf{5.30}$$

$$\Delta v_{mc} = \sum_{i=1}^{n} z_i \Delta v_{ci} \qquad \textbf{5.31}$$

The parameter B_{2m} is calculated according to:

$$B_{2m} = \sum_{i=1}^{n} z_i B_{2i} \qquad \textbf{5.32}$$

The coefficients B_{2i} are correlation parameters reported by Gmehling and Wang, [1999]. The parameter B_{1m} is computed using

$$B_{1m} = \left(\frac{c_m}{\Delta v_{cm}} - 1 - B_{1m} 0.3^{2/3} \right) \Big/ 0.3^{1/3} \qquad \textbf{5.33}$$

The temperature-dependent volume correction can be determined using:

$$c'_m = \Delta v_{cm} \left(1 - B_{1m} \left| 1 - T_{rm} \right|^{1/3} + B_{21m} \left| 1 - T_{rm} \right|^{2/3} \right) \qquad \textbf{5.34}$$

where ω is the accentric factor and T_{rm} is the reduced temperature of the mixture.

5.3.3 Gas Viscosity

Gas viscosity is determined using the Lee-Gonzalez-Eakin [1966] correlation. This correlation is given by:

$$\mu_G = 10^{-4} k_v \exp\left[x_v \left(\frac{\rho_G}{62.4} \right)^{y_v} \right]$$
$$k_v = \frac{\left(9.4 + 0.02 MW_G\right) T^{1.5}}{209 + 19 MW_G + T}$$
$$y_v = 2.4 - 0.2 x_v$$
$$x_v = 3.5 + \frac{986}{T} + 0.01 MW_G$$
$$MW_G = \sum_{i=1}^{nc} y_i MW_i$$

5.35

where the temperature is in ºR, and density is in lbm/ft^3.

5.3.4 Liquid Viscosity

Viscosity of the liquid is determined using the Jossi et al. [1962] correlation given by

$$\mu_L = \mu^* + \frac{1}{\xi_m} \left[\left(0.1023 + V_1 + V_2 + V_3 + V_4\right)^4 - 10^{-4} \right]$$
$$V_1 = 0.023364 \rho_r$$
$$V_2 = 0.058533 \rho_r^2$$
$$V_3 = -0.040758 \rho_r^3$$
$$V_4 = 0.0093724 \rho_r^4$$
$$\rho_r = \frac{\rho_L}{MW_L} V_{Pc}$$

5.36

Lohrentz et al. [1964] recommended that liquid viscosity at atmospheric pressure be evaluated using

$$\mu^* = \frac{\sum_{i=1}^{nc} x_i \mu_i^* \left(MW_L\right)^{0.5}}{\sum_{i=1}^{nc} x_i \left(MW_L\right)^{0.5}} \qquad \textbf{5.37}$$

Jossi et al. further recommended that the viscosity of each pure component be computed using

$$\mu_i^* = \frac{34.0\times10^{-5} T_{ri}^{0.94}}{\xi_i} \quad \text{for } T_{ri} \le 1.5$$
$$\mu_i^* = \frac{17.78\times10^{-5} \left(4.58T_{ri} - 1.67\right)}{\xi_i} \quad \text{for } T_{ri} \ge 1.5 \qquad \textbf{5.38}$$

for the pure component viscosities, Lohrentz et al. suggested that

$$\xi_m = \frac{5.4402 T_{Pc}^{1/6}}{\left(MW_L\right)^{0.5} P_{Pc}^{2/3}}$$
$$\xi_i = \frac{5.4402 T_{ci}^{1/6}}{\left(MW_i\right)^{0.5} P_{ci}^{2/3}} \qquad \textbf{5.39}$$

where the pseudo-critical properties are given by:

$$P_{Pc} = \sum_{i=1}^{nc} x_i P_{ci}$$
$$T_{Pc} = \sum_{i=1}^{nc} x_i T_{ci} \qquad \textbf{5.40}$$
$$V_{Pc} = \sum_{i=1}^{nc} x_i V_{ci}$$

5.3.5 Surface Tension of the Liquid

Katz et al. [1959] proposed the following expression to determine surface tension of liquid hydrocarbons:

$$P_{Pc} = \sum_{i=1}^{nc} x_i P_{ci}$$
$$T_{Pc} = \sum_{i=1}^{nc} x_i T_{ci}$$
$$V_{Pc} =$$
$$\sigma = 6.852177 \times 10^{-3} \left[\sum_{i=1}^{nc} PCH_i \left(\frac{\rho_L}{62.4 MW_L} x_i - \frac{\rho_G}{62.4 MW_G} y_i \right) \right]^4 \quad \textbf{5.41}$$

The weighting factors *PCH*s are experimental factors. The surface tension in equation [5.41] is in units of lbf/ft.

5.4 Phase Behavior Package Validation

5.4.1 Flash Calculator Validation

a) Prakih [1984] Data

Table **5.1**: Composition of sample tested by Prakih [1984] for dew and bubble point observations

Component	Mole %
N_2	0.00
CH_4	85.11
C_2H_6	10.07
C_3H_8	4.82

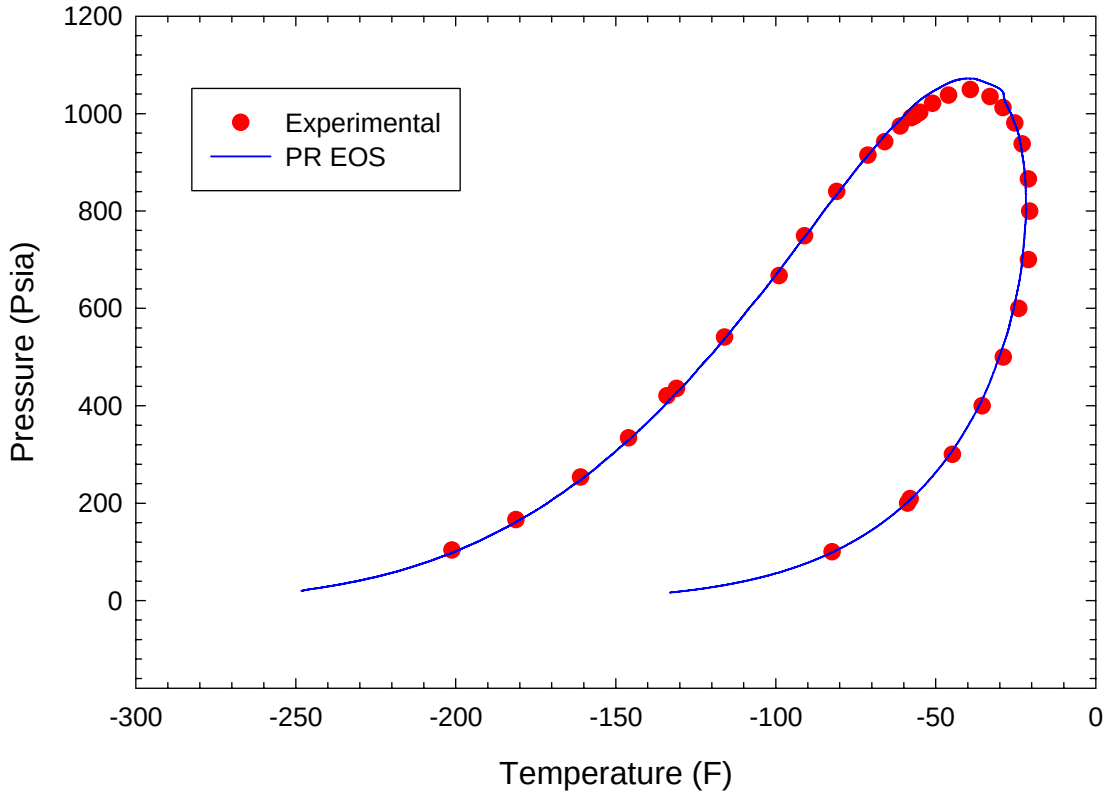

Figure **5.1**: Comparison of model performance with experimental data of Prakih [1984]

b) Data of Lee and Gonzalez [1968]

Table **5.2**: Composition of sample tested by Lee and Gonzalez [1968] for dew and bubble point observations

Component	**Mole %**

N_2	0.00
CH_4	85.11
C_2H_6	10.07
C_3H_8	4.82

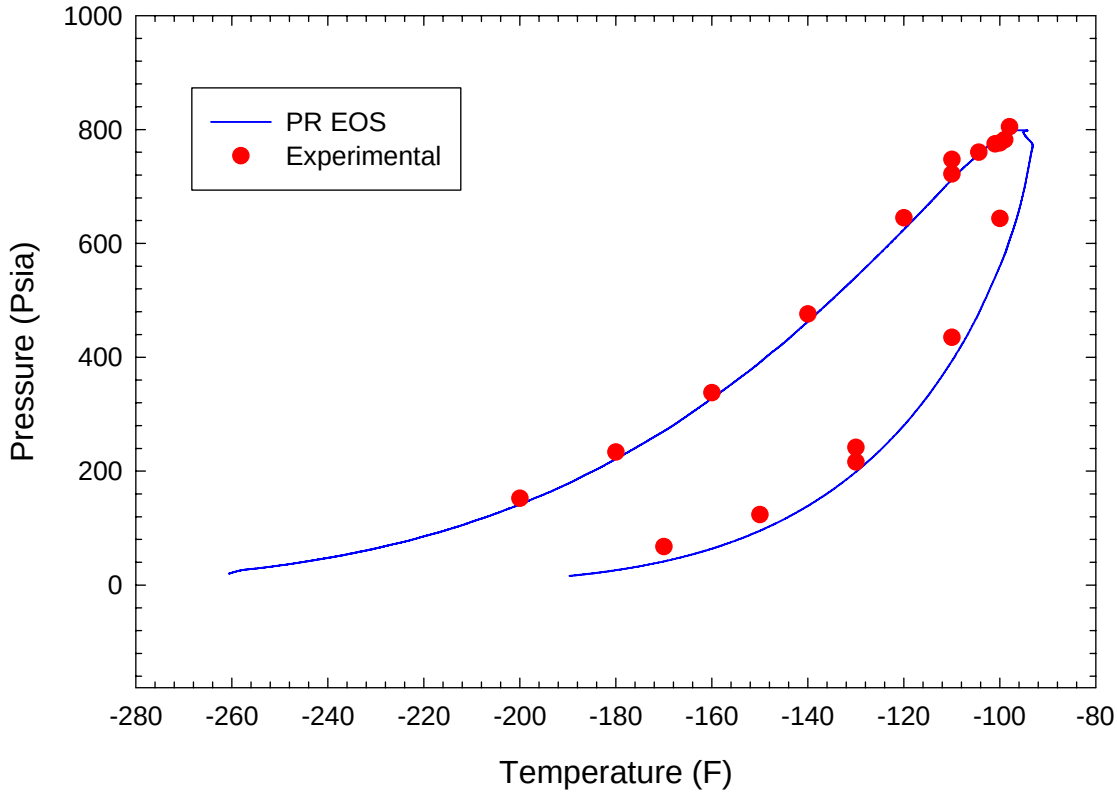

Figure **5.2**: Comparison of model performance with chilled mirror data reported by Lee and Gonzalez [1968]

5.4.2 Performance of Volume Translated PR EOS in Density Prediction

Table **5.3**: Composition of gas condensate sample used by Danesh et al.[2003] for experimental determination of liquid density

Component	**Mole %**
CH_4	82.05
C_3H_8	8.95
n-C_5H_{12}	5.00
n-$C_{10}H_{22}$	1.99
n-$C_{16}H_{34}$	2.01

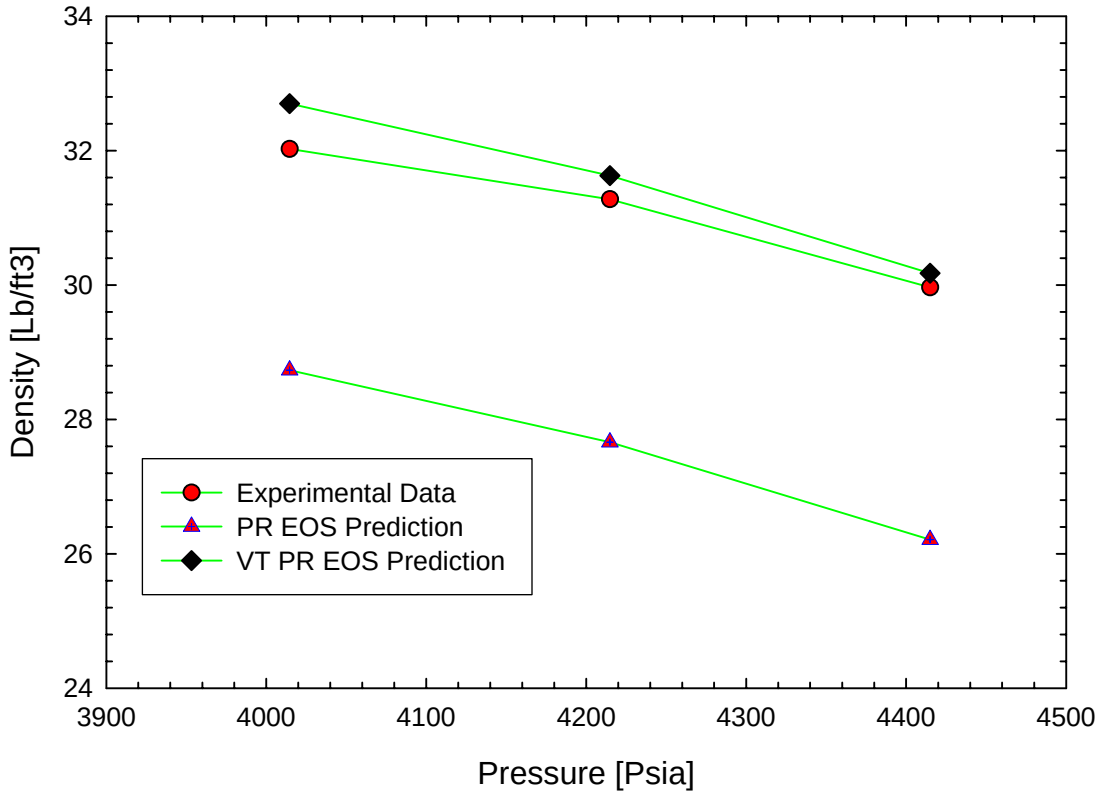

Figure **5.3**: Density prediction using volume translated PR EOS compared with experimental data reported by Danesh et al. [2003]

Chapter 6

VALIDATION OF THE WELLBORE MODEL

6.1 Introduction

After developing the hydrodynamic model, the flow regime transition model, and phase behavior model and independently testing each model, the three were integrated to form the wellbore model. Having done this, a literature search was conducted to find suitable data for validation of the model. It was found that most data in the petroleum and natural gas engineering literature pertains to flow of black oil, natural gas, and water mixtures. Only one data set provided data for multiphase flow of gas condensate or volatile oil with natural gas. This is the data set provided by Error! Not a valid link..

The data set was compiled from the public files of the Energy Conservation Board of Alberta, Canada. It comprised 102 gas/condensate well tests. The gas production rate varied from 0.144 to 27.4 MMSCFD at a gas-oil-ratio ranging from 3.9 to 1,170 MSCF/STB. The tubing strings' internal diameter varied form 1.995 to 3.958 inches and the well depths varied from 3678 to 12,073 feet. During testing, the flowing bottomhole pressure and temperature, wellhead pressure and temperature, and recombined well effluent stream flow rates and chemical composition were recorded.

It should be noted one limitation for these data is that only the mole fraction of heptane-plus fraction was reported. The specific gravity, however, was not provided.

Furthermore, the accuracy of measurement devices at the time data was compiled may be of moderate accuracy in some cases.

6.2 Field Data Set

For the data set described previously, associated formation water production was not reported for 45 tests and therefore these tests were selected for model validation. From this data set, after careful evaluation, 30 tests were selected for testing of the model. The range of significant parameters for the 30 test cases is given in Table 6-1.

Table **6-1**: Range of significant parameters used in model validation data set

	Q_G (MSCF/D)	GOR (MSCF/STB)	Methane (%)	String ID (in.)
Range	1.18 to 22.5	5.16 to 1170	62.74 to 88.21	1.99 to 4.4

6.3 Testing Procedure

To perform a simulation run, pipeline and gas quality data are entered and read. These data are:

1. Flow, wellbore, and string data
    a. Test identification tag
    b. Oil flow rate (STB/D)
    c. Gas flow rate (MSCF/D)

d. GOR (SCF/STB)

e. Combined molar flow rate (Moles/D)

f. Wellbore depth (ft)

g. String diameter (ft)

h. Surface pressure (Psia)

i. Bottomhole pressure (Psia)

j. Surface temperature (F)

k. Bottom hole temperature (F)

l. Absolute roughness of pipe (in.)

2. Fluid composition

a. Number of input array elements

b. Fluid sample tag

c. Type of EOS to be used (1 = VT-PREOS, 2 = VT-SRKEOS)

d. Number of compounds in mixtures

e. Identification tag for each compound

f. Mole fractions of all compounds

The program is then run to provide:

1. Pressure traverse
2. Surface liquid holdup
3. Gas and liquid compositions at the wellhead

6.4 Statistical Analysis

Testing results were analyzed by comparing the reported and predicted pressure drops using the Average Absolute Percent Error (AAPE) statistic. For each test, after predicting the pressure drop, the absolute value of the difference between the computed and the reported pressure drop is determined and divided by the measured pressure drop. For the tests to be analyzed, the differences are then summed and divided by the total number of tests. The result is reported as a percentage. Mathematically this is given by:

$$AAPE = 100 \frac{\sum_{i=1}^{N} \frac{\left|\Delta P_{\exp} - \Delta P_{mdl}\right|}{\Delta P_{\exp}}}{N} \qquad \textbf{6.1}$$

where:

N is the number of tests

$\Delta P_{\exp}$ is the experimental pressure drop

ΔP_{mdl} is the pressure drop estimated by model

6.5 Model Sensitivity

Before selecting the appropriate absolute roughness and pressure drop interval to be used in validation testing, the sensitivity of the model to parameters that could be most significant in introducing errors was evaluated.

The first parameter evaluated was absolute roughness of pipe. The chosen validation data set was used and the model was run with absolute rougnesses of 0.00005

ft, 0.00010 ft, 0.00015 ft, and 0.00020 ft. Comparisons of these runs are presented in Figure 6-1.

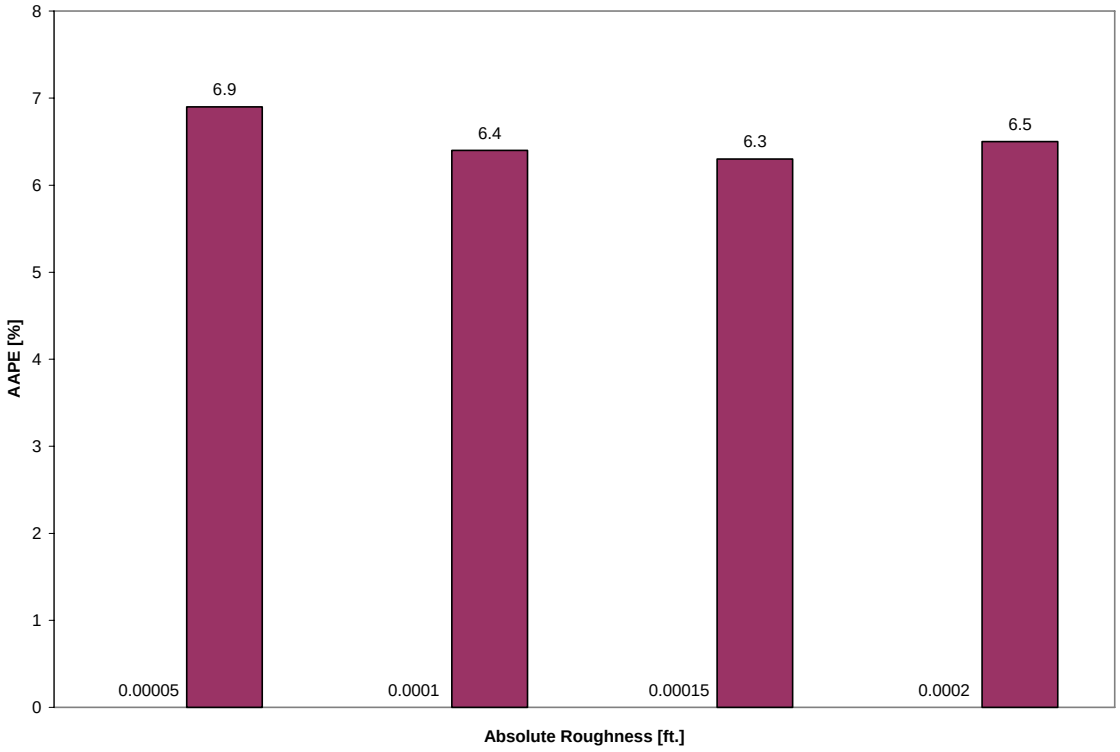

Figure **6-1**: Model sensitivity to absolute roughness of well string.

The roughness was found to have a relatively small impact on the accuracy of the model the AAPE ranged from a maximum 6.9% for a roughness of 0.00005 ft. to a minimum value of 6.3% for a roughness of 0.00015 ft. This value was thus used for all subsequent validation runs.

The pressure drop interval used in the iterative method for converging on the pressure gradient was also tested. Interval values of 5, 50, and 100 Psi were tested and the results are summarized in Figure 6-2.

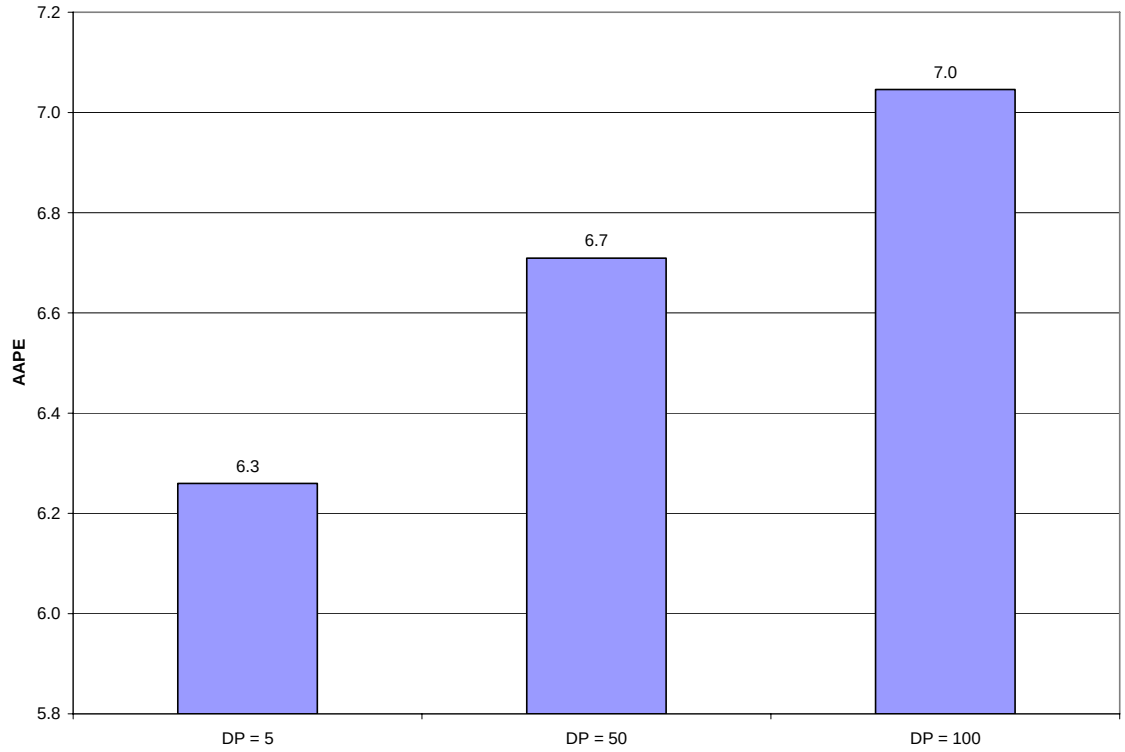

Figure **6-2**: Model sensitivity to initial pressure drop guess.

Figure 6-2 shows that the AAPE increased from 6.3% at a pressure interval of 5 Psi to 7.0% at an interval of 100 Psia. It should be noted that no significant improvement in prediction was observed for interval values lower than 5 psi. However the computation time was increased singnificantly. It was therefore decided to use an interval of 5 Psi during the reminder of the study.

It was also of interest to investigate the effect of errors in gas flow rate, well bottom hole pressure and reported methane content in the bottom hole gas stream.

Figures 6-3 to 6-5 show the results of these comparisons successively.

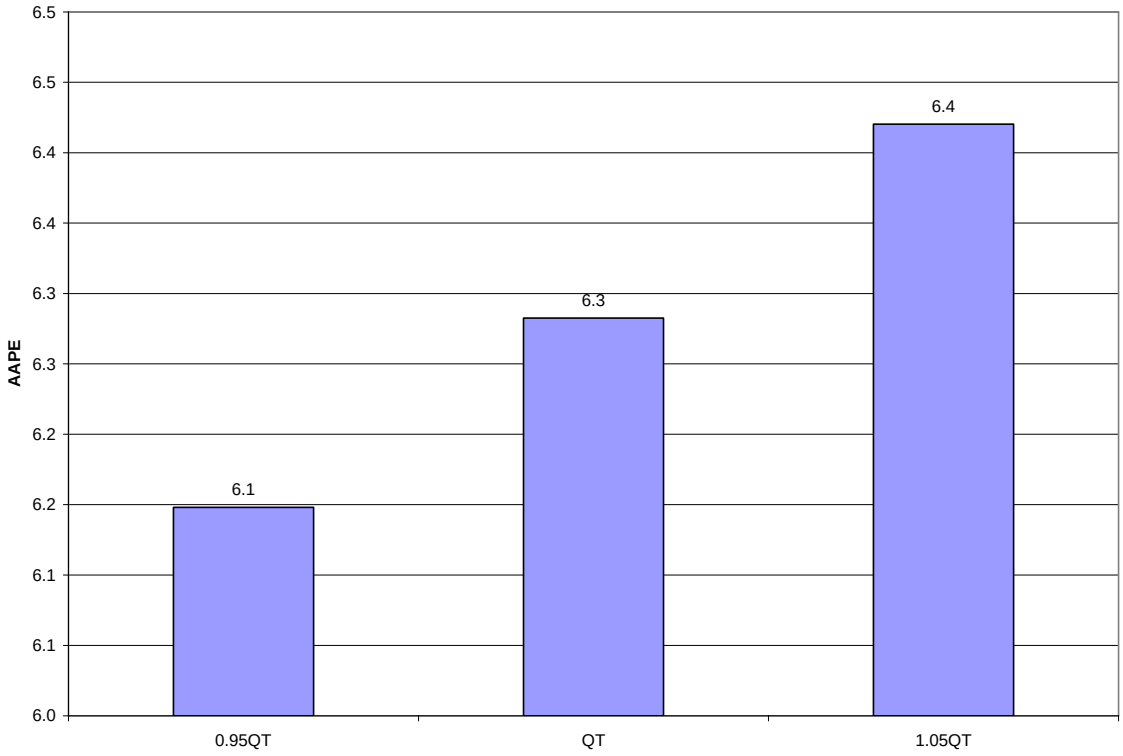

Figure **6-3**: Model sensitivity to errors in gas flow rate.

Figure 6-3 shows the results obtained when the total gas flow rate is perturbed by ±5.0%. It is seen that using flow rates having a value of 95% of the reported flow rate values actually caused a slight increase in the accuracy of the model prediction. The AAPE dropped from 6.3% to 6.1% while and a flow rate having a value 105% of the reported value actually decreased the accuracy as can be concluded from AAPE increasing from 6.3% to 6.4%.

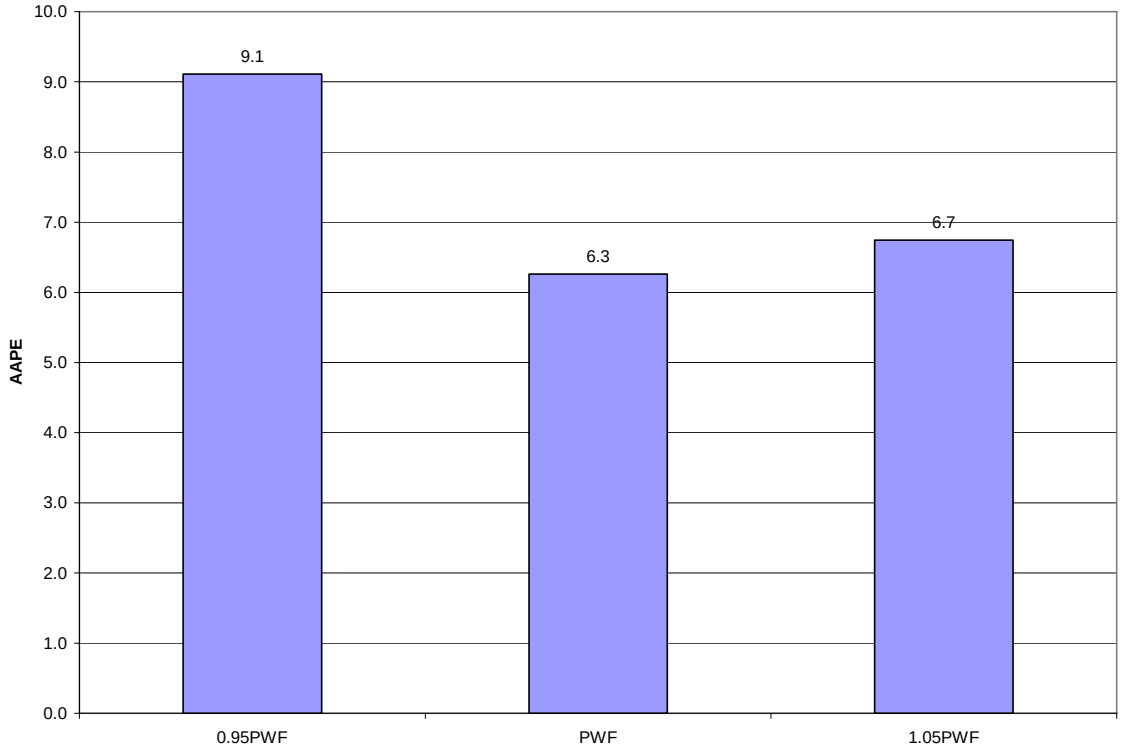

Figure **6-4**: Model sensitivity to error in reported bottom hole pressure.

The model was found more sensitive to changes in reported bottom hole pressure. In general the reported values seem to produce the most accurate predictions while increasing the reported bottom hole pressure by 5% produced a 0.4% increase in AAPE. One the other hand, decreasing the reported bottom hole pressure by 5% lead to an increase of 2.8%.

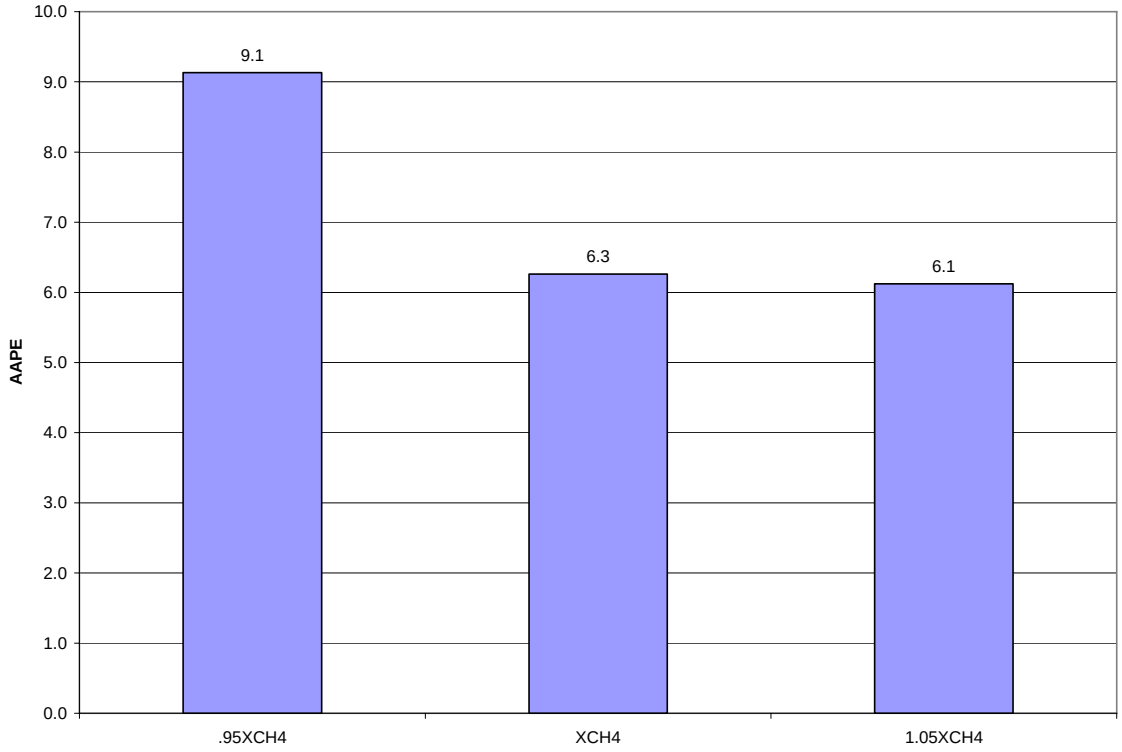

Figure **6-5**: Model sensitivity to reported percent methane

The reported composition seems to be slightly heavier (in C1+) than the actual composition. Reducing the percent methane by 5%, lead to an increase of 2.8% in AAPE.

6.6 Discussion of Results

6.6.1 Single-Phase Tests

The first set of tests discussed here are those tests for which single-phase gas flow existed throughout the entire height of the wellbore. Figure 6-6 shows a plot of the measured pressure drop versus the predicted pressure drop. It can be seen from this figure that the agreement between the model and the reported values was good. The AAPE was about 4.5 with the highest error being approximately 10.1. This error was found for test GF-0011. Since the model performed well for a very similar test (GF-0012), it is possible there was an error in the measured quantities. It is likely that this error is originated from the pressure or composition measurements.

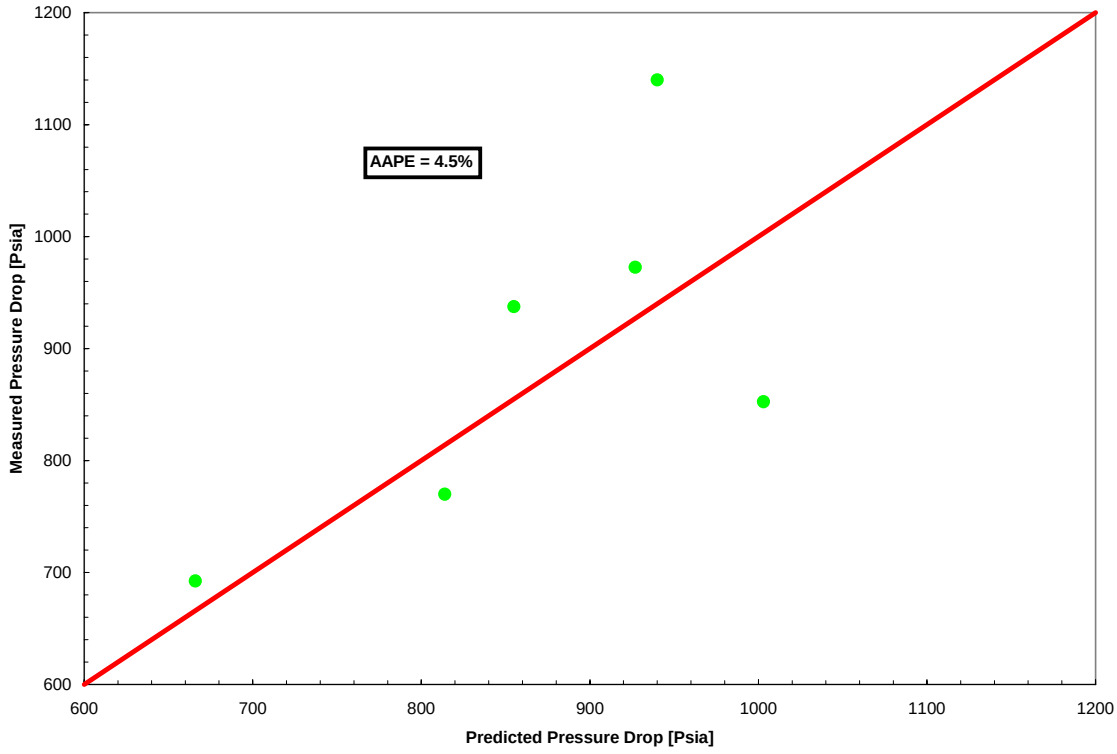

Figure **6-6**: Predicted versus measured pressure drops for the test cases where single-phase gas flow existed for entire height of wellbore

6.6.2 Single-Phase Flow at Bottomhole

The model was also tested for cases where single-phase flow existed at the bottomhole pressure and temperature conditions, but condensate dropped out as pressure and temperature decreased during fluid flow to the surface. The AAPE was 4.3 for the seven test cases with the highest difference being 10.5% for test GF-0006. Figure 6-7 graphically depicts the test data.

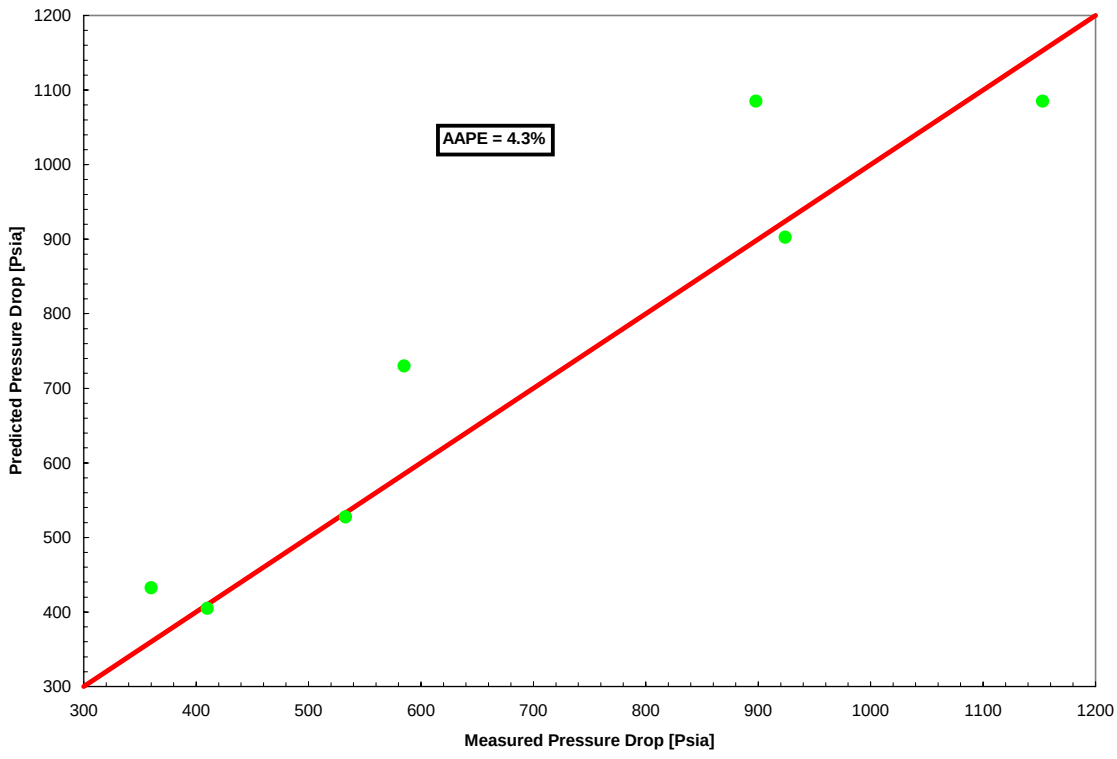

Figure **6-7**: Predicted versus measured pressure drops for the test cases where liquid

dropout occurred after single-phase gas traveled a distance up the wellbore

To analyze the performance of the model with respect to this particular test (GF-0006), we will compare the parameters and results reported for this test to all other tests in the same category which showed the trend of flow regime change from single-phase gas to mist flow. These tests are GF-0020,GF-0026, GF-0034, GF-0050, and GF-0056 (please see tables in Appendix A).

Table 6-2 shows the comparison of oil flow rate, gas flow rate, GOR, molar flow rate, diameter, depth, top and bottom flow temperatures and the top and bottom flowing pressures, and percent methane in reported composition. The table compares the quantities reported for test GF-0006 with the average for all tests in this category.

Table **6-2**: Comparison of Test GF-0006 with all tests where single-phase gas flow turned to mist flow as fluid traveled up the wellbore

Parameter	**GF-00006**	**Average**	**Difference (%)**
Oil (STB/D)	134	91	47.3
Gas (MSCFD)	10100	6540	54.4
GOR (SCF/STB)	75700	78917	-4.1
Moles/D	26800	17435	53.7
Depth (ft)	7983	7684	3.9
Diameter (ft)	0.203	0.218	-7.0
PT (Psia)	1785	1455	22.7
PB (Psia)	2683	2073	29.4
TT (F)	100	100	0.5
CH4 [%]	75	77	-2.0

From Table 6-2 it can be seen that the oil gas flow rate at a difference of 54.4%, represents the most significant differences for this test category. It is therefore possible that errors exist in the reported gas flow rate value.

It is of interest here to discuss the flow regime transitions observed. For all cases except one, the transition took place in a predictable manner; that is from single-phase gas to two-phase mist flow. For test GF-0033, a transition occurred from mist to slug flow without going through the annular mist flow regime. This could be due to the fact

that only 67% of the gas stream was methane. It is therefore possible that liquid dropout is much higher for this particular gas stream.

6.6.3 Two-phase Flow Tests

This category comprised most of the tests. The dew point of the reservoir fluid had already been reached when the fluid reached the bottom of the production string. Overall, the AAPE for this category was 7.7 with a maximum AAPE of 30.3 for test GF-0029. The results of testing are shown graphically in Figure 6-8.

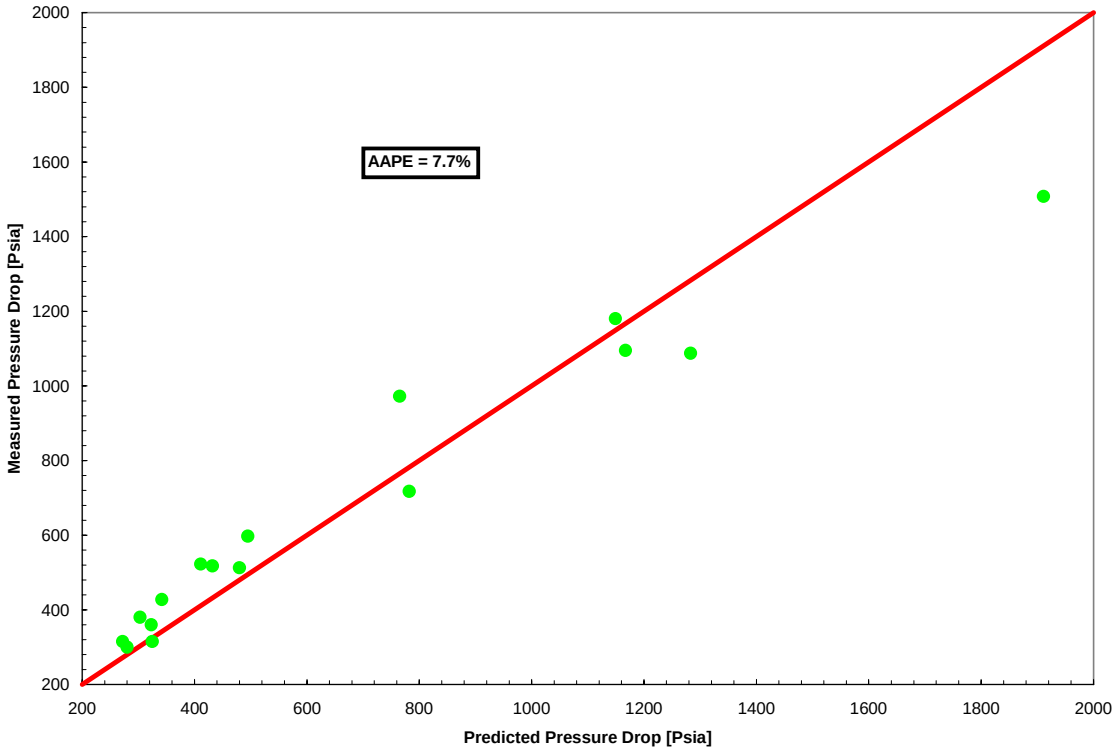

Figure **6-8**: Predicted versus measured pressure drops for the test cases where two-phase flow existed for entire well depth

Overall the data trend was good with no profound bias towards under or over-predicting pressure drop.

The predominant flow regime observed was mist flow, which prevailed for 17 test cases. This is expected due to the gas quality and high in-situ gas velocity. Slug flow was observed for test GF-0031 which could be attributed to the high oil flow rate of 774.0 STB/D compared to an average of about 247 STB/D. Another interesting case was observed for test GF-0029 where dispersed bubbly flow existed for the first 1578 feet and then slug flow prevailed to the surface. As expected, this test had the highest oil flow rate with a value of 946 STB/D.

Chapter 7

CONCLUSIONS AND RECOMMENDATIONS

7.1 Conclusions

A wellbore model based on the integration of modern methods in hydrodynamic modeling, flow regime transition prediction, and phase behavior and fluid properties calculators, was developed and tested. The model is capable of predicting pressure drop, liquid holdup and gas and/or liquid composition at the wellhead. The hydrodynamic model incorporates pressure drop prediction routine for single-phase gas or liquid flow, mist/annular mist flow, slug flow, bubbly flow and dispersed bubbly flow. The thermodynamic calculators can predict fluid split, fluid density, viscosity, and surface tension. The model was tested with 33 field cases and good agreement was observed between the predicted and the measured pressure drops. An overall average absolute percent error of 6% was observed.

The following specific conclusions were drawn from this work:

- Integrating a phase behavior package with an accurate hydrodynamic package and a flow regime transition model proved to provide good predictions of gas condensate well pressure drop using very reasonable computational resources.
- When performing multiphase flow calculations, use of physically based and internally integrated flow transition predictions eliminates the risk of

selecting inappropriate flow regime transition map by production technologists.

- Mechanistic pressure prediction models are capable of accurately predicting pressure drop and liquid holdup in gas condensate wellbore simulations.
- Relatively simple cubic equations of state can reasonably predict phase splits and necessary fluid properties.
- By integrating a phase behavior package, the mass transfer between liquid and gas phases was accounted for. To the knowledge of the author, it is the first time this important physical phenomenon has been taken into account in wellbore modeling.
- Applying the volume translation technique to the Peng-Robinson cubic equation of state leads to significant improvement in liquid density prediction. This yields more accurate prediction of hydrostatic pressure head (which accounts for about 80% of the total pressure drop) and frictional pressure drop.

7.2 Recommendations for Future Work

Having this model available, it is possible to perform many useful engineering calculations for gas condensate reservoir optimization and surface facilities design and operations. Specifically

- It is well known the best method to analyze the hydrocarbon production system is through a total systems analysis approach. Since about 70% of the total pressure drop experienced by the fluid from the reservoir to the stock tanks and the gas sales point is experienced in the wellbore it is extremely important to have at the disposal of production engineers an accurate physically based wellbore model. The model could be incorporated in a total systems analysis study of the production system by using a compositional reservoir simulator or an appropriate inflow performance relationship.
- In most instances a quantity of the formation water is produced with the hydrocarbon stream. It is important to integrate with the model discussed in this dissertation a phase behavior package capable of performing vapor-liquid-liquid equilibrium and fluid properties calculations.
- Building on the previous point, it is imperative to perform research in three-phase gas-liquid hydrocarbon-water flow regime transitions and pressure drop predictions methods.

References

Ansari et al. (1994): "A Comprehensive Mechanistic Model for Two-Phase Flow in Wellbores," SPEPF, Trans. AIME, **297**, 143.

Aziz, K.; Govier, G. W. and Fogarasi, M. (1972): "Pressure Drop in Wells Producing Oil and Gas," Cdn. J. Pet. Tech. , (July-September), **11**, 38.

Barnea, D. (1987): "A Unified Model for Predicting Flow-Pattern Transition for the Whole Range of Pipe Inclinations," Int. J. Multiphase Flow, **13**, 1.

Baxendell, P. B. and Thomas, R. (1961): "The Calculation of Pressure Gradients in High-Rate Flowing Wells," JPT, Trans. AIME, **222**, 1023.

Beggs, H. D. (1972): "An Experimental Study of Two-Phase Flow in Inclined Pipes," PhD Thesis, U. of Tulsa.

Beggs, H. D. and Brill, J. P. (1973): "A Study of Two-Phase Flow in Inclined Pipes," JPT, Trans. AIME, **255**, 607.

Bendikson, K. H.; Malnes, D.; Moe, R. and Nuland, S. (1991): "The Dynamic Two-Fluid Model OLGA: Theory and Application," SPEPE (May), 171.

Bergelin et al. (1949): "Co-Current Gas-Lift Flow," (II), "Flow in Vertical Pipes," Heat Transfer and Fluid Mechanics Institute, UC-Berkeley.

Brill, J.P., and Mukherjee, H. (1999): Multiphase flow in Wells, SPE H.L. Doherty Series, Monograph volume 17.

Brodkey, R.S. (1967): The Phenomena of Fluid Motions, Addison-Wesley Press.

Brotz, W. (1954): "Uber die Vorausberechnung der Absorptionsgeschwindigkeit von Gasen in Stromenden Flussigkeitsschichten," Chem. Ing. Tech., **26**, 470.

Colebrook, C.F. (1939): "Turbulent Flow in Pipes with Particular Reference to the Transition Region between Smooth and Rough Pipe Laws," J. Inst. Civil Eng., **11**, 133.

Danesh et. al (2003): "Vapor-Liquid Equilibrium Volume and Density Measurements of a Five-Component gas Condensate at 278.15-383.15 K," Fluid Phase Equilibria, **95**, 206.

Davis, G. J. Jr. and Weidner, C. E. (1914): "An Investigation of Air Lift Pump," Bulletin of the University of Wisconsin. Versluys, J.: "Mathematical Development of the Theory of Flow Oil Wells," Petroleum Development and Technology, **92**

Davis, R.M., and Taylor, G. (1949): "The Mechanics of Large Bubbles Rising Through Extended Liquids and Through Liquids in Tubes'" Proc., Royal Soc., London, **200A**, 375.

Duns, H. Jr. and Ros, N.C.J. (1963): "Vertical Flow of Gas and Liquid Mixtures in Wells," Proc. Sixth World Petrol. Cong., Tokyo, 451.

Fancher, G. H. Jr. and Brown, K. E. (1963): "Prediction of Pressure Gradients for Multiphase Flow in Tubing," SPEJ, Trans. AIME, **228**, 59 .

Fernandes, R. C.; Semiat, R. and Dukler, A. E. (1983): "Hydrodynamic Model for Gas-Liquid Slug Flow in Vertical Tubes" AIChE J., **29**, 981 .

Fu, X. Y. and Ishii, M. (2002): "Two-Group Interfacial Area Transport in Vertical Air-Water Flow: I. Mechanistic Model," Nuc. Eng. Design, **219**, 143.

Gmehling, J. and Wang, L. (1999): "Improvement of the SRK Equation of State for Representing Volumetric Properties of Petroleum Fluids Using Dortmund Data Bank," Chemical Engineering Science, **54**, 3885.

Govier, G. W. ; Radford, B. A. and Dunn, J. S. C. (1957): "The Upward Vertical Flow of Air-Water Mixtures , Pt. 1," Canad. J. Chem. Eng., **35**, 58.

Govier, G.W, and Fogarasi, M., (1975): "Pressure Drop in Wells Producing Gas and Condensate," Cdn. J. Pet. Tech., **14**, 28

Griffith, P. and Snyder, G. A. (1964): "The Bubbly-Slug Transition in a High Velocity Two-Phase Flow," Report No. 5003-29 (TID 20947), MIT, Cambridge, Mass

Griffith, P. and Wallis, G. B. (1961): "Two-Phase Slug Flow," J. Heat Transfer, **83**, 307.

Hagedorn, A. R. and Brown, K. E. (1965): "Experimental Study of Pressure Gradients Occurring during Continuous Two-Phase Flow in Small Diameter Vertical Conduits," JPT, Trans. AIME, **234**, 457.

Harmathy, T. Z. (1960): "Velocity of Large Drops and Bubbles in Media of Infinite or Restricted Extent," AIChE J., **6**, 281.

Hasan, A. R. and Kabir, C. S. (1988): "A Study of Multiphase Flow Behavior in Vertical Wells," SPEPE, Tans. AIME, **285**, 474

Hasan, A. R.; Kabir, C. S. and Rahman, R. (1988): "Predicting Liquid Gradient in a Pumping-Well Annulus," SPEPE, Trans. AIME, **285**, 113.

Jones Jr., O. C. and Zuber, N. (1975): "The Inter-Relation between Void Fraction Fluctuations and Flow Patterns in Two-Phase Flow" Int. J. Multiphase Flow, **2**, 273.

Jossi, J.A., Stiel, L.I, and Thodos, G. (1962): "Viscosity of Pure Substances in the Dense Gaseous and Liquid Phases," AIChE J, **8**, 59.

Katz, D.L., et al., (1959), Handbook of Natural Gas Engineering, McGraw Hill Book Co., Inc., New York.

Kaya, A. S.; Sarica, C. and Brill, J. P. (2001): "Mechanistic Modeling of Two-Phase Flow in Deviated Wells," SPEPF (August), 156.

Lee, A.L., Gonzalez, M.H, and Eakin, B.E. (1966): "The Viscosity of Natural Gases," SPE paper No. 1340.

Lockhart, R.W, and Martinelli, R.C. (1949): "Proposed Correlation of Data for Isothermal Two-Phase, Two-Component Flow in Pipes, Chem. Eng. Prog., **45**, 39.

Lohrentz, B.B, and Clark, C. (1964): "Calculating Viscosities of Reservoir Fluids from their Compositions," SPE Paper No. 915.

Moody, L.F, (1944): "Friction Factors for Pipe Flow," Trans. ASME, **66**, 671.

Moore, T. V. and Wilde, H. D. (1931): "Experimental Measurements of the Vertical Flow of Gas Liquid Mixtures in Glass Pipes" Petroleum Division meeting, AIME, New York (February).

Mukherjee, H. (1980): "An Experimental Study of Inclined Two-Phase Flow," PhD Thesis, U. of Tulsa.

Mukherjee, H. and Brill, J. P. (1985): "Pressure Drop Correlations for Inclined Two-Phase Flow," J. Energy Resources, Tech., **107**, 549.

Nicklin, D. J.; Wilkes, J. O. and Davidson, J. F. (1962): "Two-Phase Flow in Vertical Tubes" Trans. AIChE, **40**, 61.

Orkiszewski, J. (1967): "Predicting Two-Phase Pressure Drops in Vertical Pipes," JPT, Trans. AIME, **240**, 829.

Peneloux, A., Rauzy, E. and Freze, R. (1982): "Consistent Correction for Redlich-Kwong-Soave Volumes," Fluid Phase Equilibria, **8**, 7.

Peng, D. and Robinson, D.B. (1976): "A New Two-Constant Equation of State," Industrial Engineering Chemical Fundamentals, **15**, 59.

Poettman, F. H. and Carpenter, P. G. (1952): "The Multiphase Flow of Gas, Oil and Water through Vertical Flow Strings with Application to Design and Gas-Lift Installations," Drilling and Production Practices, 257.

Prakih, J.S et al. (1988): "Dew and Bubble Point Measurements for a Methane-Ethane-Propane Mixture," J. Chem. Eng. Data, **29**, 301.

Radovich, N. A. Moissis, R. (1962): "The Transition From Two-Phase Bubble Flow to Slug Flow," Report No. 7-7673-22, MIT, Cambridge, Mass.

RELAP5/MOD1 Code Manual Volume 1 (1982): System Models and Numerical Methods, NUREG/CR-1826, EGG-2070.

Schmidt, Z. (1976): "Experimental Study of Gas-Liquid Flow in a Pipeline-Riser System," MS Thesis, U. Tulsa.

Scott, S.L, and Kuba, G.E. (1990): "Advances in Slug Flow Characterization for Horizontal and Slightly Inclined Pipelines," SPE Paper No. 20628.

Spencer, C.F, and Adler, S.B. (1978): "A Critical Review of Equations for Predicting Saturated Liquid Density, J. Chem. Eng. Data, **23**, 82.

Spencer, C.F, and Danner, R.P (1973): "Prediction of Bubble Point Density of Mixtures," J. Chem. Eng. Data, **18**, 230.

Stewart, P. S. B. and Davidson, J. F. (1967): "Slug Flow in Fluidized Beds" Powder Tech., **1**, 61.

Sylvester, N. D. (1987): "A Mechanistic Model for Two-Phase Vertical Slug Flow in Pipes," J. Energy Res. Tech., **109**, 206.

Taitel, Y. M.; Barnea, D. and Dukler, A. E. (1980): "Modeling Flow Pattern Transitions for Steady Upward Gas-Liquid Flow in Vertical Tubes," AIChE J., **26**, 345.

TRAC-PF1 (1984): An Advanced Best Estimate Computer Program for Pressurized Water Reactor Analysis, NUREG/CR-3567, LA-994-MS.

Uren, L. C.; Gregory, P. P.; Hancock, R. A.; and Feskov, G.V. (1930): "Flow Resistance of Gas-Oil Mixtures through Vertical Pipes," Petroleum Development and Technology, **86**, 209.

Versluys, J (1930): "Mathematical Development of the Theory of Flowing Oil Wells," Petr. Dev. and Tech., **92**, 192.

Vo, D.T., and Shoham, O. (1989): "A Note on the Existence of a Solution for Two-Phase Slug Flow in Vertical Pipes," J. Energy Res. Tech., **111**, 64.

Wallis, G. B. (1969): One-Dimensional Two-Phase Flow, McGraw-Hill, NY.

Zuber, N. and Findley, J. A. (1965): "Average Volume Concentration in Two-Phase Flow Systems" ASME J., **87**, 453.

Zuber, N. and Hench, J. (1962): "Steady State and Transient Void Fraction of Bubbling Systems and their Operating Limit. Pt. I: Steady State Operation," General Electric Report, 62GL100.

Zuber, N; Staub, F.W., Bijwaard, G., and Kroeger, P.G. (1967): "Steady-State and Transient Void Fraction in Two-Phase Flow Systems," Report EURAEC-GEAP-5417, General Electric Co., San Jose, CA, Vol.1

Appendix A

GOVIER AND FOGARASI [1974] FIELD DATA

Table **1-1**: Well characteristics and flow parameters (tests GF-0001 to GF-0007)

Flow Conditions	Test No. GF-0001	GF-0002	GF-0003	GF-0004	GF-0005	GF-0006	GF-0007
Oil (STB/D)	775.00	200.00	380.00	141.00	118.00	134.00	138.00
Water (STB/D)	9.90	0.00	18.30	11.40	2.20	0.00	14.90
Gas(MSCF/D)	10100.00	10000.00	27400.00	10000.00	8880.00	10100.00	15200.00
GOR(SCF/STB)	13100.00	50300.00	70300.00	70900.00	75400.00	75700.00	110000.00
Moles/D	30800.00	27000.00	73100.00	26800.00	23700.00	26800.00	40200.00
Depth (ft)	10471.00	8930.00	8914.00	9959.00	7725.00	7983.00	9330.00
Diameter (ft)	0.203	0.249	0.249	0.203	0.203	0.203	0.249
PT(PSIA)	2685.00	2082.00	2672.00	2120.00	1717.00	1785.00	2815.00
PSF(PSIA)	4579.00	2937.00	4087.00	3100.00	2445.00	2683.00	3713.00
TT(F)	146.00	119.00	145.00	121.00	172.00	100.00	125.00
TB(F)	242.00	196.00	194.00	212.00	182.00	192.00	198.00

Table **1-2**: Well characteristics and flow parameters (tests GF-0008 to GF-0013)

Flow Conditions	Test No.					
	GF-0008	GF-0009	GF-0010	GF-0011	GF-0012	GF-0013
Oil (STB/D)	176.00	105.00	140.00	64.00	17.00	11.00
Water (STB/D)	0.00	0.00	54.00	0.00	0.00	0.00
Gas(MSCF/D)	22500.00	1500.00	20300.00	17900.00	11700.00	12400.00
GOR(SCF/STB)	128000.00	143000.00	145000.00	281000.00	701000.00	1170000.00
Moles/D	59600.00	39700.00	53800.00	47200.00	30800.00	32500.00
Depth (ft)	8755.00	8777.00	9421.00	8930.00	8734.00	8850.00
Diameter (ft)	0.330	0.330	0.249	0.249	0.249	0.330
PT(PSIA)	1990.00	2239.00	2120.00	1990.00	1879.00	2347.00
PSF(PSIA)	2993.00	3053.00	3202.00	2930.00	2806.00	3013.00
TT(F)	105.00	94.00	154.00	100.00	104.00	92.00
TB(F)	180.00	180.00	273.00	180.00	168.00	189.00

Table **1-3**: Well characteristics and flow parameters (tests GF-00014 to GF-0019)

Flow Conditions	Test No.					
	GF-0014	GF-0015	GF-0016	GF-0017	GF-0018	GF-0019
Oil (STB/D)	1300.00	736.00	236.00	270.00	100.00	187.00
Water (STB/D)	22.30	8.10	15.10	12.20	0.10	3.10
Gas(MSCF/D)	16300.00	13600.00	8030.00	9790.00	5480.00	10600.00
GOR(SCF/STB)	12500.00	18500.00	34100.00	36300.00	54800.00	56600.00
Moles/D	50400.00	38200.00	21600.00	26500.00	14700.00	28400.00
Depth (ft)	10948.00	8788.00	9311.00	8423.00	9313.00	8236.00
Diameter (ft)	0.249	0.203	0.203	0.203	0.203	0.166
PT(PSIA)	2147.00	1716.00	2218.00	2040.00	1812.00	1423.00
PSF(PSIA)	4066.00	3309.00	3186.00	2968.00	2614.00	2969.00
TT(F)	149.00	126.00	97.00	106.00	96.00	99.00
TB(F)	235.00	240.00	169.00	184.00	171.00	184.00

Table **1-4**: Well characteristics and flow parameters (tests GF-00020 to GF-0025)

Flow Conditions	Test No. GF-0020	GF-0021	GF-0022	GF-0023	GF-0024	GF-0025
Oil (STB/D)	84.00	97.00	102.00	131.00	26.00	57.00
Water (STB/D)	0.00	66.50	49.40	17.50	1.50	7.10
Gas(MSCF/D)	5000.00	5890.00	7330.00	11300.00	2470.00	6190.00
GOR(SCF/STB)	59200.00	60700.00	72200.00	86500.00	94700.00	109000.00
Moles/D	13400.00	15800.00	19600.00	30600.00	6580.00	16500.00
Depth (ft)	7989.00	7875.00	8025.00	8309.00	9558.00	9915.00
Diameter (ft)	0.203	0.203	0.203	0.249	0.203	0.249
PT(PSIA)	1769.00	1914.00	1822.00	1563.00	2151.00	1336.00
PSF(PSIA)	2354.00	2525.00	2524.00	2166.00	2788.00	1781.00
TT(F)	97.00	110.00	110.00	113.00	73.00	108.00
TB(F)	182.00	180.00	180.00	176.00	184.00	196.00

Table **1-5**: Well characteristics and flow parameters (tests GF-00026 to GF-0031)

COMPOUND	Test No. GF-0026	GF-0027	GF-0028	GF-0029	GF-0030	GF-0031
Oil (STB/D)	67.00	136.00	34.00	946.00	1590.00	774.00
Water (STB/D)	0.00	20.70	8.30	0.00	16.30	0.00
Gas(MSCF/D)	7700.00	20100.00	7870.00	4880.00	8320.00	9210.00
GOR(SCF/STB)	115000.00	147000.00	234000.00	5160.00	5250.00	11900.00
Moles/D	20400.00	53000.00	20800.00	15300.00	26700.00	26500.00
Depth (ft)	9733.00	9658.00	10014.00	8653.00	10540.00	8677.00
Diameter (ft)	0.203	0.249	0.203	0.166	0.203	0.203
PT(PSIA)	941.00	1303.00	1433.00	1333.00	2146.00	2214.00
PSF(PSIA)	1865.00	2585.00	2182.00	3244.00	3883.00	3363.00
TT(F)	99.00	121.00	122.00	105.00	132.00	104.00
TB(F)	200.00	220.00	208.00	181.00	211.00	176.00

Table **1-6**: Well characteristics and flow parameters (tests GF-00032 to GF-0037)

COMPOUND	Test No. GF-0032	GF-0033	GF-0034	GF-0035	GF-0036	GF-0037
Oil (STB/D)	536.00	865.00	121.00	59.00	422.00	272.00
Water (STB/D)	15.40	0.00	0.00	0.00	0.00	1.20
Gas(MSCF/D)	6860.00	13900.00	3200.00	1590.00	14400.00	9420.00
GOR(SCF/STB)	12800.00	16000.00	26400.00	26900.00	34100.00	34600.00
Moles/D	20400.00	38500.00	8810.00	4320.00	39200.00	25500.00
Depth (ft)	10410.00	10042.00	5939.00	7662.00	7415.00	11578.00
Diameter (ft)	0.203	0.367	0.203	0.203	0.203	0.249
PT(PSIA)	1840.00	2210.00	1896.00	1040.00	1485.00	690.00
PSF(PSIA)	3117.00	3363.00	2429.00	1343.00	2652.00	1398.00
TT(F)	120.00	100.00	105.00	61.00	106.00	93.00
TB(F)	235.00	168.00	193.00	178.00	119.00	180.00

Table **1-7**: Well characteristics and flow parameters (tests GF-00038 to GF-0043)

COMPOUND	Test No. GF-0038	GF-0039	GF-0040	GF-0041	GF-0042	GF-0043
Oil (STB/D)	88.00	444.00	207.00	174.00	57.00	96.00
Water (STB/D)	0.60	10.10	0.00	1.30	0.00	5.50
Gas(MSCF/D)	3130.00	15800.00	7880.00	6890.00	2470.00	4300.00
GOR(SCF/STB)	35500.00	35600.00	38100.00	39600.00	43200.00	44600.00
Moles/D	8460.00	43200.00	21200.00	18700.00	6690.00	11500.00
Depth (ft)	8612.00	8152.00	7907.00	8339.00	7665.00	6401.00
Diameter (ft)	0.203	0.249	0.203	0.203	0.203	0.166
PT(PSIA)	1099.00	1661.00	1854.00	1708.00	1603.00	897.00
PSF(PSIA)	1502.00	2445.00	2619.00	2390.00	2098.00	1462.00
TT(F)	79.00	116.00	100.00	110.00	76.00	80.00
TB(F)	185.00	181.00	182.00	186.00	180.00	169.00

Table **1-8**: Well characteristics and flow parameters (tests GF-00044 to GF-0049)

COMPOUND	Test No. GF-0044	GF-0045	GF-0046	GF-0047	GF-0048	GF-0049
Oil (STB/D)	234.00	114.00	29.00	56.00	49.00	263.00
Water (STB/D)	1.10	3.50	0.40	4.00	0.00	3.60
Gas(MSCF/D)	12100.00	5990.00	1570.00	3230.00	2940.00	17100.00
GOR(SCF/STB)	51800.00	52400.00	53300.00	58000.00	59700.00	65100.00
Moles/D	33000.00	16300.00	4820.00	8660.00	7870.00	45500.00
Depth (ft)	8943.00	8314.00	8573.00	7676.00	6631.00	7248.00
Diameter (ft)	0.203	0.249	0.203	0.203	0.203	0.249
PT(PSIA)	1351.00	1889.00	1240.00	1486.00	1130.00	1288.00
PSF(PSIA)	2487.00	2490.00	1662.00	1918.00	1472.00	2070.00
TT(F)	94.00	80.00	74.00	86.00	74.00	104.00
TB(F)	164.00	179.00	190.00	182.00	162.00	154.00

Table **1-9**: Well characteristics and flow parameters (tests GF-00050 to GF-0055)

COMPOUND	Test No. GF-0050	GF-0051	GF-0052	GF-0053	GF-0054	GF-0055
Oil (STB/D)	78.00	53.00	13.00	49.00	48.00	136.00
Water (STB/D)	0.00	0.00	1.20	1.60	0.60	13.20
Gas(MSCF/D)	5090.00	3570.00	923.00	3610.00	3850.00	11500.00
GOR(SCF/STB)	65200.00	67100.00	72100.00	73300.00	81100.00	84200.00
Moles/D	13600.00	9620.00	2450.00	9630.00	10300.00	31500.00
Depth (ft)	7917.00	7946.00	6745.00	8230.00	8203.00	8291.00
Diameter (ft)	0.249	0.166	0.166	0.203	0.203	0.249
PT(PSIA)	1294.00	1318.00	450.00	1925.00	1877.00	1580.00
PSF(PSIA)	1654.00	1857.00	653.00	2549.00	2499.00	2295.00
TT(F)	104.00	66.00	46.00	90.00	94.00	110.00
TB(F)	181.00	168.00	160.00	184.00	186.00	180.00

Table **1-10**: Well characteristics and flow parameters (tests GF-00056 to GF-0061)

COMPOUND	Test No. GF-0056	GF-0057	GF-0058	GF-0059	GF-0060	GF-0061
Oil (STB/D)	62.00	8.00	14.00	11.00	1660.00	635.00
Water (STB/D)	0.00	0.80	0.00	0.00	0.00	9.40
Gas(MSCF/D)	8150.00	1100.00	2420.00	1940.00	6480.00	3870.00
GOR(SCF/STB)	132000.00	143000.00	169000.00	183000.00	3900.00	6100.00
Moles/D	21600.00	2920.00	6380.00	5120.00	20500.00	11900.00
Depth (ft)	6545.00	6931.00	5135.00	8007.00	4473.00	11912.00
Diameter (ft)	0.249	0.203	0.203	0.203	0.166	0.249
PT(PSIA)	1045.00	654.00	787.00	597.00	839.00	1165.00
PSF(PSIA)	1455.00	786.00	981.00	877.00	2005.00	2205.00
TT(F)	92.00	60.00	73.00	70.00	122.00	101.00
TB(F)	115.00	148.00	145.00	166.00	165.00	188.00

Table **1-11**: Well characteristics and flow parameters (tests GF-00062 to GF-0067)

COMPOUND	Test No. GF-0062	GF-0063	GF-0064	GF-0065	GF-0066	GF-0067
Oil (STB/D)	134.00	480.00	1060.00	233.00	814.00	1650.00
Water (STB/D)	3.60	0.00	7.00	2.50	315.40	9.80
Gas(MSCF/D)	954.00	3930.00	9080.00	2050.00	7220.00	16200.00
GOR(SCF/STB)	7120.00	8180.00	8570.00	8820.00	8870.00	9810.00
Moles/D	2830.00	11600.00	28200.00	6340.00	22400.00	48000.00
Depth (ft)	9496.00	9496.00	10537.00	11100.00	11694.00	12073.00
Diameter (ft)	0.203	0.203	0.203	0.203	0.249	0.249
PT(PSIA)	816.00	816.00	1270.00	1413.00	1277.00	1232.00
PSF(PSIA)	1437.00	1437.00	2351.00	2400.00	2398.00	2679.00
TT(F)	65.00	65.00	116.00	86.00	144.00	108.00
TB(F)	186.00	186.00	214.00	242.00	244.00	187.00

Table **1-12**: Well characteristics and flow parameters (tests GF-00068 to GF-0073)

COMPOUND	Test No. GF-0068	GF-0069	GF-0070	GF-0071	GF-0072	GF-0073
Oil (STB/D)	68.00	720.00	832.00	252.00	810.00	232.00
Water (STB/D)	0.00	175.80	5.40	0.00	0.00	1.20
Gas(MSCF/D)	674.00	8300.00	9830.00	3210.00	11400.00	3310.00
GOR(SCF/STB)	9940.00	11500.00	11800.00	12700.00	14100.00	14200.00
Moles/D	2060.00	24000.00	28500.00	9120.00	32300.00	9240.00
Depth (ft)	5718.00	12015.00	7682.00	8483.00	7502.00	11447.00
Diameter (ft)	0.166	0.249	0.249	0.203	0.203	0.249
PT(PSIA)	809.00	1183.00	1199.00	1165.00	960.00	1058.00
PSF(PSIA)	1224.00	2269.00	2033.00	1727.00	2243.00	1729.00
TT(F)	52.00	106.00	110.00	73.00	123.00	84.00
TB(F)	122.00	180.00	157.00	172.00	173.00	185.00

Table **1-13**: Well characteristics and flow parameters (tests GF-00074 to GF-0079)

COMPOUND	Test No. GF-0074	GF-0075	GF-0076	GF-0077	GF-0078	GF-0079
Oil (STB/D)	655.00	105.00	380.00	157.00	59.00	550.00
Water (STB/D)	0.00	0.00	1.50	3.60	0.00	5.30
Gas(MSCF/D)	9510.00	1750.00	6310.00	2650.00	1000.00	10000.00
GOR(SCF/STB)	14500.00	16600.00	16600.00	16900.00	17000.00	18200.00
Moles/D	26200.00	4800.00	17500.00	7510.00	2730.00	28100.00
Depth (ft)	6043.00	7337.00	11733.00	3678.00	6293.00	11790.00
Diameter (ft)	0.203	0.203	0.203	0.166	0.203	0.249
PT(PSIA)	1438.00	626.00	663.00	839.00	485.00	1197.00
PSF(PSIA)	2196.00	883.00	1551.00	1125.00	1537.00	2205.00
TT(F)	98.00	54.00	92.00	62.00	52.00	120.00
TB(F)	170.00	156.00	181.00	96.00	154.00	184.00

Table **1-14**: Well characteristics and flow parameters (tests GF-00080 to GF-0085)

COMPOUND	Test No. GF-0080	GF-0081	GF-0082	GF-0083	GF-0084	GF-0085
Oil (STB/D)	114.00	83.00	458.00	61.00	46.00	441.00
Water (STB/D)	0.00	13.70	0.00	6.10	441.00	0.10
Gas(MSCF/D)	2100.00	1870.00	10700.00	1450.00	1100.00	11600.00
GOR(SCF/STB)	18400.00	22700.00	23300.00	23700.00	24100.00	26300.00
Moles/D	5940.00	5160.00	28900.00	3970.00	3010.00	31500.00
Depth (ft)	5261.00	8680.00	6020.00	8655.00	8542.00	7439.00
Diameter (ft)	0.166	0.203	0.203	0.166	0.166	0.249
PT(PSIA)	1253.00	1368.00	1157.00	1012.00	1008.00	1057.00
PSF(PSIA)	1909.00	1822.00	1939.00	1509.00	1349.00	1642.00
TT(F)	84.00	52.00	106.00	66.00	67.00	75.00
TB(F)	160.00	180.00	168.00	180.00	187.00	170.00

Table **1-15**: Well characteristics and flow parameters (tests GF-00086 to GF-0091)

COMPOUND	Test No. GF-0086	GF-0087	GF-0088	GF-0089	GF-0090	GF-0091
Oil (STB/D)	172.00	94.00	40.00	101.00	57.000	95.00
Water (STB/D)	1.60	1.00	0.00	0.00	0.00	0.00
Gas(MSCF/D)	4670.00	2780.00	1180.00	3100.00	2210.00	4140.00
GOR(SCF/STB)	27100.00	29600.00	29800.00	30700.00	39000.00	43400.00
Moles/D	12500.00	14700.00	3230.00	8480.00	5970.00	16100.00
Depth (ft)	7005.00	7327.00	7547.00	7615.00	7951.00	7357.00
Diameter (ft)	0.166	0.166	0.166	0.203	0.203	0.203
PT(PSIA)	1063.00	1380.00	1428.00	1452.00	973.00	438.00
PSF(PSIA)	1716.00	1909.00	1908.00	1859.00	1322.00	800.00
TT(F)	72.00	68.00	64.00	75.00	64.00	70.00
TB(F)	142.00	162.00	165.00	172.00	162.00	141.00

Table **1-16**: Well characteristics and flow parameters (tests GF-00082 to GF-0097)

COMPOUND	Test No. GF-0092	GF-0093	GF-0094	GF-0095	GF-0096	GF-0097
Oil (STB/D)	23.00	391.00	84.00	144.00	150.00	42.00
Water (STB/D)	0.00	7.20	0.00	0.00	7.20	1.10
Gas(MSCF/D)	1110.00	19900.00	4790.00	8960.00	10500.00	3250.00
GOR(SCF/STB)	49000.00	50800.00	57400.00	62400.00	70100.00	78100.00
Moles/D	2960.00	33800.00	12700.00	24000.00	27900.00	8800.00
Depth (ft)	7516.00	8071.00	7196.00	5967.00	5797.00	6701.00
Diameter (ft)	0.203	0.249	0.166	0.249	0.249	0.203
PT(PSIA)	908.00	1135.00	958.00	1349.00	1430.00	1169.00
PSF(PSIA)	1211.00	2089.00	1622.00	1781.00	1901.00	1495.00
TT(F)	58.00	108.00	60.00	108.00	105.00	61.00
TB(F)	166.00	158.00	146.00	170.00	174.00	154.00

Table **1-17**: Well characteristics and flow parameters (tests GF-00098 to GF-0102)

COMPOUND	Test No. GF-0098	GF-0099	GF-0100	GF-0101	GF-0102
Oil (STB/D)	112.00	66.00	12.00	25.00	7.00
Water (STB/D)	0.00	0.00	0.00	0.00	0.00
Gas(MSCF/D)	9020.00	6880.00	1330.00	3230.00	1010.00
GOR(SCF/STB)	80800.00	104000.00	116000.00	127000.00	141000.00
Moles/D	24100.00	18400.00	3540.00	8570.00	2690.00
Depth (ft)	6746.00	6189.00	6600.00	6190.00	6540.00
Diameter (ft)	0.249	0.249	0.203	0.249	0.203
PT(PSIA)	1079.00	1064.00	988.00	1109.00	954.00
PSF(PSIA)	1490.00	1387.00	1260.00	1434.00	1443.00
TT(F)	90.00	88.00	88.00	82.00	98.00
TB(F)	178.00	170.00	123.00	170.00	150.00

Appendix B

CHEMICAL COMPOSITION OF FLUID STREAMS [GOVIER AND FOGARASI, 1974]

Table **2-1**: Chemical Compositions for tests (GF-0001 to GF-0006)

COMPOUND	Test No. GF-0001	GF-0002	GF-0003	GF-0004	GF-0005	GF-0006
H_2S	17.06	0.66	0.00	1.26	12.31	10.00
CO_2	3.20	4.72	1.37	4.14	4.85	6.20
N_2	1.92	0.42	0.26	0.17	3.51	4.44
C1	59.03	80.00	85.41	87.82	74.91	75.48
C2	7.27	7.51	7.94	3.62	2.10	2.11
C3	2.97	2.97	2.26	0.91	0.52	0.51
i-C4	0.79	0.68	0.40	0.29	0.09	0.08
n-C4	1.44	0.98	0.60	0.34	0.30	0.33
i-C5	0.59	0.38	0.24	0.17	0.13	0.13
n-C5	0.62	0.34	0.18	0.14	0.12	0.12
C6	1.20	0.33	0.27	0.20	0.19	0.12
C7+	3.91	1.00	1.07	0.94	0.97	0.48
MW C7+	124.00	125.00	145.00	128.00	137.00	128.00
Sum	**100.00**	**99.99**	**100.00**	**100.00**	**100.00**	**100.00**

Table **2-2**: Chemical Compositions for tests (GF-0007 to GF-0012)

COMPOUND	Test No. GF-0007	GF-0008	GF-0009	GF-0010	GF-0011	GF-0012
H_2S	1.15	0.57	0.67	1.91	0.66	0.74
CO_2	4.03	4.85	4.83	3.58	5.43	4.47
N_2	0.16	0.44	0.43	0.13	0.43	0.38
C1	88.18	81.96	82.74	88.11	82.41	75.86
C2	3.64	7.76	7.83	3.68	8.02	7.62
C3	0.94	2.17	1.76	0.95	1.64	7.31
i-C4	0.26	0.42	0.31	0.28	0.25	1.23
n-C4	0.31	0.60	0.45	0.30	0.36	1.72
i-C5	0.15	0.22	0.18	0.16	0.12	0.25
n-C5	0.13	0.17	0.16	0.12	0.11	0.19
C6	0.22	0.20	0.14	0.15	0.11	0.11
C7+	0.83	0.64	0.50	0.64	0.45	0.11
MW C7+	127.00	120.00	123.00	138.00	119.00	121.00
Sum	**100.00**	**100.00**	**100.00**	**100.01**	**99.99**	**99.99**

Table **2-3**: Chemical Compositions for tests (GF-0013 to GF-0018)

COMPOUND	Test No. GF-0013	GF-0014	GF-0015	GF-0016	GF-0017	GF-0018
H_2S	0.57	18.52	0.53	3.30	0.54	5.16
CO_2	4.86	3.80	4.98	1.90	4.43	1.97
N_2	0.45	1.89	0.44	1.83	0.55	2.23
C1	84.62	55.11	78.31	79.92	79.59	77.78
C2	7.75	8.05	7.15	5.73	7.51	5.23
C3	1.18	3.36	2.90	2.21	3.00	2.96
i-C4	0.11	0.87	0.70	0.50	0.66	0.59
n-C4	0.17	1.57	1.11	1.04	0.95	1.30
i-C5	0.05	0.61	0.42	0.44	0.34	0.40
n-C5	0.04	0.68	0.41	0.48	0.32	0.51
C6	0.07	0.95	3.05	0.64	0.49	0.51
C7+	0.12	4.59	0.00	2.01	1.62	1.36
MW C7+	119.00	123.00	121.00	128.00	117.00	124.00
Sum	**99.99**	**100.00**	**100.00**	**100.00**	**100.00**	**100.00**

Table **2-4**: Chemical Compositions for tests (GF-0019 to GF-0024)

COMPOUND	Test No. GF-0019	GF-0020	GF-0021	GF-0022	GF-0023	GF-0024
H_2S	0.10	11.32	9.25	12.21	0.41	0.55
CO_2	5.44	5.24	5.53	7.10	4.72	3.84
N_2	0.71	4.24	4.36	4.45	0.41	0.18
C1	80.72	74.04	75.44	71.40	82.79	88.97
C2	7.15	2.26	2.39	2.11	6.31	3.81
C3	2.46	0.73	0.67	0.55	2.17	0.98
i-C4	0.57	0.11	0.12	0.09	0.50	0.28
n-C4	0.78	0.36	0.40	0.36	0.70	0.33
i-C5	0.35	0.17	0.18	0.19	0.31	0.15
n-C5	0.34	0.15	0.19	0.17	0.28	0.13
C6	0.33	0.27	0.30	0.25	0.37	0.20
C7+	1.06	1.11	1.16	1.11	1.03	0.58
MW C7+	118.00	117.00	117.00	119.00	128.00	128.00
Sum	**100.01**	**100.00**	**99.99**	**99.99**	**100.00**	**100.00**

Table **2-5**: Chemical Compositions for tests (GF-0025 to GF-0030)

COMPOUND	Test No. GF-0025	GF-0026	GF-0027	GF-0028	GF-0029	GF-0030
H_2S	1.45	1.57	1.92	1.81	0.00	7.24
CO_2	3.98	3.66	4.31	4.12	1.57	2.33
N_2	0.22	0.31	0.15	0.15	1.25	4.45
C1	87.34	88.21	87.05	86.87	67.58	60.77
C2	3.63	3.59	3.67	3.48	11.27	6.52
C3	1.14	0.87	0.91	0.90	5.67	3.64
i-C4	0.30	0.24	0.27	0.29	0.85	0.97
n-C4	0.40	0.30	0.30	0.34	2.21	1.89
i-C5	0.18	0.15	0.17	0.18	0.71	0.93
n-C5	0.16	0.13	0.13	0.17	0.85	0.91
C6	0.27	0.20	0.24	0.27	1.19	1.79
C7+	0.92	0.77	0.88	1.41	6.85	8.56
MW C7+	131.00	121.00	118.00	131.00	128.00	143.00
Sum	**99.99**	**100.00**	**100.00**	**99.99**	**100.00**	**100.00**

Table **2-6**: Chemical Compositions for tests (GF-00315 to GF-0036)

COMPOUND	Test No. GF-0031	GF-0032	GF-0033	GF-0034	GF-0035	GF-0036
H_2S	0.00	17.76	16.15	1.44	0.00	14.71
CO_2	0.62	3.35	4.02	1.27	0.83	2.15
N_2	0.57	1.13	0.90	1.54	0.58	9.01
C1	76.34	56.99	67.41	73.68	80.87	65.46
C2	9.19	7.40	3.89	10.87	8.87	2.89
C3	5.14	3.07	1.34	4.79	4.53	1.44
i-C4	0.79	0.88	0.32	0.76	0.53	0.27
n-C4	1.73	1.62	0.81	1.83	1.47	0.69
i-C5	0.65	0.75	0.41	0.73	0.44	0.25
n-C5	0.66	0.83	0.42	0.74	0.50	0.29
C6	1.06	1.30	0.88	0.82	0.46	0.44
C7+	3.26	4.92	3.45	1.53	0.89	2.40
MW C7+	130.00	123.00	133.00	119.00	114.00	122.00
Sum	**100.01**	**100.00**	**100.00**	**100.00**	**99.97**	**100.00**

Table **2-7**: Chemical Compositions for tests (GF-0037 to GF-0042)

COMPOUND	Test No. GF-0037	GF-0038	GF-0039	GF-0040	GF-0041	GF-0042
H_2S	2.83	0.67	0.08	13.13	0.67	1.39
CO_2	4.38	3.82	5.29	2.06	4.37	2.60
N_2	1.07	0.47	0.44	8.37	0.59	5.08
C1	79.06	81.39	80.91	65.69	77.48	81.83
C2	6.66	7.06	6.80	3.52	9.64	4.19
C3	2.19	2.64	2.37	2.11	2.92	1.43
i-C4	0.49	0.61	0.56	0.45	0.64	0.27
n-C4	0.92	0.91	0.81	1.18	0.94	0.77
i-C5	0.35	0.37	0.36	0.47	0.33	0.34
n-C5	0.34	0.34	0.33	0.57	0.32	0.33
C6	0.48	0.47	0.49	0.64	0.47	0.50
C7+	1.23	1.24	1.54	1.81	1.62	1.28
MW C7+	128.00	124.00	128.00	128.00	124.00	128.00
Sum	**100.00**	**99.99**	**99.98**	**100.00**	**99.99**	**100.01**

Table **2-8**: Chemical Compositions for tests (GF-0043 to GF-0048)

COMPOUND	Test No. GF-0043	GF-0044	GF-0045	GF-0046	GF-0047	GF-0048
H_2S	0.00	12.11	0.63	0.63	1.73	0.00
CO_2	1.84	2.55	6.44	4.43	2.59	2.70
N_2	0.20	0.68	0.38	0.51	5.79	0.73
C1	88.88	72.16	79.11	80.17	80.41	78.83
C2	5.79	6.13	6.93	7.36	4.20	9.65
C3	1.57	2.06	2.42	2.87	1.51	4.23
i-C4	0.26	0.56	0.58	0.67	0.31	0.67
n-C4	0.32	1.01	0.84	1.01	0.89	1.16
i-C5	0.13	0.45	0.41	0.38	0.39	0.36
n-C5	0.09	0.37	0.37	0.34	0.38	0.37
C6	0.05	0.55	0.51	0.37	0.60	0.43
C7+	0.88	1.37	1.38	1.26	1.17	0.87
MW C7+	260.00	128.00	128.00	125.00	111.00	119.00
Sum	**100.01**	**100.00**	**100.00**	**100.00**	**99.97**	**100.00**

Table **2-9**: Chemical Compositions for tests (GF-0049 to GF-0054)

COMPOUND	Test No. GF-0049	GF-0050	GF-0051	GF-0052	GF-0053	GF-0054
H_2S	1.07	7.73	0.00	0.00	12.75	16.15
CO_2	5.05	4.55	4.34	1.23	5.82	7.24
N_2	0.51	4.51	0.73	1.29	4.07	3.72
C1	81.44	77.13	79.93	80.31	71.83	68.00
C2	6.68	2.70	8.16	9.55	2.24	1.90
C3	2.16	0.86	3.41	4.13	0.64	0.66
i-C4	0.50	0.15	0.50	0.53	0.09	0.11
n-C4	0.70	0.47	1.02	1.19	0.38	0.32
i-C5	0.28	0.21	0.33	0.35	0.20	0.13
n-C5	0.26	0.21	0.31	0.38	0.20	0.13
C6	0.34	0.35	0.39	0.32	0.35	0.29
C7+	1.02	1.13	0.88	0.71	1.41	1.33
MW C7+	122.00	120.00	128.00	183.00	128.00	134.00
Sum	**100.01**	**100.00**	**100.00**	**99.99**	**99.98**	**99.98**

Table **2-10**: Chemical Compositions for tests (GF-0055 to GF-0060)

COMPOUND	Test No. GF-0055	GF-0056	GF-0057	GF-0058	GF-0059	GF-0060
H_2S	0.47	9.21	0.00	0.00	0.00	15.63
CO_2	5.89	4.89	2.46	1.18	1.62	6.64
N_2	0.39	0.50	0.28	0.90	3.78	0.58
C1	79.56	73.65	84.70	84.13	78.25	51.75
C2	6.91	7.01	7.50	7.88	9.46	5.55
C3	2.49	2.29	2.88	3.11	3.89	2.07
i-C4	0.65	0.46	0.40	0.57	0.63	0.49
n-C4	0.90	0.87	0.67	0.93	1.03	1.39
i-C5	0.44	0.34	0.19	0.30	0.31	0.87
n-C5	0.39	0.27	0.20	0.29	0.31	0.94
C6	0.49	0.18	0.25	0.28	0.25	2.06
C7+	1.42	0.35	0.47	0.44	0.47	12.03
MW C7+	128.00	108.00	108.00	235.00	117.00	164.00
Sum	**100.00**	**100.02**	**100.00**	**100.01**	**100.00**	**100.00**

Table **2-11**: Chemical Compositions for tests (GF-0061 to GF-0066)

COMPOUND	Test No. GF-0061	GF-0062	GF-0063	GF-0064	GF-0065	GF-0066
H_2S	2.70	4.49	0.00	8.87	19.97	19.61
CO_2	3.59	1.74	0.63	2.99	3.37	3.09
N_2	1.02	1.83	0.25	4.39	1.14	0.98
C1	76.06	72.76	71.78	64.32	56.84	56.86
C2	7.52	4.66	10.03	5.75	7.30	7.47
C3	2.78	2.33	5.57	2.95	3.09	3.11
i-C4	0.63	0.53	1.00	0.75	0.83	0.88
n-C4	1.29	1.14	2.10	1.42	1.56	1.58
i-C5	0.53	0.47	0.80	0.67	0.66	0.66
n-C5	0.48	0.64	0.83	0.68	0.69	0.74
C6	0.73	1.13	1.32	1.27	0.93	1.20
C7+	2.67	8.10	5.70	5.94	3.61	3.82
MW C7+	129.00	142.00	163.00	142.00	123.00	128.00
Sum	**100.00**	**99.82**	**100.01**	**100.00**	**99.99**	**100.00**

Table **2-12**: Chemical Compositions for tests (GF-0067 to GF-0072)

COMPOUND	Test No. GF-0067	GF-0068	GF-0069	GF-0070	GF-0071	GF-0072
H_2S	2.68	0.00	2.81	0.35	0.00	14.59
CO_2	3.90	0.46	4.99	5.18	0.63	2.10
N_2	0.96	0.60	0.94	0.73	0.51	8.41
C1	74.11	78.13	74.20	79.83	76.31	62.74
C2	7.38	8.39	7.18	7.09	8.66	2.91
C3	2.82	5.18	2.73	2.47	4.80	1.68
i-C4	0.75	0.80	0.78	0.53	0.74	0.35
n-C4	1.42	1.97	1.24	0.87	1.71	1.20
i-C5	0.72	0.69	0.45	0.31	0.73	0.46
n-C5	0.70	0.69	0.42	0.39	0.71	0.61
C6	1.14	1.10	0.73	0.33	1.08	0.97
C7+	3.44	2.00	3.53	1.91	4.12	3.99
MW C7+	132.00	128.00	138.00	128.00	130.00	147.00
Sum	**100.02**	**100.01**	**100.00**	**99.99**	**100.00**	**100.01**

Table **2-13**: Chemical Compositions for tests (GF-0073 to GF-0078)

COMPOUND	Test No. GF-0073	GF-0074	GF-0075	GF-0076	GF-0077	GF-0078
H_2S	2.75	1.12	0.00	3.07	0.00	0.68
CO_2	3.72	1.75	2.91	3.63	0.26	2.63
N_2	1.06	1.68	0.51	1.05	3.86	0.54
C1	76.11	72.81	77.87	76.29	83.69	83.85
C2	6.95	10.34	9.08	6.92	4.07	5.49
C3	2.48	4.70	3.65	2.44	2.42	2.30
i-C4	0.56	0.75	0.63	0.58	0.60	0.31
n-C4	1.15	1.77	1.00	1.18	1.02	0.76
i-C5	0.54	0.64	0.40	0.57	0.49	0.24
n-C5	0.50	0.68	0.46	0.51	0.51	0.28
C6	0.74	1.08	0.56	0.84	0.84	0.38
C7+	3.44	2.68	2.93	2.92	2.23	2.56
MW C7+	131.00	164.00	194.00	128.00	103.00	227.00
Sum	**100.00**	**100.00**	**100.00**	**100.00**	**99.99**	**100.02**

Table **2-14**: Chemical Compositions for tests (GF-0079 to GF-0084)

COMPOUND	Test No. GF-0079	GF-0080	GF-0081	GF-0082	GF-0083	GF-0084
H_2S	3.19	0.00	0.00	1.22	0.44	0.23
CO_2	4.41	0.38	2.82	1.60	4.01	3.93
N_2	0.97	3.79	0.32	2.00	0.60	0.52
C1	76.61	77.52	73.80	72.91	80.85	78.86
C2	7.00	9.18	10.61	11.38	6.69	7.95
C3	2.21	4.15	4.99	4.92	2.50	3.24
i-C4	0.67	0.65	0.83	0.77	0.63	0.71
n-C4	1.05	1.37	1.64	1.61	0.88	1.22
i-C5	0.40	0.43	0.55	0.60	0.34	0.50
n-C5	0.39	0.46	0.58	0.64	0.32	0.52
C6	0.62	0.54	0.85	0.75	0.39	0.64
C7+	2.48	1.55	3.01	1.60	2.35	1.68
MW C7+	120.00	214.00	132.00	144.00	160.00	128.00
Sum	**100.00**	**100.02**	**100.00**	**100.00**	**100.00**	**100.00**

Table **2-15**: Chemical Compositions for tests (GF-0085 to GF-0090)

COMPOUND	Test No. GF-0085	GF-0086	GF-0087	GF-0088	GF-0089	GF-0090
H_2S	0.00	0.00	0.00	0.00	0.00	0.00
CO_2	4.22	2.22	0.91	1.93	1.00	0.51
N_2	1.51	0.62	0.55	0.37	0.72	1.04
C1	74.99	73.68	78.71	78.98	78.33	79.97
C2	9.69	10.03	8.61	10.51	9.87	9.61
C3	4.11	6.15	5.44	3.78	4.62	4.57
i-C4	0.70	1.32	0.84	0.58	0.51	0.63
n-C4	1.34	1.89	1.46	0.87	1.54	1.25
i-C5	0.44	0.61	0.36	0.36	0.40	0.41
n-C5	0.59	0.63	0.46	0.35	0.48	0.37
C6	0.59	0.81	0.57	0.46	0.92	0.43
C7+	1.82	2.04	2.09	1.81	1.61	1.20
MW C7+	128.00	128.00	128.00	129.00	117.00	121.00
Sum	**100.00**	**100.00**	**100.00**	**100.00**	**100.00**	**99.99**

Table **2-16**: Chemical Compositions for tests (GF-0091 to GF-0096)

COMPOUND	Test No. GF-0091	GF-0092	GF-0093	GF-0094	GF-0095	GF-0096
H_2S	0.00	2.21	0.48	0.00	8.10	8.18
CO_2	0.63	4.22	6.07	4.27	3.20	3.65
N_2	0.51	5.00	0.44	0.47	0.48	0.22
C1	76.31	83.85	78.54	81.31	74.67	73.55
C2	8.66	1.73	6.66	7.94	7.40	7.61
C3	4.80	0.55	2.46	2.90	2.58	2.76
i-C4	0.74	0.10	0.60	0.48	0.48	0.54
n-C4	1.71	0.30	0.91	0.79	0.97	1.04
i-C5	0.73	0.15	0.42	0.22	0.40	0.43
n-C5	0.71	0.13	0.43	0.26	0.32	0.36
C6	1.08	0.16	0.70	0.30	0.48	0.53
C7+	4.12	1.60	2.29	1.05	0.91	1.13
MW C7+	130.00	124.00	128.00	186.00	110.00	118.00
Sum	**100.00**	**100.00**	**100.00**	**99.99**	**99.99**	**100.00**

Table **2-17**: Chemical Compositions for tests (GF-0097 to GF-0102)

COMPOUND	Test No. GF-0097	GF-0098	GF-0099	GF-0100	GF-0101	GF-0102
H_2S	0.00	8.78	8.33	9.10	8.57	8.00
CO_2	4.70	5.05	3.08	4.33	2.98	2.98
N_2	0.46	0.46	0.48	0.47	0.47	0.53
C1	78.90	73.18	75.29	73.78	75.60	75.51
C2	8.51	7.00	7.39	7.15	7.23	7.42
C3	3.61	2.31	2.49	2.35	2.51	2.57
i-C4	0.56	0.48	0.46	0.46	0.46	0.49
n-C4	1.07	0.92	0.93	0.90	0.90	0.94
i-C5	0.35	0.37	0.36	0.36	0.36	0.37
n-C5	0.38	0.30	0.29	0.28	0.28	0.30
C6	0.41	0.46	0.33	0.31	0.29	0.33
C7+	1.05	0.69	0.56	0.50	0.37	0.57
MW C7+	122.00	110.00	128.00	110.00	108.00	112.00
Sum	**100.00**	**100.00**	**99.99**	**99.99**	**100.02**	**100.01**

Appendix C

PRESSURE TRAVERSE CURVES

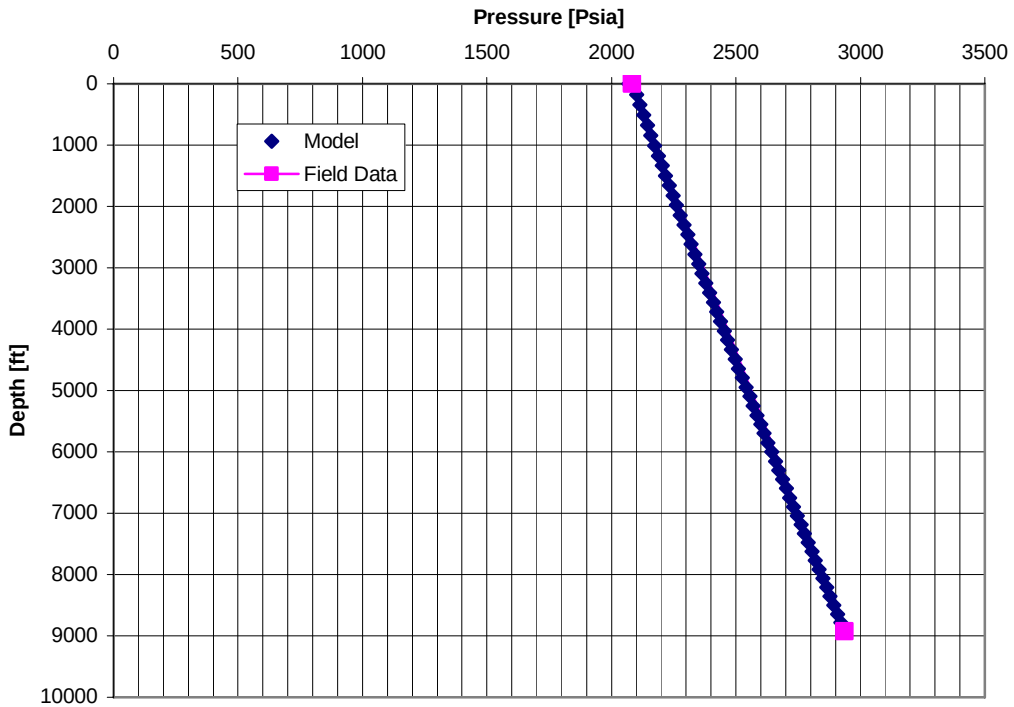

Figure **3-1**: Test GF-0002

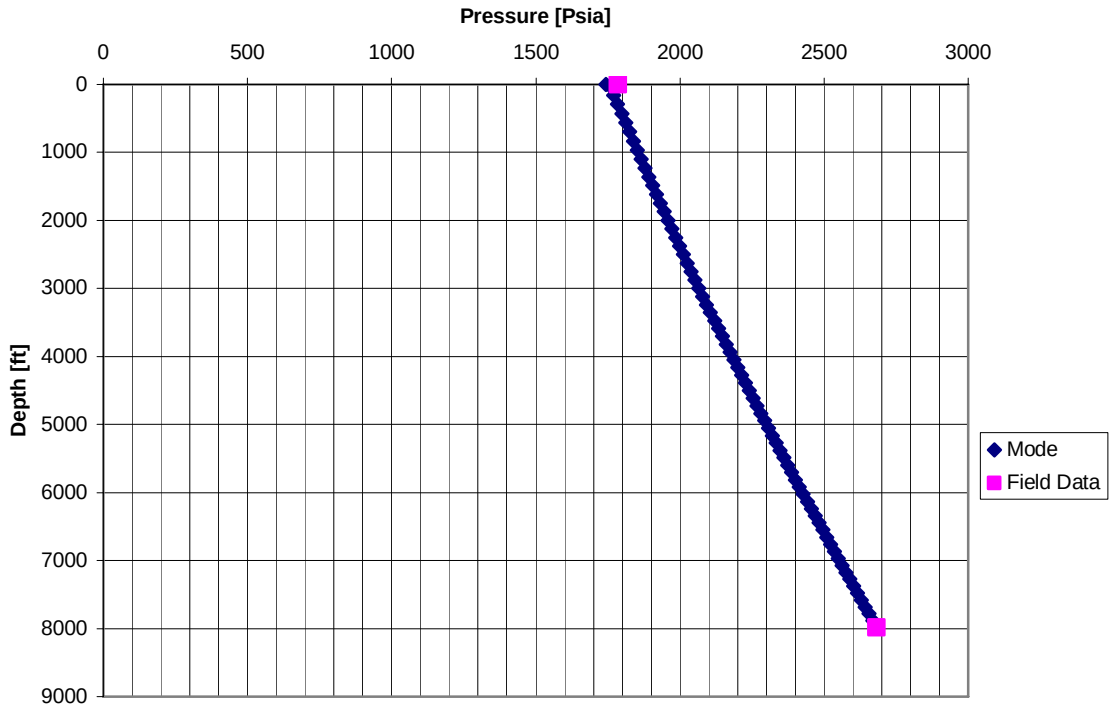

Figure **3-2**: Test GF-0006

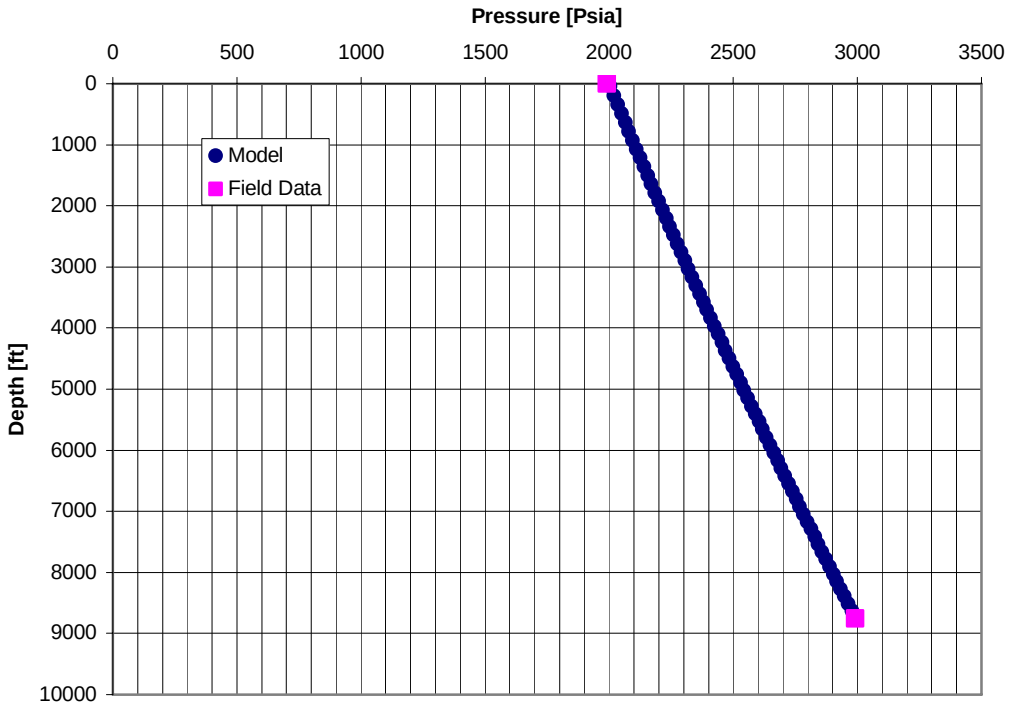

Figure **3-3**: Test GF-0008

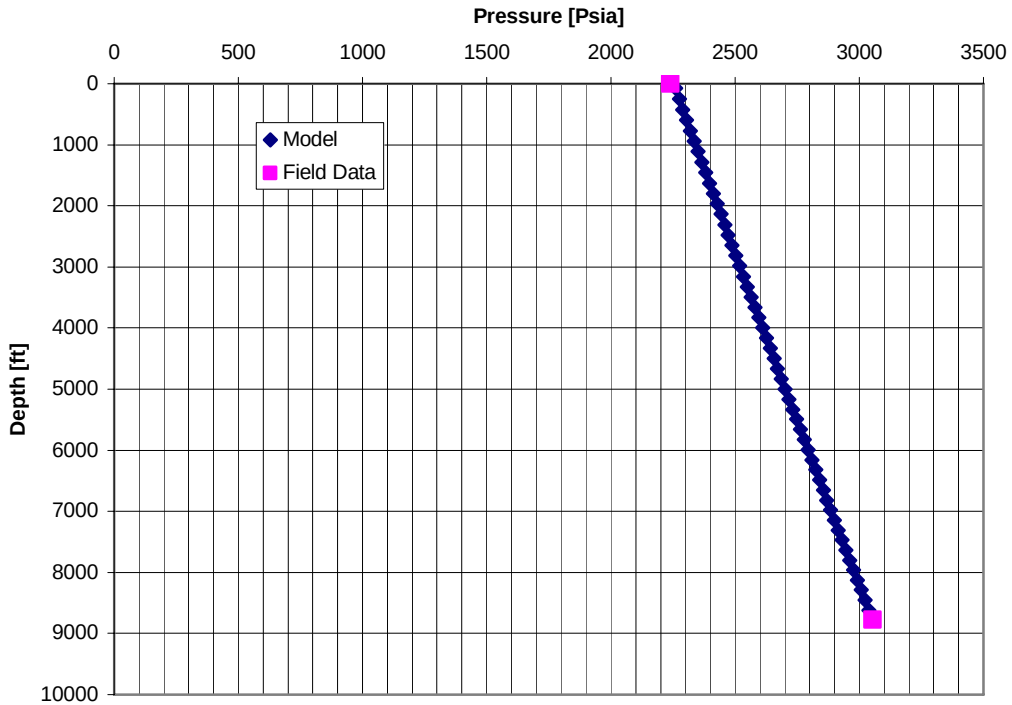

Figure **3-4**: Test GF-0009

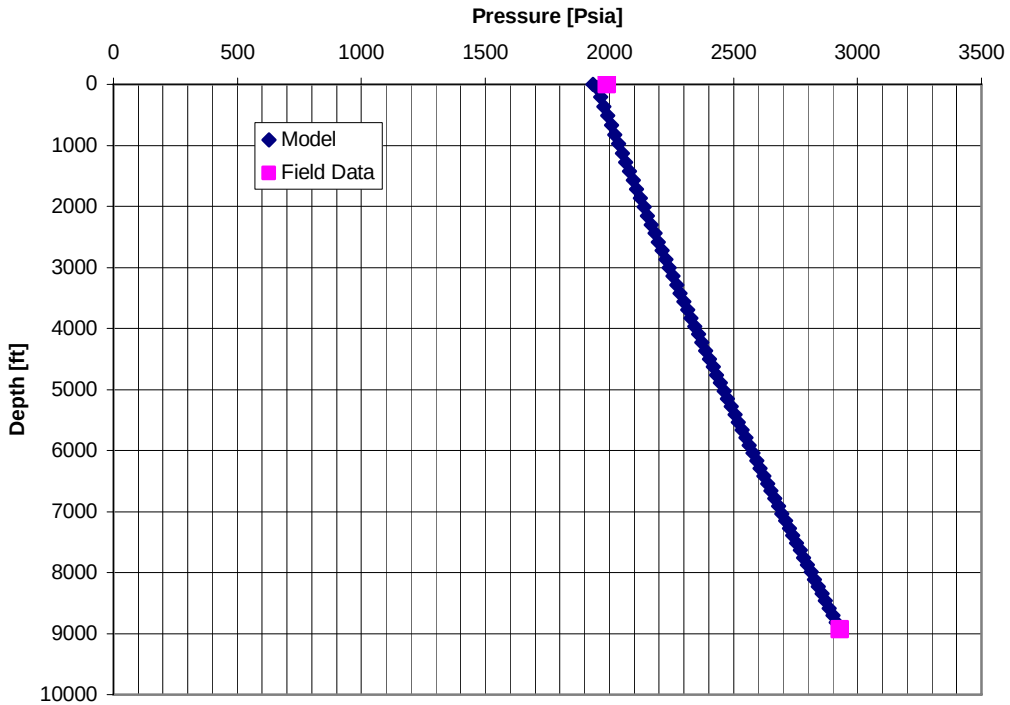

Figure **3-5**: Test GF-0011

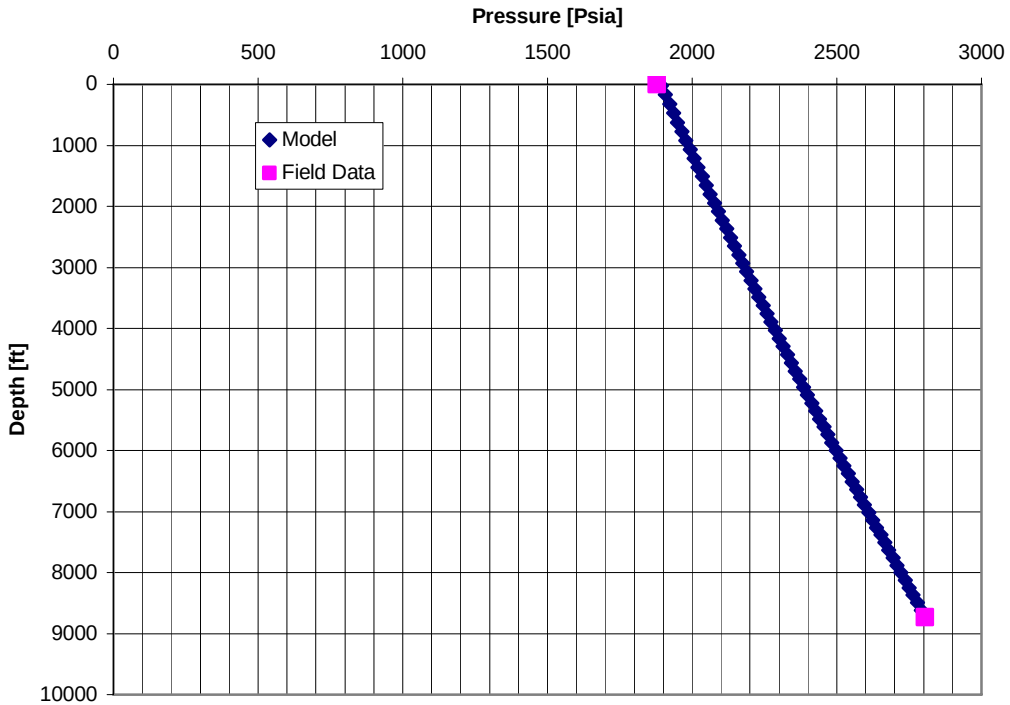

Figure **3-6**: Test GF-0012

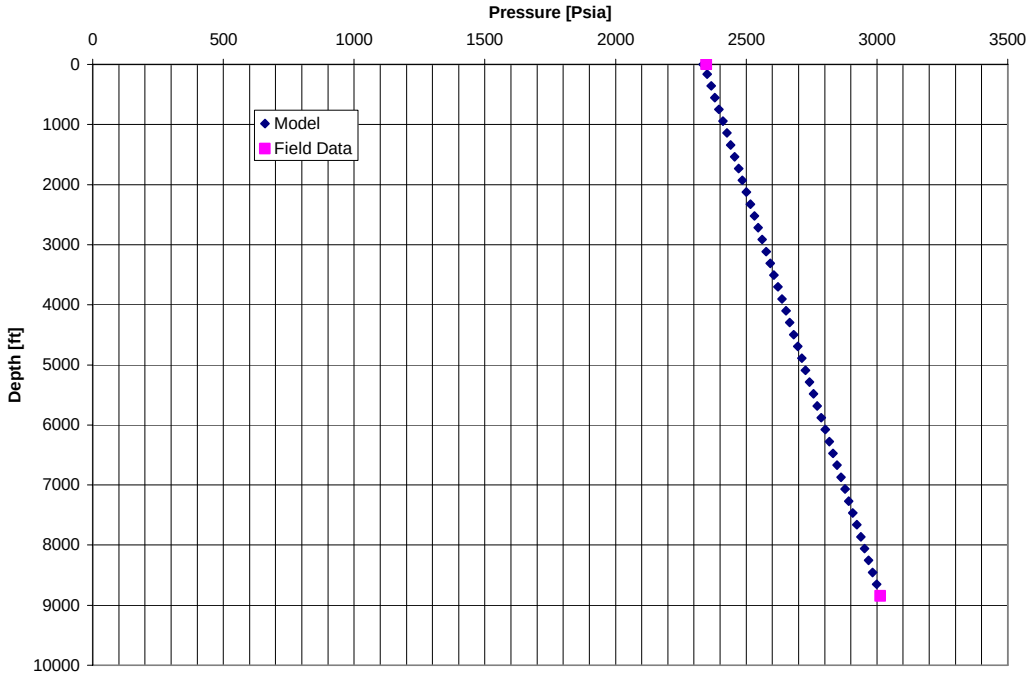

Figure **3-7**: Test GF-0013

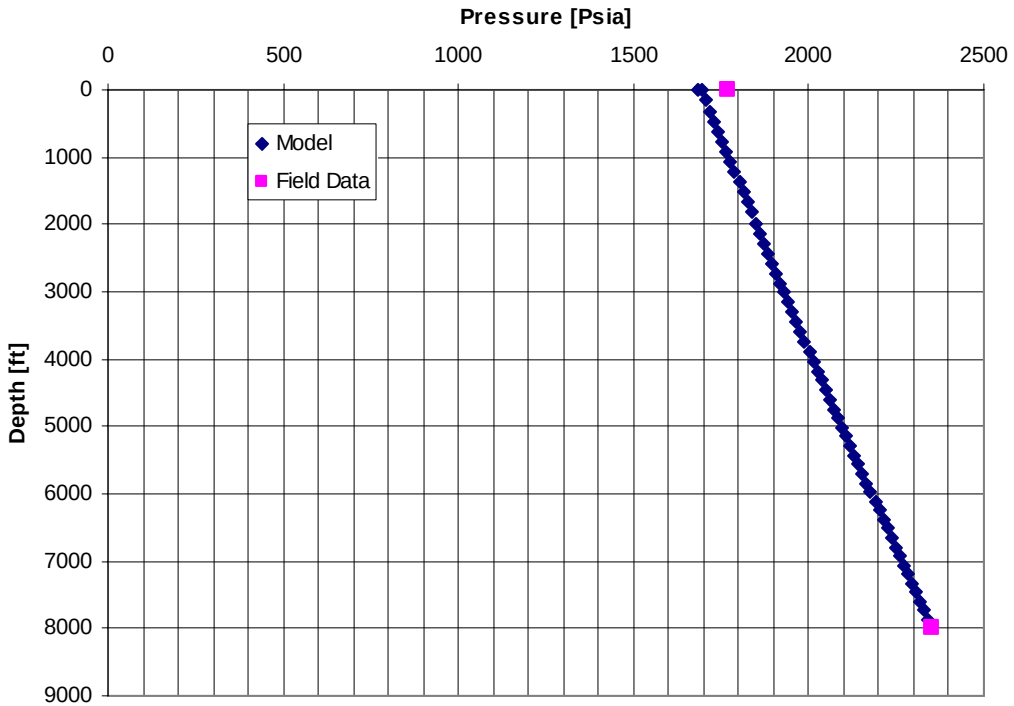

Figure **3-8**: Test GF-0020

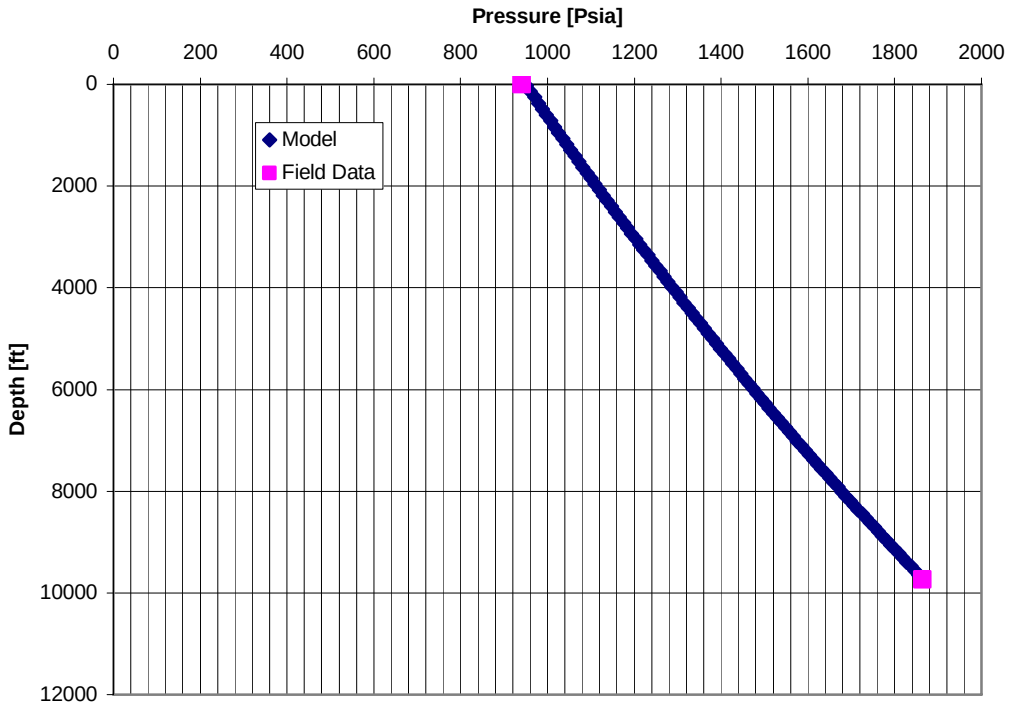

Figure **3-9**: Test GF-0026

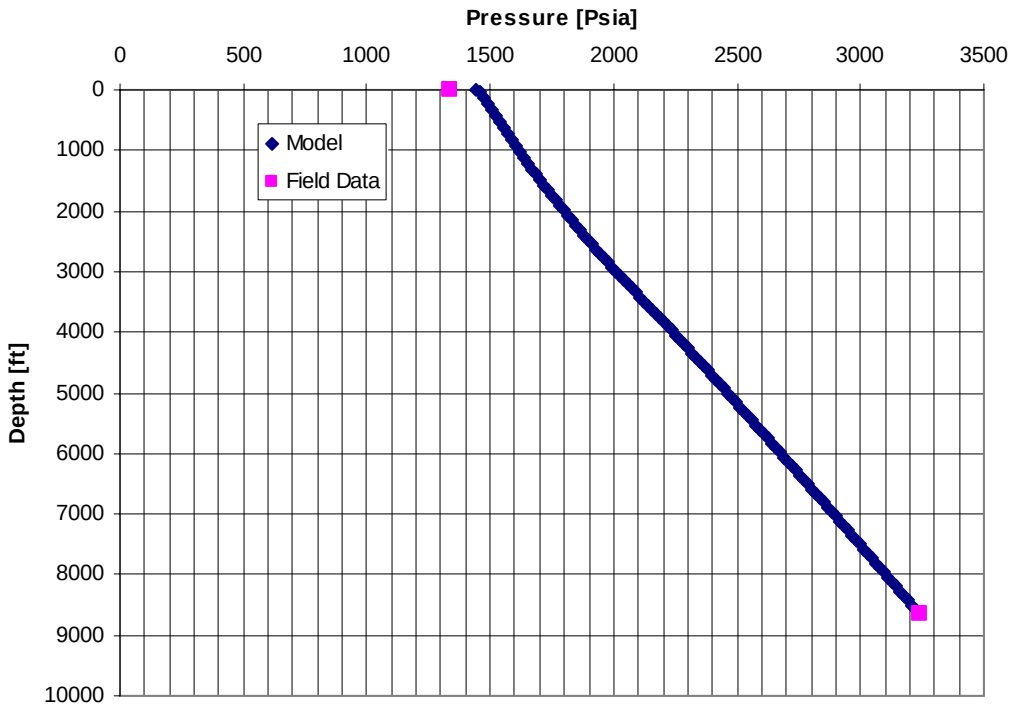

Figure **3-10**: Test GF-0029

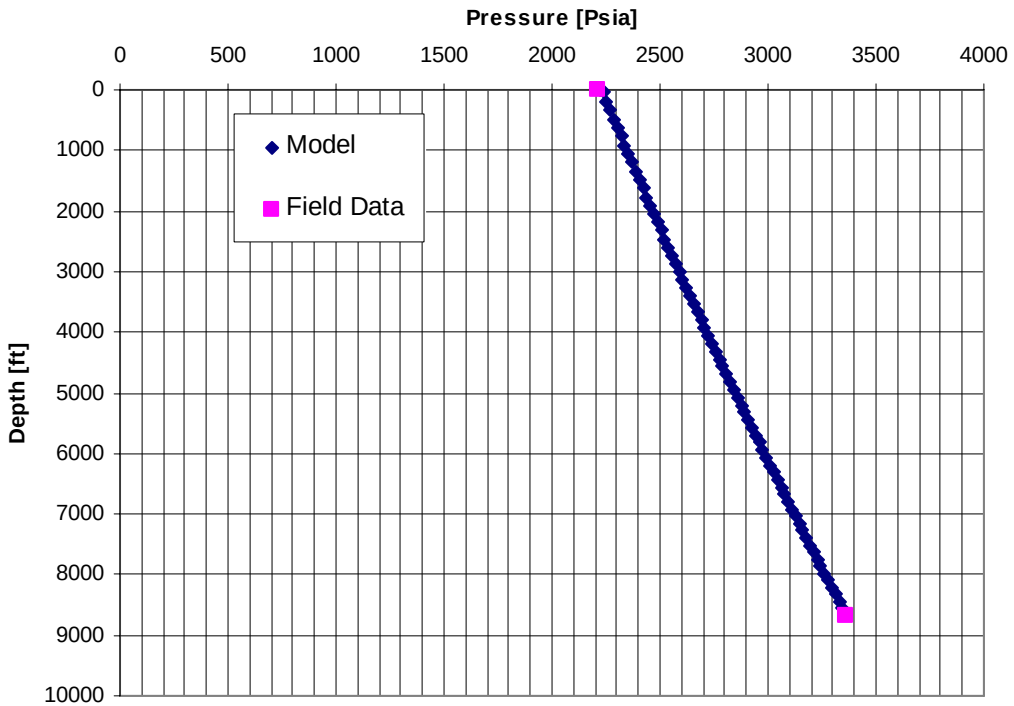

Figure **3-11**: Test GF-0031

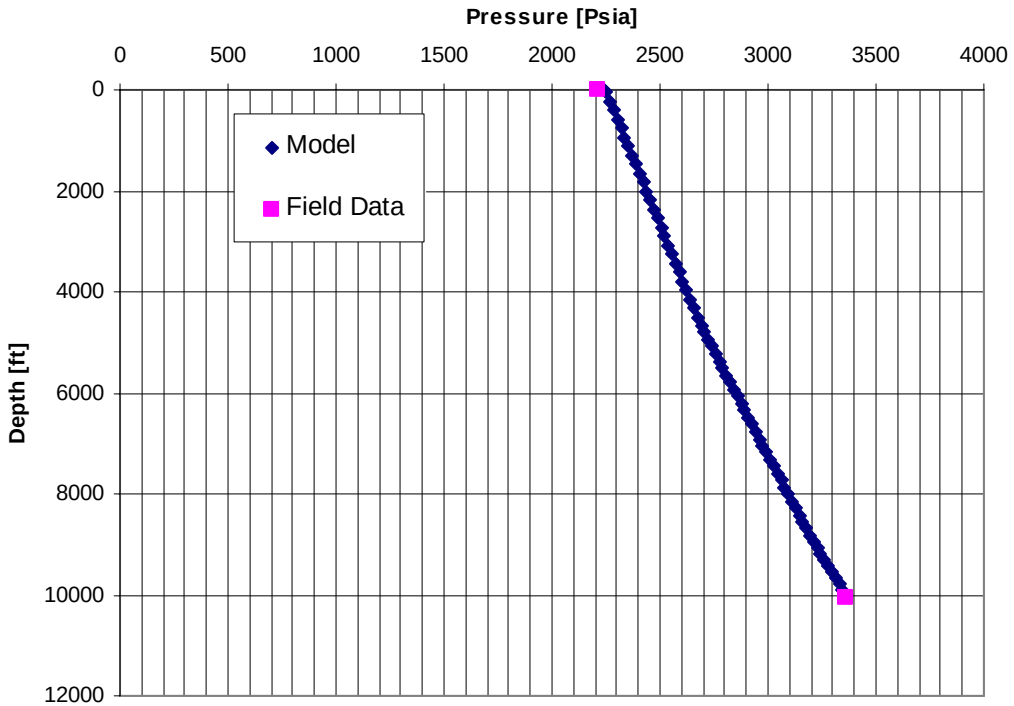

Figure **3-12**: Test GF-0033

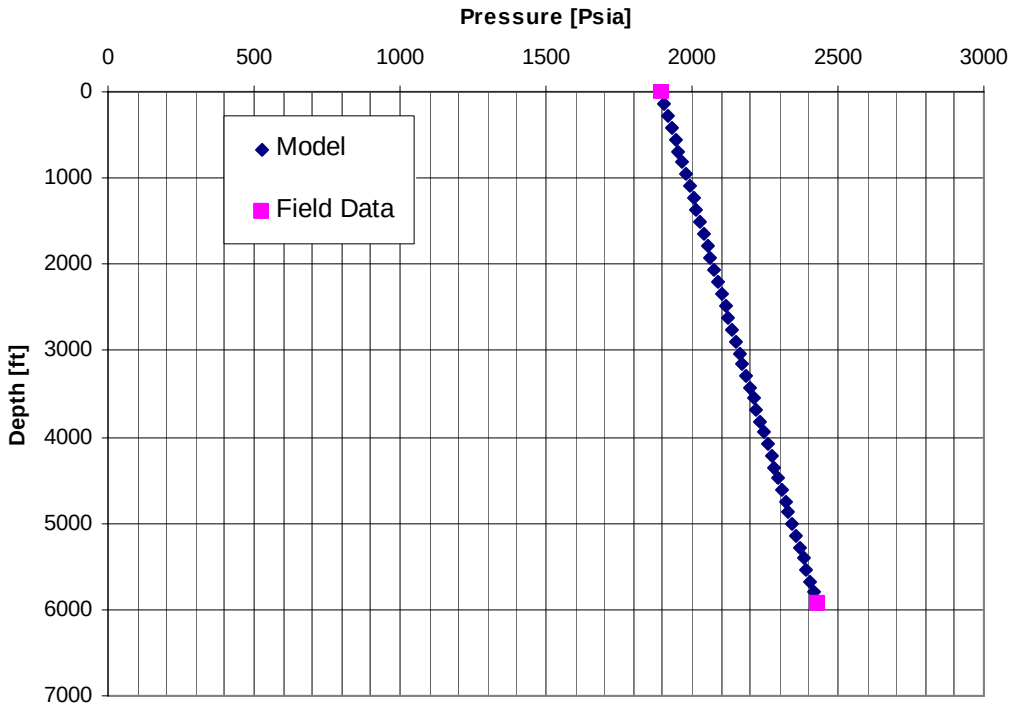

Figure **3-13**: Test GF-0034

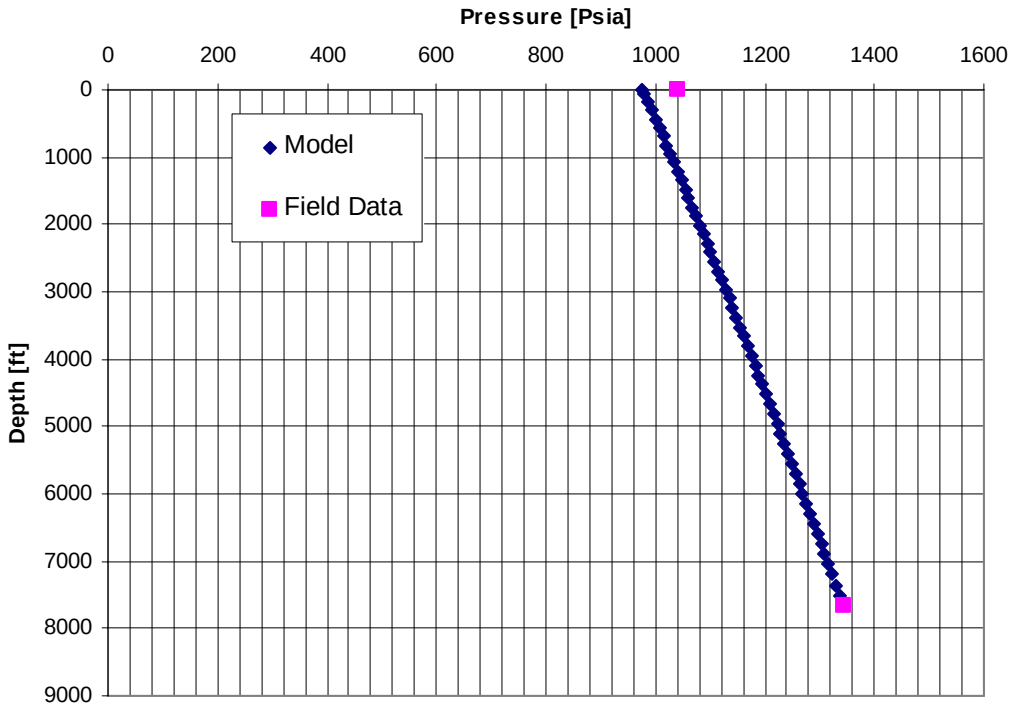

Figure **3-14**: Test GF-0035

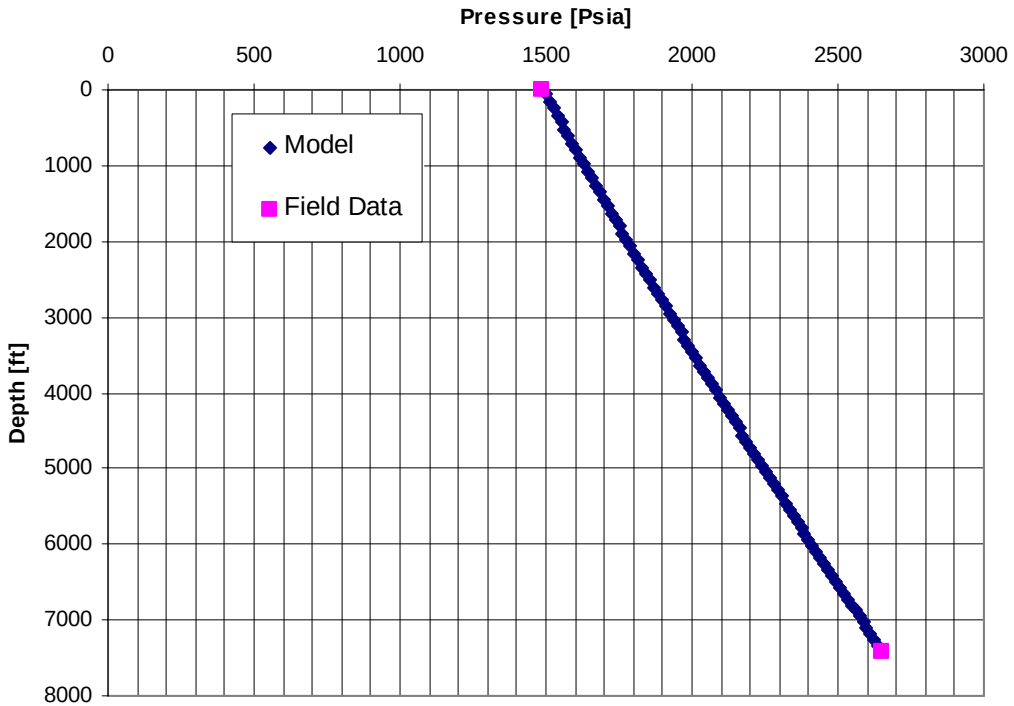

Figure **3-15**: Test GF-0036

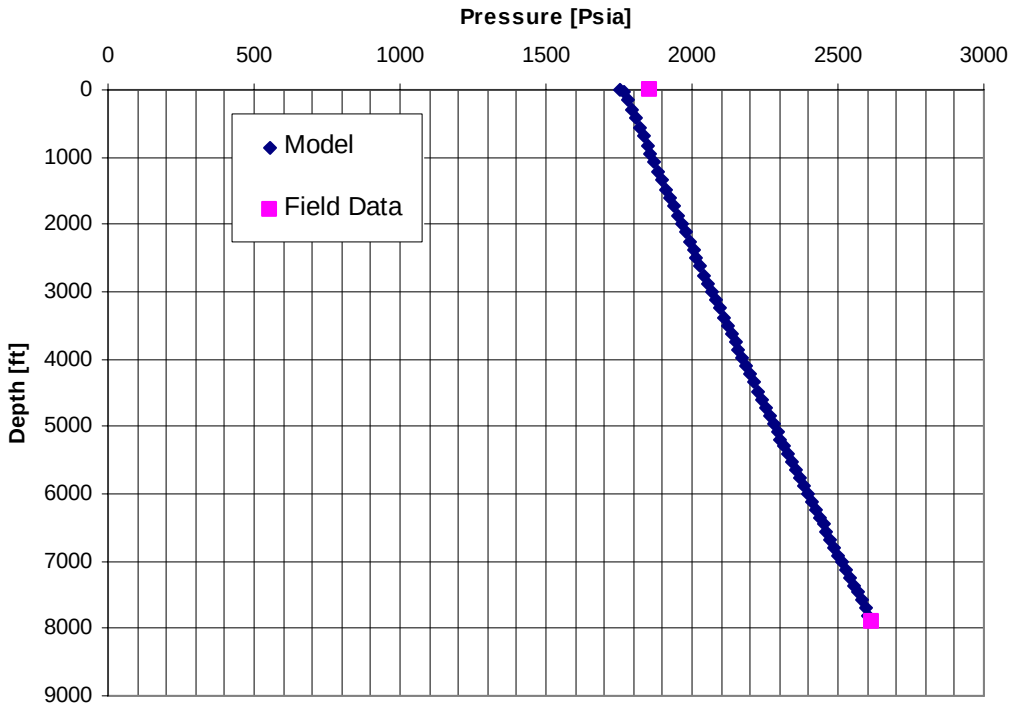

Figure **3-16**: Test GF-0040

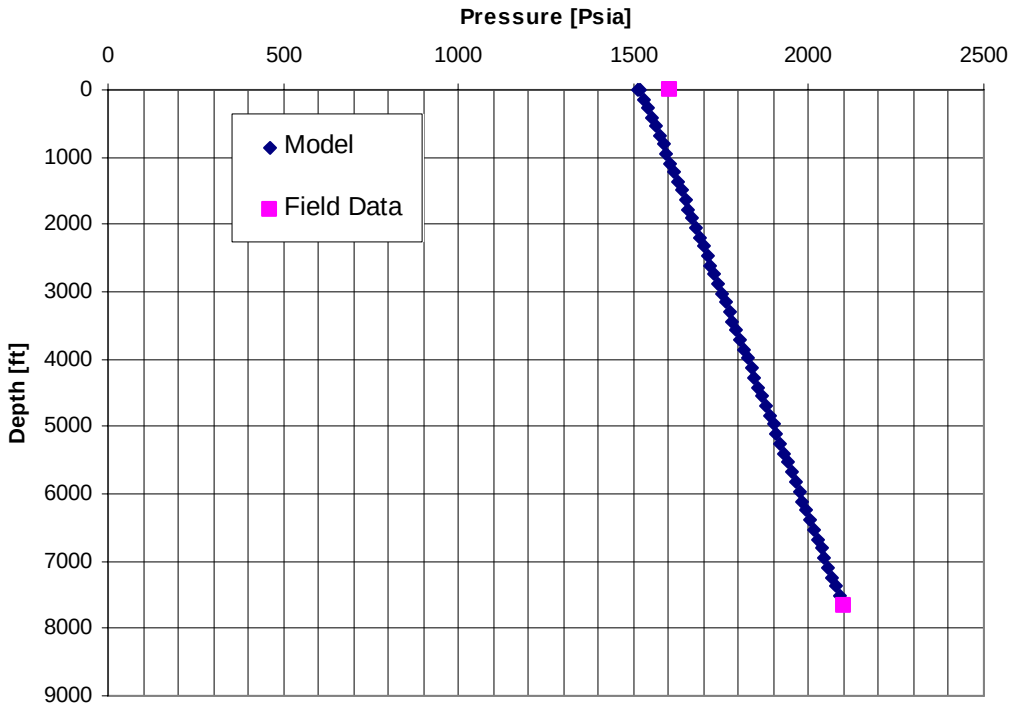

Figure **3-17**: Test GF-0042

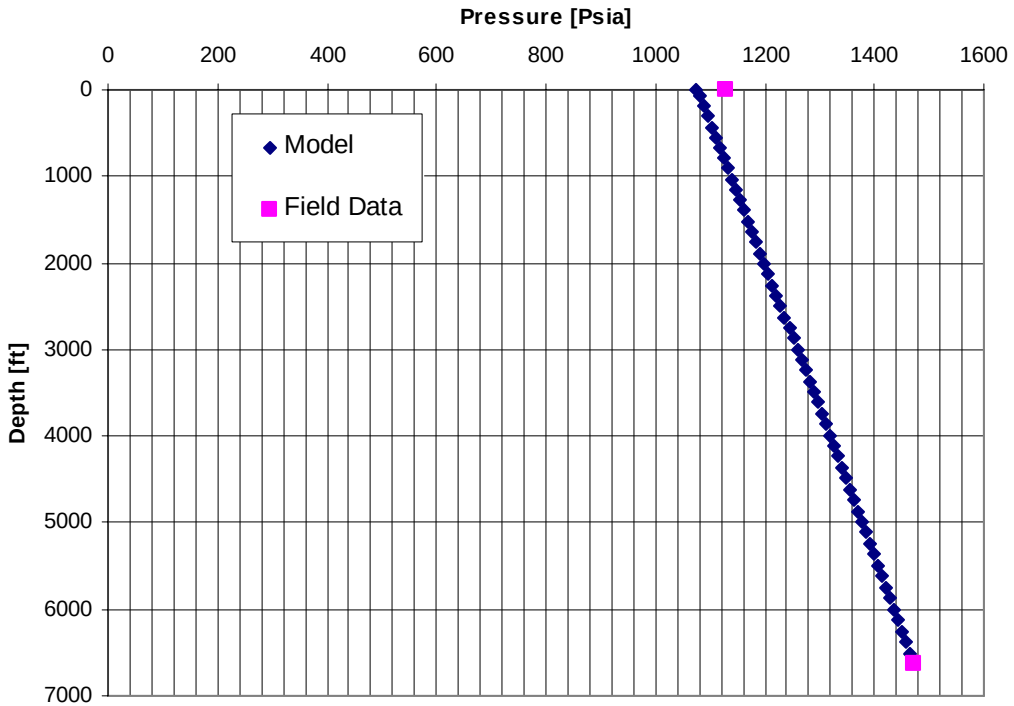

Figure **3-18**: Test GF-0048

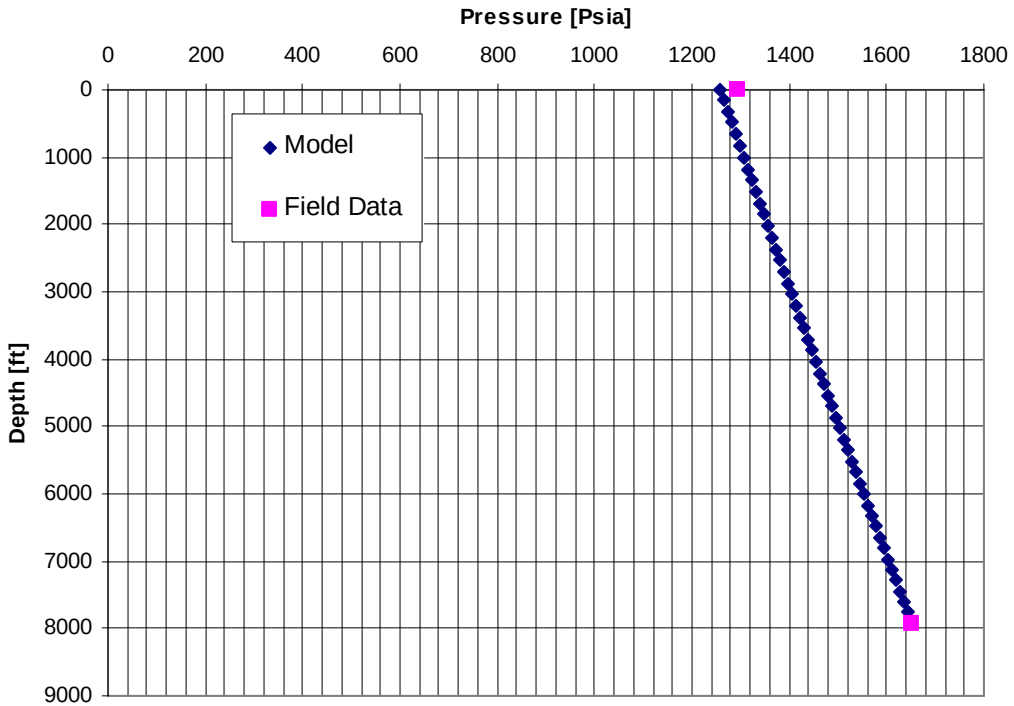

Figure **3-19**: Test GF-0050

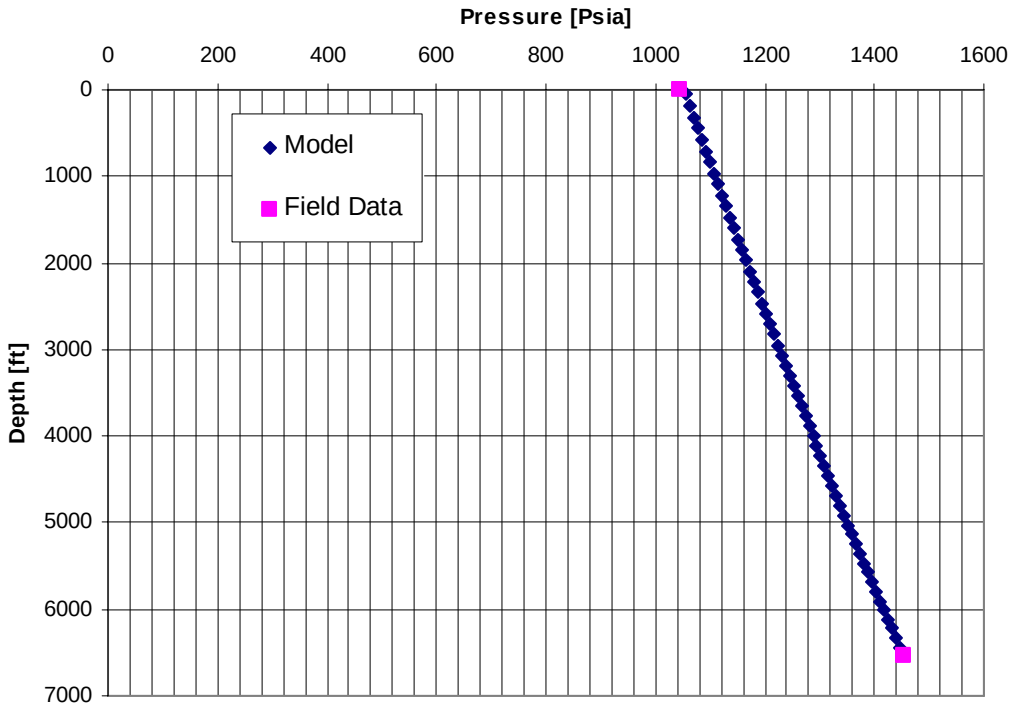

Figure **3-20**: Test GF-0056

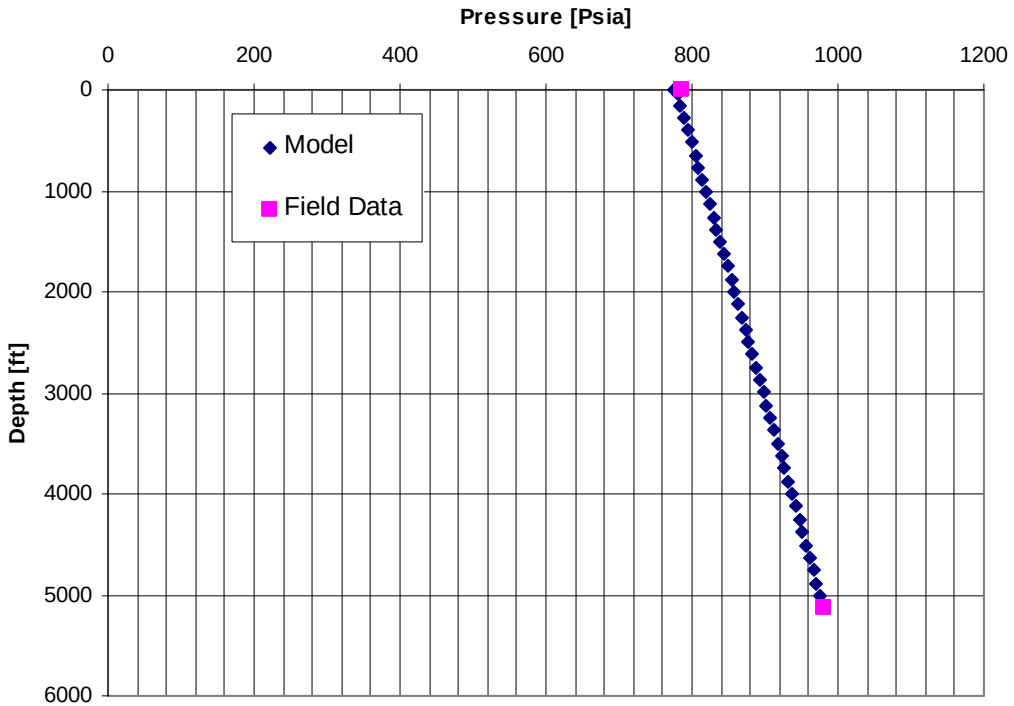

Figure **3-21**: Test GF-0058

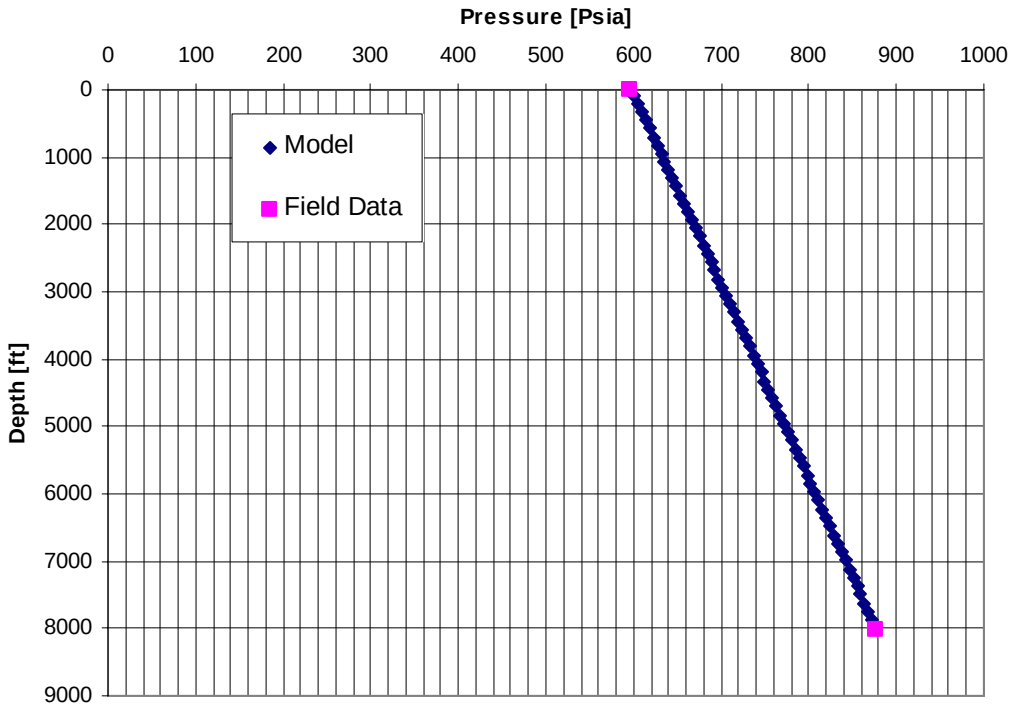

Figure **3-22**: Test GF-0059

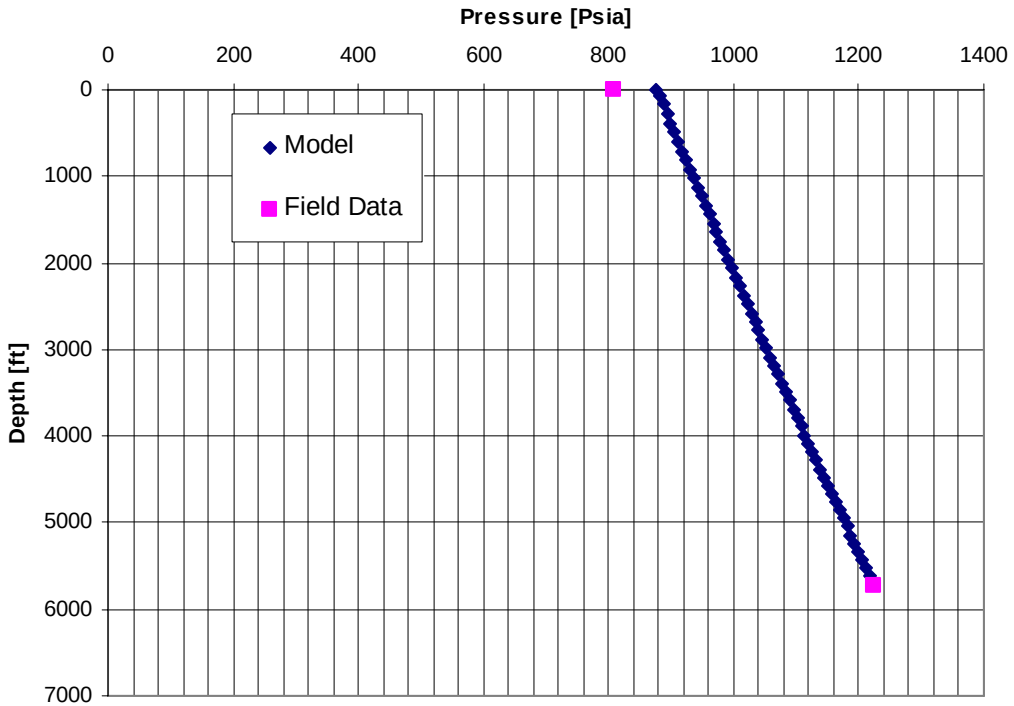

Figure **3-23**: Test GF-0068

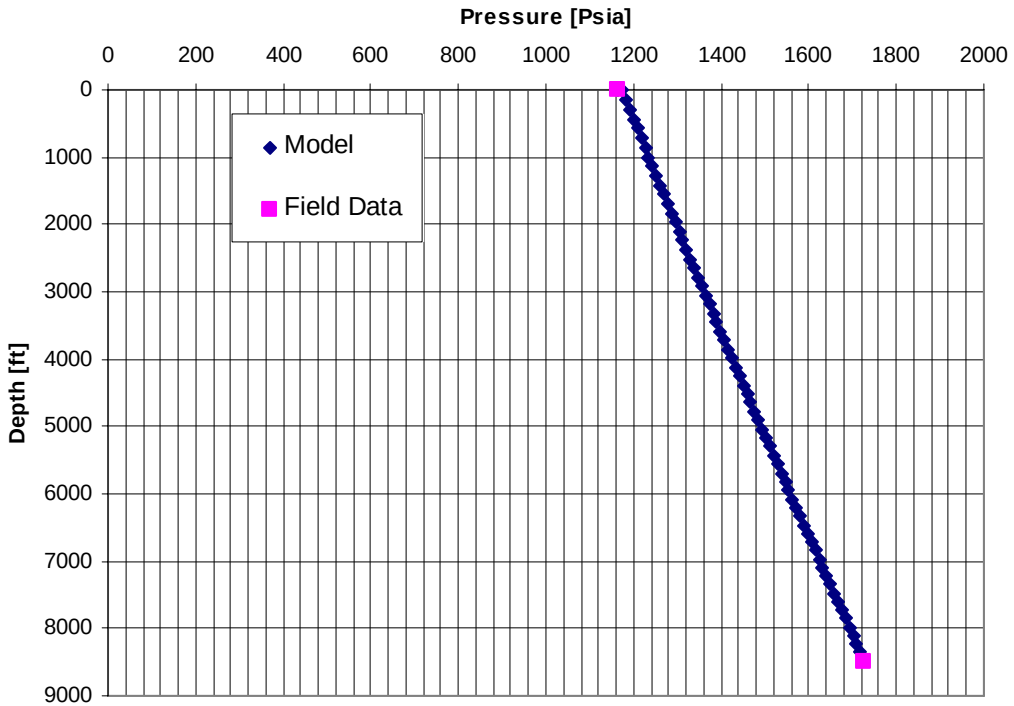

Figure **3-24**: Test GF-0071

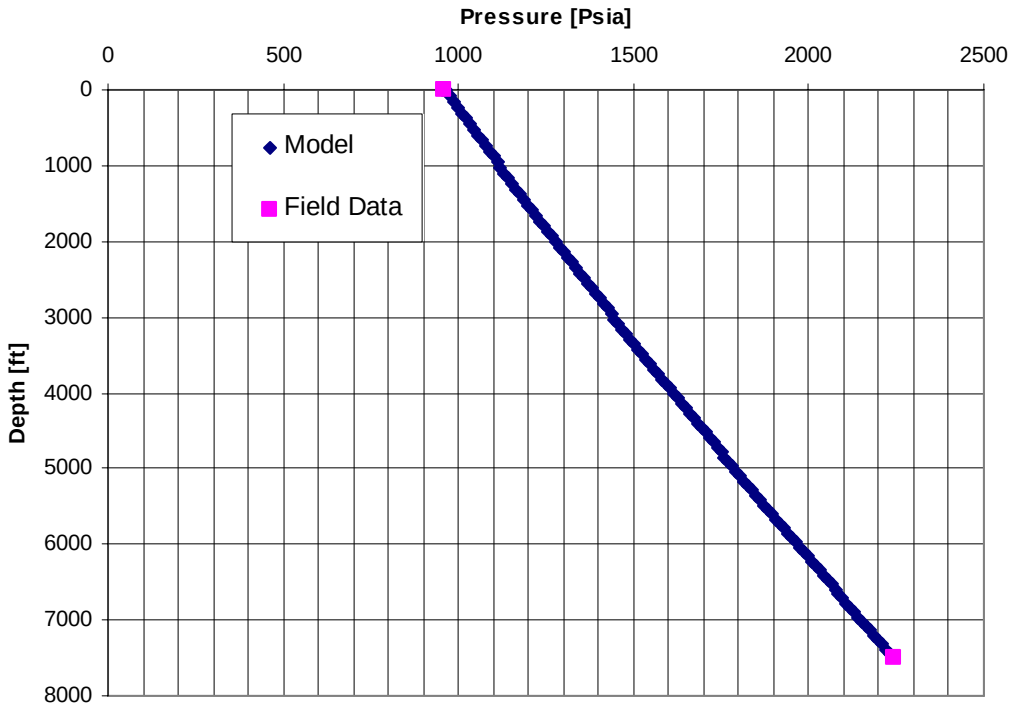

Figure **3-25**: Test GF-0072

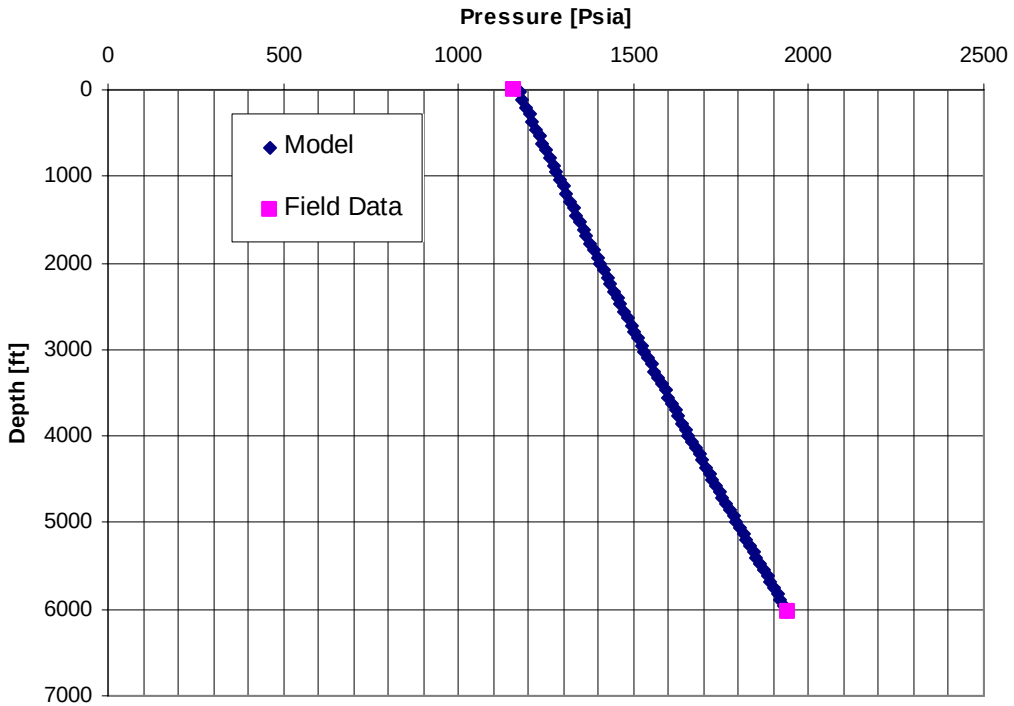

Figure **3-26**: Test GF-0082

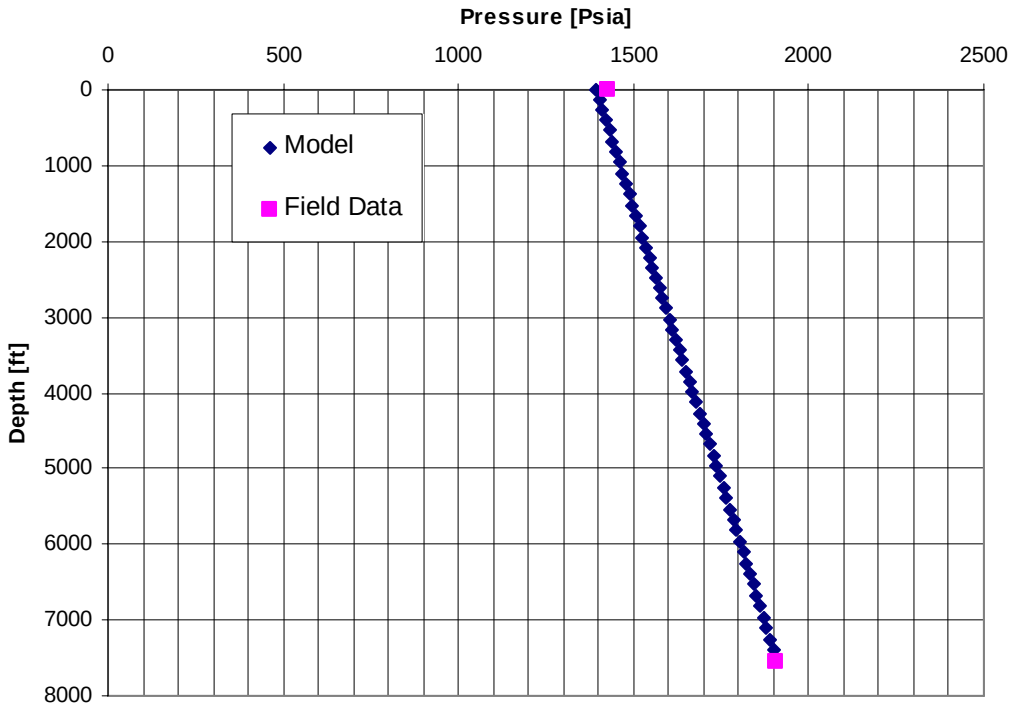

Figure **3-27**: Test GF-0088

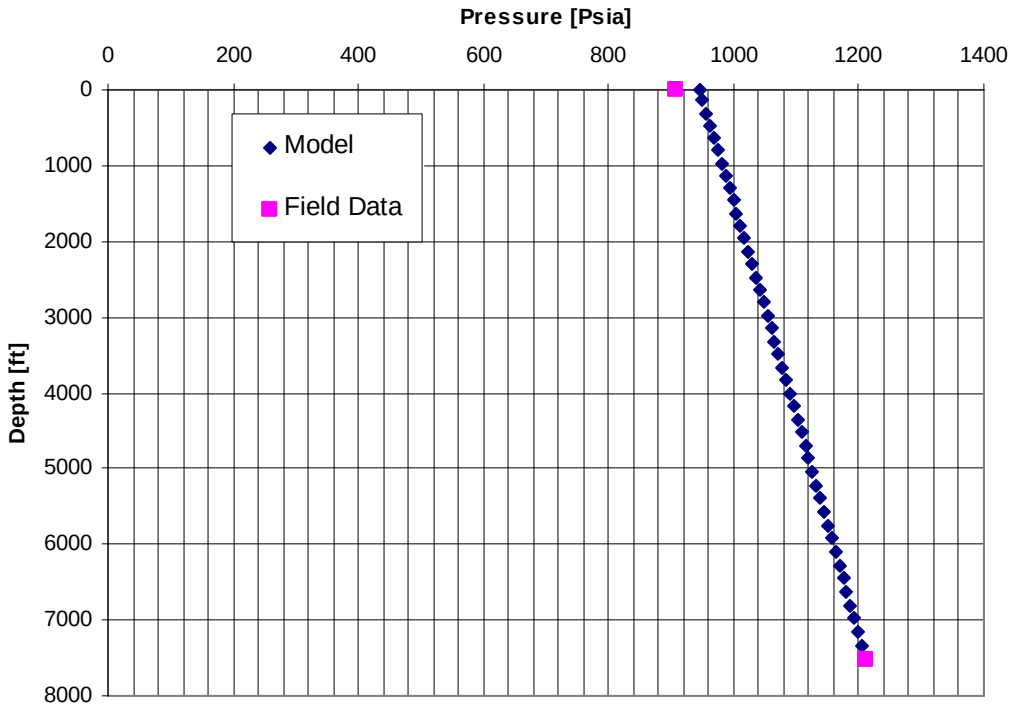

Figure **3-28**: Test GF-0092

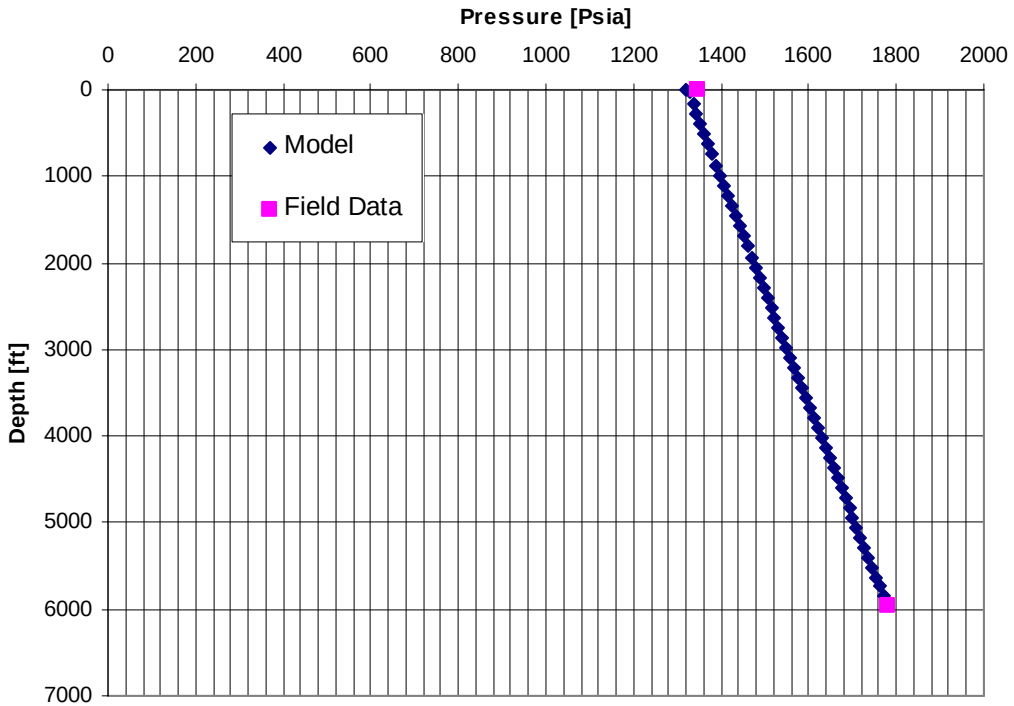

Figure **3-29**: Test GF-0095

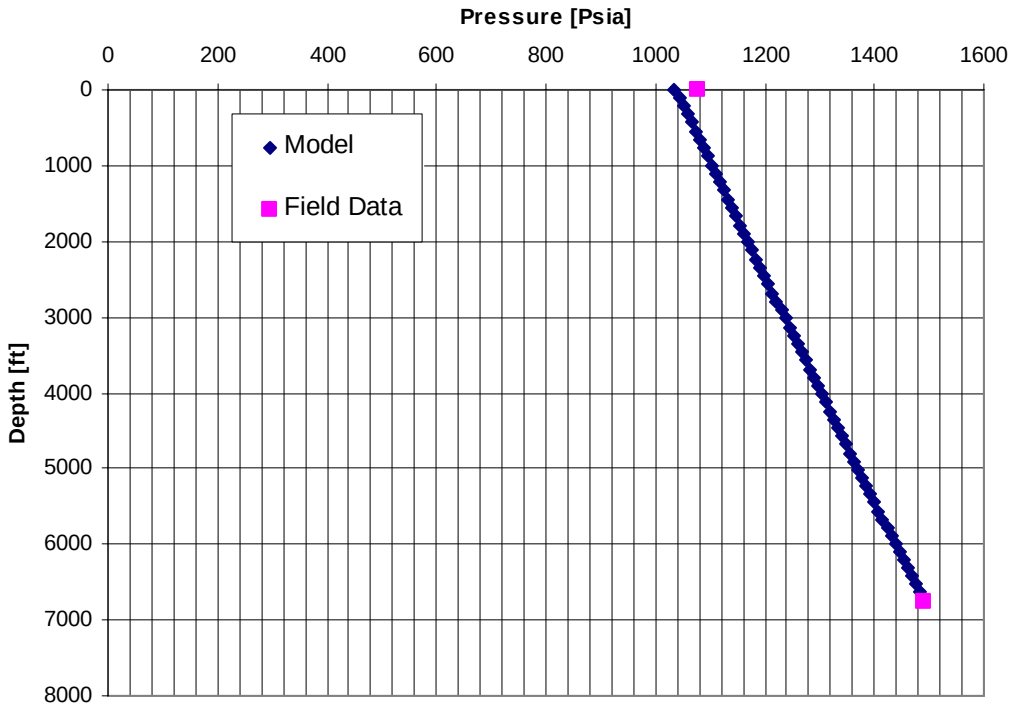

Figure **3-30**: Test GF-0098

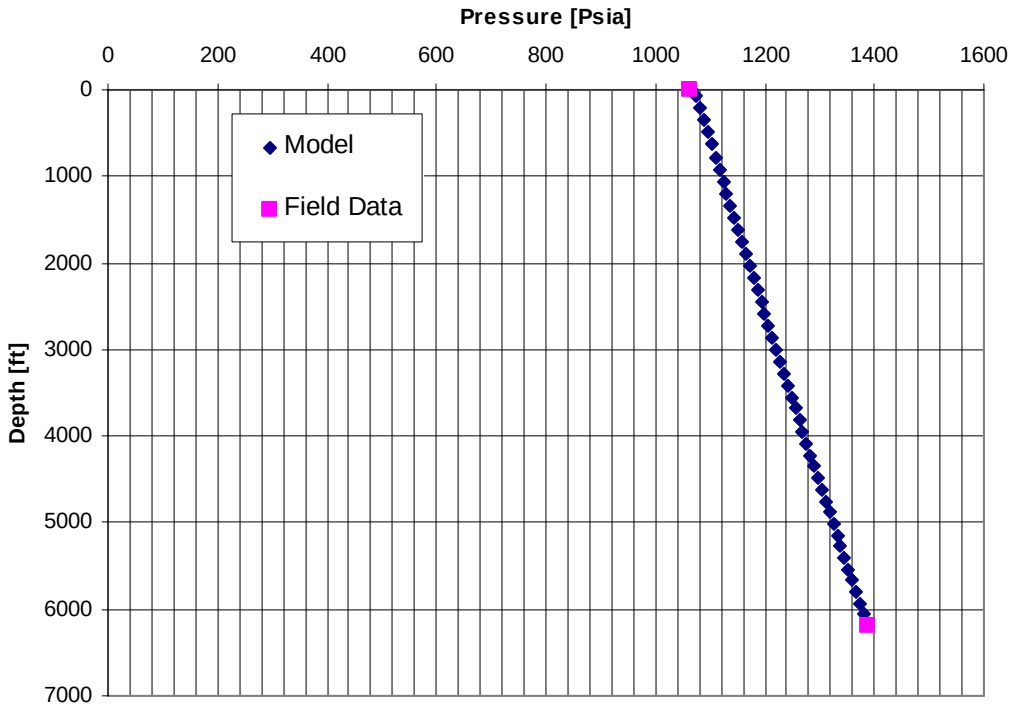

Figure **3-31**: Test GF-0099

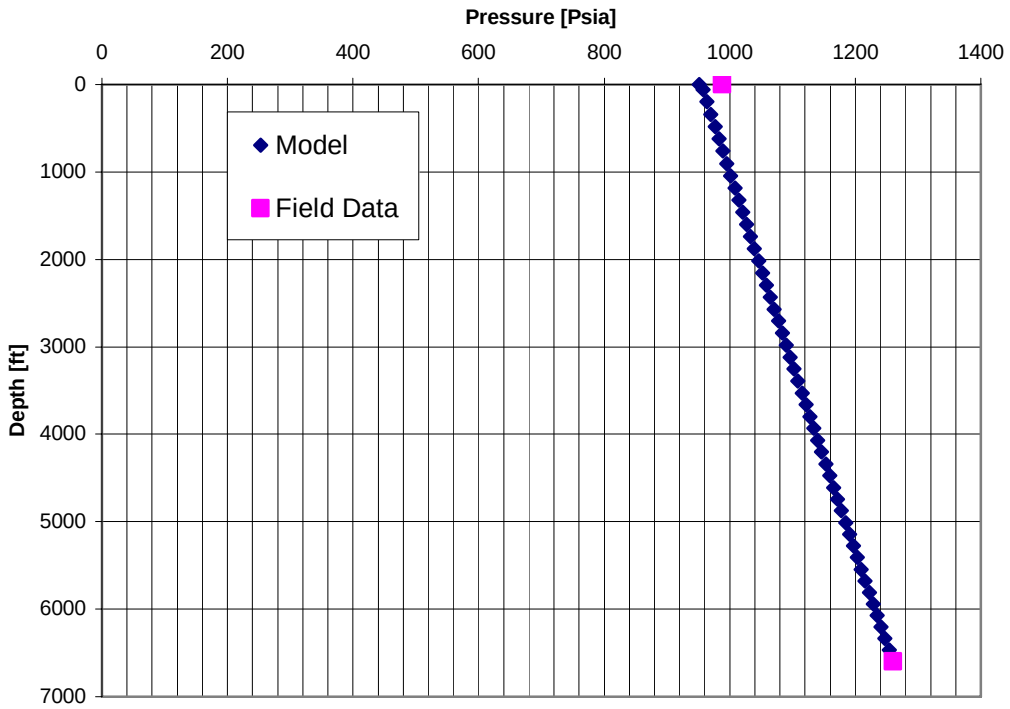

Figure **3-32**: Test GF-0100

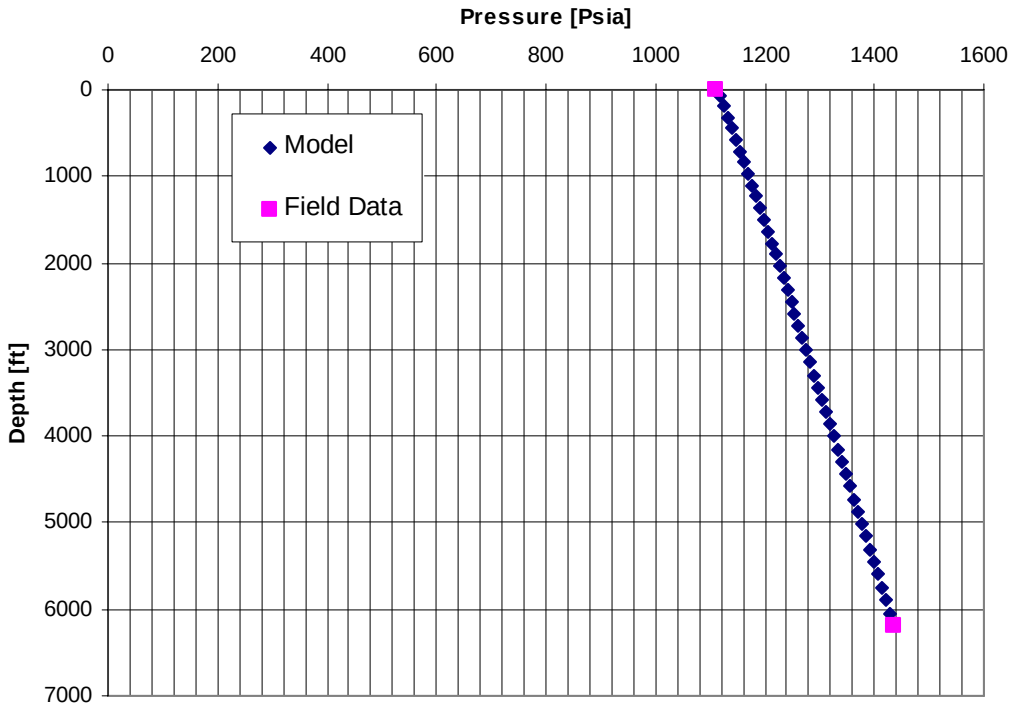

Figure **3-33**: Test GF-0101

VITA

Abdallah Ahmed Sadegh

Abdallah A. Sadegh was born on May 11, 1976 in Nouakchott, Mauritania. He attended Leycèe Arabe High School and graduated in June 1994. He was ranked 5th in the country in the national high school examination (Bac. C). He completed an intensive English language training course at the University of Arizona, Tucson, and graduated with outstanding recognition. Abdallah attended the University of Missouri-Rolla, and earned BS honors (*Cum Laude*) in Metallurgical Engineering. He then earned his Master of Science degree in Mineral Processing in 2002 from the Pennsylvania State University and then went on to join the PhD program in Petroleum and Natural Gas Engineering. He has published several technical papers and given presentations at technical conferences. He is an active member of the Society of Petroleum Engineers and the Society for Mining Metallurgy and Exploration. He is also a member of the Phi Eta Sigma National Honor Society and of Alpha Sigma Mu (Honor Society for Materials Science and Engineering).